CHAPTER 5

AN ANALYSIS OF FLOW AT THE ZEDEX GALLERY BY USING A COUPLED HYDRO-CHEMICAL APPROACH

5.1 INTRODUCTION

Unsaturated and saturated flow has been numerically investigated in the ZEDEX gallery. When analysing the behaviour of a deep repository, the unsaturated state of the clayey components of the engineered barrier represents a short transient period if compared with the long life of the nuclear waste. However, unsaturated flow became critical within the schedule of the Backfill and Plug Test Project, as backfill hydration was slower than expected a priori from the results in laboratory. Therefore, the study of the backfill unsaturated flow was a key issue in the simulations carried out throughout the project.

Several models were proposed in order to study the flow in this project: different geometries, different boundary conditions, different backfill parameters, different formulations, etc. The aim of this study was to establish a proper model able to reproduce the flow conditions at the barrier. After all the calculations performed, a model which took into account the reactive transport of salts was the most suitable to reproduce the measurements from different devices located in the backfill. The key point of the conceptual model presented is the variation of osmotic suction with time due to the transport of solutes. The range of total suction measured in the BPTP is low if compared with pure bentonites in other projects dealing with engineered barriers. Therefore, the variation of osmotic suction may become significant under these conditions. Moreover, the increase of backfill hydraulic conductivity due to its hydration with salt water had to be taken into account to correctly reproduce the measurements. This increase, though not very important, was proved from different experimental results in chapter 3.

Due to the considerable experimental testing research carried out on unsaturated and saturated compacted bentonite-granular material mixtures in the last years, necessity and concern on modelling tools have increased but at a slower rate. Difficulties to formulate mathematical models able to reproduce the coupled interaction between pore fluid chemistry and hydro-mechanical behaviour are quite notorious until the last few years. Nowadays, some models, taking into account the chemical coupling, are available in the literature (Murad & Cushman, 1998; Guimarães et al. 2001; Hueckel et al. 2001; Molenaar & Huyghe, 2001; Thomas et al. 2001) but much more work is still necessary to incorporate the geochemical variables in the current understanding of soil behaviour. In this chapter, a new-coupled thermo-hydro-mechanical-chemical (THMC) formulation (Guimarães, 2002) was used to simulate the backfill saturation and global flow tests at the ZEDEX gallery at the Äspö Hard Rock Laboratory (ÄHRL) within the Backfill and Plug Test Project (BPTP). This mixture was compacted in-situ and is being saturated with salt water to speed up the saturation process. The effects of salt water on the unsaturated and saturated backfill behaviour were investigated. At this stage, only the hydro-chemical coupling was considered after the results of oedometer tests in Rowe cells which confirmed that backfill compressibility was not influenced by changes in pore fluid chemistry. An experimental intrinsic permeability law, obtained from oedometer tests in Rowe cells, was proposed. This law was implemented into

the finite element code and used to compute the variation of intrinsic permeability depending on pore fluid chemistry.

5.2 HYDRAULIC CONDUCTIVITY AND ITS MATHEMATICAL STUDY

Hydraulic conductivity is one of the most important parameters in soil mechanics and above all, one of the most complex to estimate with accuracy due to its enormous variation depending on changes in fabric, void ratio, water content, temperature and pore fluid chemistry. One of the very first models of hydraulic conductivity was the well-known Kozeny-Carman equation obtained by assuming laminar flow of a fluid in a net of channels when the hydraulic radius concept is applied. The grain size distribution was also used in the past to obtain expressions of the hydraulic conductivity and the water retention curve (Kovács, 1981; Fredlund et al. 1997). Kozeny-Carman law and grain size distribution models have been widely and successfully used in uniformly graded sands but, as it was stated by Olsen (1962), they were not suitable for compacted clayey soils due to the heterogeneity of the pore size distribution of such soils. Olsen indicated that flow is limited only to the *inter-cluster* pores (macropores) and fluid filling the *intra-cluster* pores (micropores) should be less mobile or immobile. Therefore, hydraulic permeability models based only on volumetric or grain size parameters cannot accurately reflect the complexity of compacted finer soil fabric.

Some works related the pore size distribution to hydraulic conductivity, soil retention curve and relative liquid permeability (Marshall, 1958; Garcia-Bengochea & Lovell, 1981; Elzeftawy & Cartwright, 1981; Kosugi, 1996; Arya et al. 1999; Romero et al. 1999; Watabe et al. 2000; Tuli et al. 2001). These models represented an important improvement respect to those related to grain size distribution or void ratio. However, such models are only applicable to inert soils but not to soils containing expanding clay minerals as bentonites, where pore fabric changes as a result of clay-fluid interactions. Lapierre et al. (1990) showed that there is not a one-to-one relationship between pore size distribution of a soil and hydraulic conductivity after flow tests, scanning electron microscopy (SEM) tests and mercury intrusion porosimetry (MIP) tests in grey marine plastic clay from Quebec. They finally concluded that direct measurements of this parameter are necessary.

Nowadays, some techniques are available to determine directly the volumetric pore size as MIP tests, capillary condensation method, or removal of water by suction or air pressure (Mitchell, 1993). MIP is, doubtless, the most common among soil scientists but its use still presents important uncertainties and limitations and its results have to be carefully considered. Despite of these limitations, MIP has become an important and useful tool to study the fabric (micro and macrostructure of soils).

Garcia-Bengochea & Lovell (1981) found that permeability generally varied with the magnitude and frequency of the large pore mode after tests carried out in different artificial soils obtained by mixing silt and kaolin. Acar & Olivieri (1989) also pointed up that mercury porosimetry provides information of the *microfabric* and hydraulic conductivity might be dependent on *macrofabric* features after conducting MIP and flow tests on compacted clayey soils taking into account the molding water. Barbour & Yang (1993) found no evidence that microstructure of a soil was altered after permeation by concentrated NaCl solutions of Canadian clays, however, important variations of hydraulic conductivity were observed after permeation with brine. They stated that these variations were due to significant changes in the macrostructure level. Mata et al. (2002a) checked out the influence of clay-fluid interaction on micro and macro-structure after four MIP tests performed on bentonite-sand mixtures (70/30

by weight) at different dry specific weights. When soil specimens were hydrated with salt water, intruded volume of mercury in the first mode of pores (macrostructure) in the specimens hydrated with salt water was bigger than volume of mercury intruded in the first mode of pores (macropores) when specimens were hydrated with distilled water. Similar results were obtained after tests in specimens compacted at two dry specific weights. However, Hueckel et al. (1997) developed a theoretical model of hydraulic conductivity, from an idealisation of the fine fraction as a two-dimensional organised periodic structure of solid particles, which is mainly controlled by the size of the smaller channels connected in series with the larger channels. They correlated the measured intrinsic permeability in flow tests, performed in specimens permeated with organic fluids as ethanol and dioxane, to measured changes in pore size distributions. Finally, concluded that the increase of intrinsic permeability observed after permeation with those organic fluids could not be explained by changes in the pore size distribution and intrinsic permeability was mainly controlled by the size of micropores connecting macropores.

As it can be observed, factors that control permeability of clays are not clear yet and important and big discussions arise from the interpretation of different experimental data available in the literature. Consequently, in the past two decades, several mathematical models of the hydraulic conductivity were proposed taking into account the pore fluid chemistry and the interactions in the soil-fluid system as a next step. The variety, origin, hypotheses and mechanisms are indeed wide and only few of them will be revised here. Experimental investigation of hydraulic conductivity variation with pore fluid chemistry is more advanced than conceptual understanding of all the phenomena involved in such a problem. Nevertheless, conceptual understanding of all the phenomena occurring at the micro and macrostructural levels is difficult due to the obvious "deficiencies" of the traditional experimental work performed in soil mechanics. Sophisticated techniques as MIP, scanning electron microscope (SEM) are necessary to overcome the problem of scale when studying the micro and macrostructural behaviour of active clays. Nevertheless, once more, deducing macroscopic patterns from microstructure behaviour is also complicated.

- Russo & Bresler (1977)

They modelled the effect of electrolyte concentration and Na/Ca ratio on the unsaturated hydraulic conductivity of a mixed sodium-calcium soil system. When an active clay (mostly smectites) swells due to hydration, a decrease in the pore diameter is measured and therefore, a subsequent reduction in hydraulic conductivity is observed. Their model estimates the unsaturated hydraulic conductivity by calculating the effective porosity in a homogeneous and isotropic porous medium with uniform porosity by means of the diffuse double layer theory. Each elementary volume of the soil (V) is subdivided into l equal subvolumes (v_i). The number of platelets in a mixed Na-Ca system at the same fluid pressure is calculated as a function of the exchangeable sodium percentage (ESP) as

$$N_i = \begin{cases} N_i^{Ca} & for\ 0 \le ESP < ESP^1 \\ N_i^{Ca} - \Delta N_i & for\ ESP^1 \le ESP < ESP^2 \\ N_i^{Na} & for\ ESP \ge ESP^2 \end{cases} \quad (1)$$

where N_i^{Ca} is the number or clay platelets per particle of Ca-saturated montmorillonite and depends on fluid pressure. ESP^l is the critical value above which the number of platelets in a

particle decreases, ESP^2 is the value at which there is only a single platelet in a particle, ΔN_i is the number of clay platelets which are broken off the Ca-montmorillonite particle and N_i^{Na} is the number of platelets per particle of Na-saturated montmorillonite. The volume of water retained in the clay fraction by unit of soil, u_i, can be estimated by means of the diffuse double layer theory as

$$u_i = \begin{cases} \left(\frac{S}{2N_i^{Ca}}\right)\left(2b_i + b_0\left(N_i^{Ca} - 1\right)\right)\rho_b \\ \left(\frac{S}{2N_i^{Ca}}\right)\left(2b_i + b_0\left(N_i - 1\right) - 2b_i\Delta N_i\right)\rho_b \end{cases} \quad (2)$$

where S is the specific surface of the soil, b_0 is the thickness of the water film between two adjacent clay platelets within a clay particle, b_i is the half distance between two adjacent clay particles and ρ_b is the bulk density of the soil. In a confined volume (V) using equation (2), the pore space (H_i) in which water flow takes place is computed and from this value, the effective porosity (n_i) is calculated. Finally, hydraulic conductivity is estimated depending on the volumetric water content, θ, concentration of the solution, C, and composition of the equilibrium soil solution $\left(R = [Na][Ca]^{-0.5} \text{ in } (\text{meq/L})^{0.5}\right)$ by means of Marshall's equation (Marshall, 1958).

$$k(\theta, C, R) = \left(\frac{n_i}{l - i + 1}\right)^2 \cdot \frac{\rho g}{8\eta} \cdot \sum_{i=1}^{l} (2i - 1)\, a_i^2 \qquad a_i > a_{i+1} \quad (3)$$

Where a_i is the mean equivalent radius of the pores depending on the i subvolume, effective porosity of the subvolume, soil porosity and surface tension of the soil solution and η is the dynamic viscosity of the fluid. The model so defined is little sensitive to the pore size distribution or specific surface of the soil, however, it was checked out that the model was strongly sensitive to the relationship between the number of platelets per clay particle and ESP, which, finally, is depending on soil water pressure, soil solution concentration and composition.

The model introduced some important features as the unsaturated soil behaviour, the effect of the change of the concentration in the soil-water system and the study of the Na-Ca system in an integrated manner. However, it has some problems related to the use of the diffuse double layer theory. Therefore, it is only valid for very dilute solutions and colloidal systems, and some parameters of the model are very difficult to estimate as, for example, b_0. Furthermore, the model does not take into account other different reactions as dissolution or precipitation of chemical species that can change the flow paths and the "immobile" water content altering the hydraulic conductivity. The model also assumes a reversible behaviour of the hydraulic properties of the soil, and this is not likely as Di Maio (1996) stated depending on the substituted cation or cycles of exposure to different solutions after performing oedometer tests in Ponza bentonite by changing the solution in contact with the soil specimens.

- Mehnert & Jennings (1985).

They presented one of the very first works where intrinsic permeability was updated depending on total salt concentration in the liquid phase following a mathematical expression while studying salt intrusion episodes in saturated coastal aquifers. Three different intrinsic permeability functions were implemented and compared in a finite element code that solves the solute mass balance on salt concentration in the mobile and immobile fluid phase. In this study, they pointed out the importance of the intrinsic permeability, k_0, variation due to change in pore fluid chemistry, C_m. The three laws implemented were

$$k_0^1(C_m) = k_0^* + \left(k_s - k_0^*\right)\frac{C_m}{C_s}$$

$$k_0^2(C_m) = \begin{cases} k_0^* & C_m < C_t \\ k_0^* + \left(k_s - k_0^*\right)\left(\dfrac{C_m - C_t}{C_s - C_t}\right) & C_m > C_t \end{cases} \qquad (4)$$

$$k_0^3(C_m) = \begin{cases} k_0^* & C_m < C_t \\ k_s & C_m > C_t \end{cases}$$

where C_s is the source strength concentration of salt on the seaward domain boundary, C_t is the threshold concentration at which permeability changes may be detected, k_s is the domain permeability measured for C_s, and k_0^* is the intrinsic permeability measured when C_m = 0. Figure 5.1 shows the shape of these three intrinsic permeability functions and the meaning of the symbols. Nevertheless, it was not the intention of the authors to present proper permeability functions, but only to compare and study the variation of the solution when variations of hydraulic conductivity depending on pore fluid chemistry were considered. This formulation is, as a main advantage, very easy to implement and experimental information can be provided to simulate the soil behaviour. However, the model is not able to distinguish among the effects that different reactions can have on the hydraulic conductivity. Effects on hydraulic conductivity due to ion exchange reactions can be different from the effects due to dissolution/precipitation of minerals, for example, depending on the soil mineralogical composition, concentration, charge of exchanging cations, temperature, etc. It also predicts a reversible behaviour of the hydraulic conductivity when pore fluid concentration changes.

- Suarez & Šimůnek (1997)

They studied the water movement and the ion chemistry in soils that contain $CaCO_3$ in arid and semiarid regions by means of a new finite element code to study the chemo-hydraulic behaviour of porous media. The main reactions considered in the original model were carbonate-solution and ion exchange. They considered that soil hydraulic conductivity decreased because of pore fluid chemistry changes and proposed a model to take into account the effect of pH and presence of considerable amount of exchangeable sodium as, for example, in sodium bentonites. Therefore, they presented a phenomenological model to take into account both effects on the variation of the hydraulic conductivity. It was proposed an expression of the unsaturated hydraulic conductivity as

$$k = rk_s k_{r\ell} \qquad (5)$$

where k_s is the saturated hydraulic conductivity, $k_{r\ell}$ is the liquid phase relative permeability law and r is the reduction function, calculated as $r = r_1 \cdot r_2$, where r_1 is the reduction due to low salinity and high exchangeable sodium fractions in the clay and r_2 is the reduction due to the effect of pH. The r_1 term is given by

$$r_1 = 1 - \frac{cx^n}{1 + cx^n} \tag{6}$$

where c and n are empirical factors and x depends on the mass fraction of montmorillonite in the soil, the interlayer spacing and the exchangeable sodium percentage in the soil. Finally, the reduction factor r_2 is calculated from experimental results as

$$r_2 = \begin{cases} 1 & pH < 6.83 \\ 3.46 - 0.36 \cdot pH & 6.83 \le pH \le 9.3 \\ 0.1 & pH > 9.3 \end{cases} \tag{7}$$

The model is simple to implement in a finite element code and all the variables can be easily computed during the calculations of the reactive transport problem. The main problem of this model is, doubtless, its lack of generality since it is extremely difficult to introduce the effects of different chemical reactions in a complex geochemical problem on hydraulic conductivity.

- Hueckel et al. (1997)

In this work, the authors presented different geometrical models using a two-dimensional organised periodic structure of solid particles. One of the mechanisms presented to explain the evolution of permeability due to interaction between liquid organic chemicals and clays was flocculation. This mechanism was observed in clay suspensions (van Olphen, 1963). They considered that this mechanism is found in all kind of clays that exhibit a variation of permeability when permeated with organic chemicals. The model is able to reproduce the increase of permeability in clayey soils in such conditions without changing the pore size distribution. In compacted soils it is assumed that the attraction forces (such as Van der Waals and Coulomb forces) affect the particles and clusters only in its vicinity, resulting in a slight body rotation as shown in figure 5.2a. This body rotation creates diverging and converging pores. Flow in this new channel network was studied by means of an approximated solution for a perfectly radial, incompressible and at a low ratio of inertial to viscous stresses flow (figure 5.2b). After several hypothesis and calculations and assuming that the angle of rotation between clusters is smaller than 18º, an expression of the intrinsic permeability was provided as

$$k_0 = \frac{\left(\delta^2\right)^3}{12a} R = \frac{\left(\delta^2\right)^3}{12a} \cdot \frac{8}{\left(\frac{\delta^2}{\delta^1}\right) + \left(\frac{\delta^2}{\delta^1}\right)^2} \tag{8}$$

where R is the microstructure factor of this model, a is the length of a single divergent channel, δ^1 is the size of the entrance of the pore and δ^2 is the size of the exit of the pore. This model was successfully used to estimate the intrinsic permeability of Sarnia clay after experimental tests on specimens permeated with ethanol conducted by Fernandez & Quigley

(1988, 1991). The authors of the model believe that permeability is mainly controlled by change in the size and shape of some of the micropores. Some experimental works did not corroborate this hypothesis, but, at this moment, fully understanding of all the factors affecting the evolution of hydraulic conductivity and its interaction with the soil-fluid system is not available. In any case, the model predicted the increase of permeability without changes in pore size distribution. Finally, as the authors pointed it out, more experimental information provided by indirect methods is needed to support this mechanism. A numerical application of this permeability model was presented by Kaczmarek et al. (1997). They introduced an exponential law between the size of the small channels and the total salts concentration in pore fluid to study in a numerical way the conservative transport. They also introduced the fluid viscosity dependency on total salt concentration in pore fluid.

5.3 FORMULATION OF THE REACTIVE TRANSPORT PROBLEM

A new formulation was used to study backfill hydro-chemical behaviour. This formulation is a fully coupled combination of a pre-existing code (CODE_BRIGHT) to solve non-isothermal multi-phase flow of brine and gas through deformable and unsaturated geological media problems (Olivella et al. 1994 and Olivella et al. 1996) and the reactive transport equations. CODE_BRIGHT is mainly applied to study the behaviour of engineered barriers for nuclear waste in THM problems (Gens et al. 1998; Gens & Olivella, 2000). At this moment, the main application of this new fully THMC formulation is also in this matter (Guimarães et al. 1999; Guimarães et al. 2002), although the code can be used in environmental engineering or petroleum engineering as well (Guimarães, 2002). The formulation considers that geochemical variables, as osmotic suction and concentration of chemical species in the liquid phase and solid phase, can affect the hydro-mechanical behaviour of clayey soils.

Only the hydro-chemical problem was solved during the simulation of the hydration process at the BPTP. Temperature was assumed constant, gas phase was not taken into account and osmotic gradient due to different saltwater concentrations in mixing and hydrating water was not considered in these analyses. The processes considered were:

- Advective flow of water and solutes (Darcy's law).
- Molecular diffusion of solutes (Fick's law).
- Mechanical dispersion of solutes (Fick's law).
- Ion exchange of Na^+ and Ca^{2+}.

The basis of this formulation can be found in (Guimarães, 2002). A brief summary of the chemical fully coupled formulation is described here. In the reactive transport formulation proposed, several dissolved solutes in the liquid phase are transported through a porous medium and react chemically among themselves in the liquid phase (homogeneous reactions) or with other species in the solid phase (heterogeneous reactions). Chemical reactions considered in this formulation include:

- Homogeneous reactions: aqueous complex formation, acid/base and oxidation/reduction.
- Heterogeneous reactions: Dissolution/precipitation of minerals and cation exchange.

Local equilibrium is assumed for all chemical reactions except dissolution/precipitation of minerals where kinetics can also be considered. The development of the reactive transport equations uses a general approach as, for example, Lichtner (1996). From the mass balance equations of every species present in the medium, the final independent transport equations

are obtained using the restrictions arising from the various reversible chemical reactions (local equilibrium hypothesis). Let us consider the reactive transport of N chemical species in a deformable unsaturated porous medium. If N_x is the number of reversible independent reactions in a system containing N species, the number of independent chemical components is $N_c = N - N_x$. It is now possible to classify the system in N_c primary species and N_x secondary species. Reversible reactions between the two types of species can be expressed as

$$A_i = \sum_{j=1}^{N_c} \nu_{ij} A_j \quad (i = 1, ..., N_x) \tag{9}$$

where A_j and A_i are the chemical formulas of the primary and secondary species respectively and ν_{ij} the number of moles of the primary species j in a mol of the secondary species i. The resultant transport equations and the variables used are briefly listed in table 5.1.

In that table, U_j is the total analytical concentration and Ua_j is the total aqueous concentration of the primary species j. C_j and X_i are the concentrations of the primary and secondary species respectively. λ_j and λ_i are the mobilities of the primary and secondary species respectively (1 if the chemical species are in the liquid phase and 0 if the chemical species are in the solid phase). Total analytical concentrations U_j are the unknowns of the transport equations, and Ua_j and R_j are considered non-linear functions of U_j. The link between the unknowns U_j and the dependent variables Ua_j and R_j is the geochemical model described in next section.

This type of unknown exhibits the interesting property of being independent of chemical equilibrium. Regarding the chemical equilibrium, an approach based on the direct minimization of Gibbs free energy to solve the chemical equilibrium is used instead of the mass action law in this new formulation. This approach has a wider application range and it was extended to non-ideal brine systems (Harvie et al. 1987). To compute the concentrations of the species in equilibrium, a Newton-Raphson algorithm is applied to the minimization of Gibbs free energy. Lagrange multipliers are used to incorporate the restrictions of the problem.

Transport Equations	$\frac{\partial}{\partial t}(\phi S_l \rho_l U_j) + \nabla \cdot \left(\rho_l Ua_j \mathbf{q}_l + \mathbf{D}_l \nabla Ua_j + \phi S_l \rho_l U_j \dot{\mathbf{u}} \right) + R_j = 0 \quad (j = 2, ..., N_c)$ $U_j = C_j + \sum_{i=1}^{N_x} \nu_{ij} X_i \quad (i = 2, ..., N_c) \quad Ua_j = \lambda_j C_j + \sum_{i=1}^{N_x} \nu_{ij} \lambda_i X_i \quad (i = 2, ..., N_c)$
THM Variables	ϕ = *porosity* — S_l = *Degree of saturation* ρ_l = *liquid phase density* — $\mathbf{u}$ = *solid phase displacement*
Chemical Variables	U_j = *total analitical concentration* — Ua_j = *total aqueous concentration* R_j = *internal/external supply (precipitation/dissolution of minerals in kinetics)*
Mechanisms of flow of species (liquid phase)	$\mathbf{q}_l$ = *Darcy's law (advective flux)* — $\mathbf{D}_l$ = *Hydrodynamic dispersion tensor (molecular diffusion + mechanical dispersion)*

Table 5.1: Main variables and processes simulated by the implemented THMC formulation (Guimarães, 2002).

5.4 GEOCHEMICAL MODEL SOLVED IN THESE CALCULATIONS

To speed up the backfill saturation, the salinity of the Äspö water was increased adding NaCl and $CaCl_2$ up to 16 g/L of salt concentration (50/50 by mass). Main chemical species in injected water to saturate the backfill are shown in table 5.2. The number of species in a real geochemical problem should be bigger and the necessary geochemical model would be more complex because of all the chemical reactions in the bentonite-fluid system as, for example, dissolution-precipitation of carbonates, chlorides, chalcedony and sulphates, ion exchange reactions among others. As available backfill geochemical information was limited, the geochemical model was simplified to its maximum and only the exchange reaction of Na^+/Ca^{2+} was considered. Table 5.3 shows the assumed geochemical model.

Cl^- (mols/L)	Ca^{2+} (mols/L)	Na^+ (mols/L)	pH
0.2807	0.0720	0.1367	7.3

Table 5.2: Chemical analysis of the injected hydration water in the BPTP (Clay Technology, 1999).

Primary aqueous species	H_2O, Ca^{2+}, Na^+ and Cl^-
Species in the solid phase	NaX and CaX_2
Ion exchange reaction	$2NaX + Ca^{2+} = CaX_2 + 2Na^+$

Table 5.3: Scheme of the solved geochemical model during the simulation of backfill hydration.

5.4.1 *Geochemical initial conditions*

There is not information on the geochemical initial conditions of this material. Therefore, some assumptions and hypothesis were assumed before performing the calculations. The correct determination of the geochemical initial conditions of an active clay-fluid system is very important, although usually very difficult. Initial exchangeable cation contents and solutes in the bentonite are necessary to simulate such geochemical problems. The available experimental techniques to study these conditions are the squeezing technique and aqueous extract tests (Iyer, 1990). Initial backfill pore fluid concentrations were obtained by interpolating experimental data obtained in compacted MX-80 specimens (Muurinen & Lehikoinen, 1998a and 1998b). The authors compacted different MX-80 specimens at different dry specific weights and put them in contact with different volumes of two external solutions, which ionic strengths were also different. After an interaction of about 300 days, some pore fluid of the specimens was squeezed out and chemistry of the external solution was analysed. They defined the bentonite-water ratio (B/W) as the total mass of bentonite divided by the volume of water connected to the specimen. The bentonite-water ratio in the case of the ZEDEX gallery should be zero as backfill is connected to an open system (the Baltic Sea). However, if data with B/W = 0 is used, concentrations in the open system remain constant. This might be the direction to which the process is going. However, in the repository, the surrounding system can be more closed and time dependent while full saturation and chemical equilibrium is reached (Muurinen, 2002).

The lowest B/W = 15 kg/m^3 reported in Muurinen & Lehikoinen (1998b) was used to determine the initial geochemical conditions. Therefore, it was assumed that geochemical initial conditions were in equilibrium, as data coming from the tests by Muurinen &

Lehikoinen was already in equilibrium. Figure 5.3 shows the evolution of concentration of [NaX] and [CaX_2] in meq/100g when the compacted MX-80 specimens were connected to two different salt solutions (0.19 g/L and 23.5 g/L of total dissolved salts). A linear variation of [NaX] and [CaX_2] with the concentration of dissolved total salts in the connected solutions was assumed. The evolution of these two species were reduced to take into account the 30% of mass of bentonite in the backfill, and finally the values at 6 g/L of salts were used as the initial [NaX] and [CaX_2]. Table 5.4 shows the concentrations of the two exchangeable cations (10 and 9 meq/100g respectively). Equation (10) shows the mass action law of the exchange reaction written by following the Gaines-Thomas convention. $K_{Na/Ca}$ is the equilibrium constant of the exchange reaction, $K_{Na/Ca} = 0.4$ (Appelo & Postma, 1993).

$$K_{Na/Ca} = \frac{a_{Na^+} \cdot x_{Ca}^{0.5}}{a_{Ca^{2+}}^{0.5} \cdot x_{Na}} \tag{10}$$

Where x_{Na} and x_{Ca} are the equivalent fractions of the exchangeable cations NaX and CaX_2, and a_{Na^+} and $a_{Ca^{2+}}$ are the chemical activities of the cations in the solution. The equivalent fraction of the exchangeable cation *i* can be calculated using (11) and they are subjected to the following restriction (12). CEC is the cation exchange capacity of the soil.

$$x_i = \frac{\text{concentration of exchangeable cation (meq/100g of solid)}}{\text{CEC (meq/100g of solid)}} \tag{11}$$

$$\sum x_i = 1 \qquad 0 \le x_i \le 1 \tag{12}$$

Chemical activities of the aqueous species were computed by the Harvie & Weare (1980) model, which belongs to the Pitzer family, valid for concentrated saline solutions. The concentrations of the aqueous primary species were calculated by using the amount of exchangeable cations shown in table 5.4 and the initial concentration of chloride was estimated considering the added water during the backfill mixing process with water containing 6 g/L of salt taking into account the bentonite initial water content prior to the mixing (10%). The so-calculated concentration of chloride was 0.0789 mol/kg of liquid phase. The distribution of calcium and sodium was calculated with the code by assuming that the two species were in chemical equilibrium with the calculated chloride concentration.

Exchangeable cations (meq/100g)		Aqueous primary species (mol/kg liquid phase)		
NaX	CaX_2	Na^+	Ca^{2+}	Cl^-
10.0	9.0	0.075	0.002	0.079
$x_{Na} = 0.55$	$x_{Ca} = 0.45$			

Table 5.4: Geochemical initial conditions of backfill used in the computations.

5.5 SUMMARY OF BACKFILL EXPERIMENTAL CHARACTERISATION

Different hydro-mechanical tests were performed on this backfill as it was detailed in chapter 3. Influence of salt concentration on final saturated hydraulic conductivity was studied by using oedometer tests performed in Rowe cells. Salt concentration influence on unsaturated hydraulic conductivity was studied by means of water uptake tests. Backfill matric suction

was obtained by means of filter paper technique and its osmotic suction, due to salt water, was indirectly studied measuring drying and wetting retention curves in a mixture of bentonite and sand, using the vapour transfer technique.

5.5.1 *Intrinsic permeability variation with pore fluid chemistry*

During the saturation phase of backfill specimens in the Rowe's cell compacted at a dry specific weight of 16.6 kN/m^3, some outgoing water was collected and chemically analysed. The results of the chemical analyses are shown in tables 3.11 and 3.12 (chapter 3). From the chemical tests, it was observed that chloride transport was approximately conservative and how important the exchange process between Na^+/Ca^{2+} was. Therefore, sodium bentonite was transforming into a calcium bentonite. After the experimental works by Lehikoinen et al. (1997), Muurinen & Lehikoinen (1998a) and Muurinen & Lehikoinen (1998b) studying the geochemical behaviour of compacted MX-80 sodium bentonite, the measured chemical concentrations in the collected water from the oedometer tests were higher than the real pore fluid ones obtained by squeezing, for instance.

Three values of backfill intrinsic permeability were estimated after oedometer tests at a void ratio of 0.4, 0.54 and 0.6 when salinity of water used to saturate the specimens was changed (tap water, 6 g/L and 16 g/L). Due to low content of bentonite of this mixture, range of salt concentration and scarce geochemical information available, it was assumed that the predominant chemical components in the pore fluid of the mixture came from the injected water. Nowadays, further studies of backfill geochemical initial conditions are being carried out to improve this hypothesis, but in this work, salt concentration in the injected water was used to update the intrinsic permeability due to low bentonite content and range of salt concentrations. Figure 5.4 shows the so-obtained expression that relates the pore fluid chemistry and the hydraulic conductivity. An empirical model of the intrinsic permeability (13) was proposed by introducing a linear dependency of natural logarithm of hydraulic conductivity on void ratio and concentration of chemical species in pore fluid.

$$\ln\left(\frac{k_0}{k_0^*}\right)=\alpha_1\left(e-e_0\right)+\alpha_2\sum_i\left(C^i-C_0^i\right)+\alpha_3 \qquad (13)$$

Where α_1, α_2 and α_3 are the coefficients of the model. They can be calculated from fitting flow tests by means of back-analysis. k_0 is the current intrinsic permeability depending on void ratio and salt concentration in pore fluid, e is the void ratio, e_0 is the initial void ratio, k_0^* is the intrinsic permeability at the initial chemical and mechanical conditions, C^i is molar concentration of the i chemical species in pore fluid (in mol/kg liquid phase) and C_0^i is the initial molar concentration of i chemical species in pore fluid. Figure 5.5 shows the shape of this empirical model. This model was implemented in the finite element code that takes into account the reactive transport of chemical species in a porous medium (Mata et al. 2001).

It was assumed in this chapter that hydraulic conductivity depends only on changes of concentration of salt in pore fluid and degree of saturation ($\alpha_1 = \alpha_3 = 0$) and equation (13) was implemented to compute the advective flow of liquid phase by means of the generalised Darcy's law (Bear, 1972).

$$\boldsymbol{q}_\ell = -\boldsymbol{K}_\ell \left(\nabla p_\ell - \rho_\ell \boldsymbol{g}\right) = -k_0 \frac{k_{r\ell}\gamma_\ell}{\mu_\ell} \boldsymbol{I} \left(\nabla p_\ell - \rho_\ell \boldsymbol{g}\right) = -k_0^* e^{\alpha_2 (C - C_0)} \frac{k_{r\ell}\gamma_\ell}{\mu_\ell} \left(\nabla p_\ell - \rho_\ell \boldsymbol{g}\right) \qquad (14)$$

Where $\boldsymbol{q}_\ell$ is the advective flow of liquid phase, $\boldsymbol{K}_\ell$ the hydraulic conductivity tensor, $\boldsymbol{I}$ the identity tensor. p_ℓ the liquid pressure, $\boldsymbol{g}$ the gravity vector, $k_{r\ell}$ is the liquid phase relative permeability law depending on the effective degree of saturation (S_e), μ_ℓ is the viscosity of the liquid phase, γ_ℓ is the specific weight of the liquid phase, ρ_ℓ is the density of the liquid phase, C is the total molar concentration of salts in the liquid phase, k_0^* is the intrinsic permeability when $C = C_0 = \left[\mathrm{Na}^+\right]_0 + \left[\mathrm{Ca}^{2+}\right]_0 + \left[\mathrm{Cl}^-\right]_0$ from table 5.4, and α_2 is the chemical parameter obtained from the empirical model of intrinsic permeability. As it was previously said the other parameters, α_1 and α_3, were assumed as zero and no mechanical influence was considered on backfill hydraulic conductivity.

The model used to compute the liquid phase relative permeability was proposed after Nielsen et al. (1986) depending on the effective degree of saturation. This model has an experimental parameter, m.

$$k_{r\ell} = \sqrt{S_e} \cdot \left\{1 - \left(1 - S_e^{\frac{1}{m}}\right)^m\right\}^2 \qquad (15)$$

Where S_e is the effective degree of saturation.

5.5.2 *Osmotic suction*.

Osmotic suction was studied by analysing bentonite-sand mixtures, because of the grain size of the backfill. Total suction of specimens of MX-80/sand mixture (30/70 by mass) mixed with water containing 6 g/L of salt and saturated with water containing 16 g/L of salt and compacted at a dry specific weight of 16.6 kN/m^3 was measured by means of psychrometers. Total suction measured at the saturated state was 1.7 MPa (figure 3.43, chapter 3). Since the specimens were already saturated, total suction measured in such conditions was assessed as the osmotic suction of the sodium bentonite – sand mixture and, as an extension, as backfill osmotic suction. The main hypothesis assumed is that osmotic suction was independent of soil structure. However, measured osmotic suction close to saturation in some psychrometers is around 1 MPa (Goudarzi et al. 2002). This value could be unrealistic and low, but also it could be only a measurement of total suction before chemical equilibrium would have been reached.

5.5.3 *Matric suction law*

Clay Technology AB studied the backfill retention curve at different stages of the project. An experimental relationship between backfill matric suction and degree of saturation was provided. The van Genuchten model (16) was used to fit the experimental results.

$$S_e = \frac{S_\ell - S_{r\ell}}{S_{\ell s} - S_{r\ell}} = \left(1 + \left(\frac{p_g - p_\ell}{p_0} \right)^{\frac{1}{1-\lambda}} \right)^{-\lambda} \tag{16}$$

S_ℓ is the degree of saturation of the liquid phase, $S_{r\ell}$ is the residual degree of saturation and $S_{\ell s}$ is the maximum of the degree of saturation, p_g is the gas pressure, p_ℓ is the liquid pressure, and p_0 and λ are the parameters of this model. The objective function was defined by using the Van Genuchten model and the measured data following the same procedure as detailed in chapter 4 in order to back-analyse the parameters of this mathematical model. The minimum of the objective function was determined and the parameters (p_0 and λ) obtained. The best fit of the experimental results was obtained by using the following parameters: p_0 = 0.105 MPa, λ = 0.205. Residual water content was 2% and therefore, the value of the residual degree of saturation, $S_{r\ell}$, was 0.10 and $S_{\ell s}$ = 1. Figure 5.6 shows the objective function and its minimum. The main assumed hypothesis was that backfill void ratio was constant during the experimental determination of the wetting retention curve. This is not true because of the experimental procedure is under free swelling conditions. Figure 5.7 shows the best fit of backfill matric suction by means of the van Genuchten model.

5.5.4 Non-advective transport.

Dispersive and diffusive fluxes were calculated using Fick's law. The non-advective flow of solute *i* in the liquid phase, $\boldsymbol{j}_i$, is expressed as

$$\boldsymbol{j}_i = -\boldsymbol{D}_\ell \nabla C_i = -\left(\phi \rho_\ell S_\ell \tau D_m \boldsymbol{I} + \rho_\ell \boldsymbol{D}_\ell^{'} \right) \nabla C_i \tag{17}$$

where τ is the soil tortuosity, ϕ is the soil porosity, D_m is the molecular diffusion and $\boldsymbol{D}_\ell^{'}$ is the mechanical dispersivity tensor defined by (18) depending on the longitudinal and transverse dispersivities of solutes, d_l and d_t, in the liquid phase respectively.

$$\boldsymbol{D}_\ell^{'} = d_t \left| \boldsymbol{q}_\ell \right| \boldsymbol{I} + \left(d_l - d_t \right) \frac{\boldsymbol{q}_\ell \boldsymbol{q}_\ell^t}{\left| \boldsymbol{q}_\ell \right|} \tag{18}$$

Due to the importance of the non-advective transport of chemical species (controlled by the soil diffusion), some attention was paid to this parameter and its influence on the calculations. Backfill diffusion of ions has not been experimentally determined and it is a challenging task. It is expected that effect of granite is not important at this bentonite content as concluded by Mingarro et al. (1991) in mixtures of an illitic clay and crushed granite and montmorillonite and crushed granite rock.

Miehe et al. (2000) performed gas diffusion tests in mixtures of sand and calcium bentonite (calcigel) varying the sand content and the degree of saturation of the mixture. They proved the importance of the density and above all the effects of the degree of saturation on diffusion of gases. The results by Miehe et al. (2000) are depicted in figure 5.8. The authors varied the sand content, the degree of saturation (saturated and dry) and the bulk density by increasing the compaction pressure. After these tests, it was concluded that diffusion considerably decreased after wetting the mixtures due to a change of structure of the bentonite during the

wetting process with water and because pores were then filled with water and not air as in the dry state. Bentonite or clay content is an important parameter to take into account when studying diffusion, however, from the results by Miehe et al. (2000) when bentonite content was higher than 25%, gas diffusivity was more or less constant. It could be concluded that diffusive behaviour is not dependent on the bentonite content when it is higher than 25 or 30% of the mixture (by weight). This result is supported by the clogging properties of bentonite in mixtures as observed in 20/80 Kunigel sodium bentonite-sand mixtures after MIP tests performed in dry compacted soil specimens and MIP tests in the same specimens after wetting (Romero et al. 2002).

Herein, diffusion of pure MX-80 bentonite was used in the simulations. Two different values of diffusion were used. The first one was obtained by Kim et al. (1993) after NaCl diffusion tests in compacted and saturated specimens of pure MX-80 sodium bentonite. Backfill molecular diffusion chosen after the diffusion tests performed by the authors was of $2 \cdot 10^{-10}$ m^2/s corresponding to diffusion of Cl^- at a bulk density of 11.4 kN/m^3. Figure 5.9 shows the evolution of the chloride diffusion at different bulk densities after Kim et al. (1993). It is clear that the higher the density, the lower the diffusion. The other value was chosen one order of magnitude higher than the measured by Kim et al. (1993) in order to study its influence on the results. This higher value is justified because of measured Na^+ molecular diffusion in compacted specimens of pure MX-80 at a dry specific weight of 17.6 kN/m^3 (Pusch et al. 1989) was $2 \cdot 10^{-10}$ m^2/s, therefore, it is expected that Na^+ diffusion could be higher at lower dry densities.

5.6 NUMERICAL SIMULATION OF A SERIES OF WATER UPTAKE TESTS.

Clay Technology (1999) performed some series of water uptake tests (WUT) at different salt concentrations to study the backfill hydration process and the influence of saltwater content on unsaturated hydraulic conductivity. Dynamically compacted backfill specimens (5 layers) of 10 cm at initial water content from 10% to 13% were saturated at atmospheric pressure with different waters. The initial dry specific weight of these specimens was 17.1 kN/m^3 (void ratio of 0.54). Tests hydrated with 16 g/L saltwater were simulated by UPC in order to estimate the potential coefficient of the liquid phase relative permeability (m, equation 15) and the intrinsic permeability (k_0^*, equation 13).

These water uptake tests were simulated using the hydro-chemical formulation of CODE_BRIGHT with the assumptions above indicated. Two values of the backfill molecular diffusion were used in these simulations $2 \cdot 10^{-10}$ and $2 \cdot 10^{-9}$ m^2/s, backfill tortuosity was 1.0 and longitudinal dispersivity was 0.01 m (10% of the total length of the one-dimensional specimen). Figure 5.10 shows the results after fitting the experimental data from WUT when water with 16 g/L of salt concentration was used to hydrate the soil specimens at atmospheric pressure. The chemical parameter α_2 (= 3.50) was calculated from the exponential relationship of intrinsic permeability after the oedometer tests. The total initial concentration of salts in the liquid phase was 0.1556 mols/kg H_2O. The back-analysed initial intrinsic permeability, k_0^*, necessary to simulate these tests was $3.5 \cdot 10^{-19}$ m^2 and the potential parameter of the liquid phase relative permeability, m, was 0.6. After saturation of backfill, final intrinsic permeability was $6.7 \cdot 10^{-19}$ m^2. This value is slightly lower than the obtained value from the oedometer tests when backfill was hydrated and saturated with saltwater containing 16 g/L ($k_0 = 1.7 \cdot 10^{-18}$ m^2, figure 5.4 for a void ratio of 0.54). Therefore, the

estimated hydraulic conductivity from the oedometer tests was 2.5 times bigger than the estimated one fitting the results of the WUT.

As it was expected, the effect of diffusion on the evolution of hydraulic conductivity has proven to be important in this problem, since the evolution of intrinsic permeability was dependent on the non-advective flow of solutes. In this respect, the correct determination of backfill ion diffusion and longitudinal dispersivity would be important when reactive transport is considered. Figure 5.11 shows the evolution of computed total concentration and figure 5.12 shows the evolution of the intrinsic permeability. Intrinsic permeability reached a maximum close to the water inlet after 3000 hours, decreasing when solutes were transported due chemical gradient in the soil. Calculated time for full specimen saturation was 5000 hours, however, chemical equilibrium was reached after 9000 hours. Figures 5.13 and 5.14 show the calculated time evolution of intrinsic permeability and degree of saturation in different points of the backfill.

When backfill diffusion was increased up to $2 \cdot 10^{-9}$ m^2/s, the results were significantly different. The fit was even much better than the previous results when backfill diffusion of $2 \cdot 10^{-10}$ m^2/s was used. Figure 5.15 shows the evolution of water content. Figures 5.16 and 5.17 show the evolution of intrinsic permeability, which is different from the evolution calculated by using the lower diffusion. When lower diffusion is used, no peak of intrinsic permeability is observed. Figure 5.18 shows the evolution of the degree of saturation. Time of saturation is approximately 6000 hours and chemical equilibrium is reached after 5500 hours. The saturation process is a little bit longer than the one simulated by using the lowest diffusion. Additionally, for the analysis using the lower diffusion, backfill intrinsic permeability showed a peak on its evolution close to the water inlet and then the saturation process was faster (figures 5.13 and 5.14). The peak in the evolution of intrinsic permeability is not observed in figure 5.17 (higher backfill diffusion).

To prevent numerical oscillations in the finite element solution, the local Peclet number should be less than or equal to two (Huyakorn & Pinder, 1983). This number is defined by (19) for the numerical scheme that approaches the problem in a one-dimensional geometry and by using equations (17) and (18).

$$P_e = \frac{|q_\ell|\Delta x}{D_\ell} \leq 2 \rightarrow \Delta x \leq 2\frac{D_\ell}{|q_\ell|} = 2\frac{D_\ell}{k\left|\frac{\partial h}{\partial x}\right|} = 2\frac{\left(\phi\rho_\ell S_\ell \tau D_m + \rho_\ell d_t k\left|\frac{\partial h}{\partial x}\right|\right)}{k\left|\frac{\partial h}{\partial x}\right|} \qquad (19)$$

Where D_ℓ is the effective diffusion in a one-dimensional problem, k is the hydraulic conductivity and h is the total water head. Therefore, the length of the elements was chosen in agreement with this condition. The time-step size was chosen by imposing that the local Courant number is less than or equal to one (Huyakorn & Pinder, 1983). This number is defined by (20) for the numerical scheme.

$$Co = \frac{|q_\ell|\Delta t}{S_\ell R\phi\Delta x} \leq 1 \rightarrow \Delta t \leq \frac{S_\ell R\phi\Delta x}{|q_\ell|} = \frac{S_\ell R\phi\Delta x}{k\left|\frac{\partial h}{\partial x}\right|} \qquad (20)$$

Where Δt is the size of time step, S_ℓ is the degree of saturation, ϕ is the soil porosity and R is a factor that depends on the transport problem and mainly of the chemical reactions considered in the problem (R = 1 if conservative transport is solved and R is bigger than one when reactive transport is solved).

5.7 NUMERICAL SIMULATION OF THE BACKFILL SATURATION PROCESS AT ÄHRL

Wescor PST-55 psychrometers are being used to monitor the evolution of backfill total suction in the ZEDEX gallery. Evolution of total suction measured by 6 psychrometers in sections A3 and A4 was simulated. The mats surrounding these two sections are D3, D4 and D5. The history of the evolution of the injected water pressure of all mats is shown in figure 5.19. Injected water pressure at mats was at the beginning of the saturation process lower than 0.1 MPa to prevent backfill hydraulic fracture. Due to headwater loses and different problems related to such an in-situ test, important variations of water pressure at mats were monitored (Goudarzi et al. 2002). Owing to the slow saturation process, water pressure at mats was increased up to 0.5 MPa after some leakages that appeared in the concrete plug were solved.

Figure 5.20 shows the geometry of the two-dimensional problem solved. Only backfill was considered in these two-dimensional calculations. Granite rock and altered granite rock were not considered because of their little influence on the saturation process as it was also checked in the inner part of the backfill. It is necessary to point out that dry specific weight at specimens used to perform the water uptake tests was 17.1 kN/m^3, however, the compaction of backfill in the ZEDEX gallery provided smaller dry specific weights close to 16.6 kN/m^3 or lower (chapter 2, figure 2.12). Thus, it is expected a higher backfill intrinsic permeability to simulate the saturation process than intrinsic permeability back-analysed from the water uptake tests ($3.5 \cdot 10^{-19}$ m^2, figures 5.10 and 5.15). Evolution of measured total suction in 6 psychrometers in sections A3 and A4 is shown in figures 5.21 and 5.22. The initial total suction of the backfill is around 2.7 – 3.0 MPa. Close to saturation, total suction provided by Wescor psychrometers could be not realistic if free water has come into the device.

Osmotic flow of water was not considered. The unknowns are the liquid pressure in the nodes (matric suction) and concentrations of chemical species in the nodes. Usually a constant value of the osmotic suction is subtracted to the total suction measurements to compare them with the computed matric suction (Fredlund & Rahardjo, 1993). However, in our case, this is not correct and it is expected that osmotic suction will change due to an increase of salt concentration and evolution of the degree of saturation. From the performed laboratory tests, the osmotic suction at the saturated state was estimated as 1.7 MPa, which it is expected to be a maximum of this variable. Finally, due to the low water potential at initial water content from 11% to 13% (2.5 MPa to 3.0 MPa), the role of a non-constant osmotic suction is important in this problem. At the beginning of the saturation process, osmotic suction is minimum due to the salt water, containing 6 g/L (NaCl and $CaCl_2$ 50/50 by mass), and other salts coming from the bentonite during the mixing process of bentonite and crushed granite rock. After saturation with water containing a higher salt concentration it is expected that osmotic suction reaches a maximum and matric suction a minimum. Figure 5.23 shows the evolution of total, matric and osmotic suction in a representative elementary volume of soil, which is wetted by liquid mass transfer of salt water and soil diffusion is high enough to assure that advective transport of water and non-advective transport of ions have similar times.

Backfill initial matric suction was assumed as 2.3 MPa corresponding to an initial degree of saturation of 50.5% (w = 11%), which is in agreement with values measured by Clay Technology when studying backfill matric suction. Temperature at the ZEDEX gallery is more or less constant to 15ºC (Clay Technology, 2002). This value was used to compute the osmotic suction. Initial osmotic suction is 0.37 MPa computed by using the geochemical initial conditions and temperature in the gallery. Assumed geochemical initial conditions for the two-dimensional simulation were the same as the one-dimensional simulations (table 5.4). Backfill parameters were the same as those obtained after the one-dimensional calibration although mechanical dispersivity was changed for the two-dimensional simulations because of its dependence on the geometry. However, backfill hydraulic conductivity was slightly increased in the two-dimensional simulations in order to account for the lower backfill dry specific weight in situ if compared with dry specific weight measured in the specimens prepared for the water uptake tests. Backfill diffusion was set to $2 \cdot 10^{-10}$ m^2/s and $2 \cdot 10^{-9}$ m^2/s to compare the effects of molecular diffusion on the results. Backfill parameters are summarised in table 5.5. Evolution of injected water pressure at mats D3, D4 and D5 was previously shown in figure 5.19. Water injected contained 16 g/L of salt (table 5.2).

Ion exchange reaction $k_{Na/Ca} = 0.4$	CEC (meq/100g)	20.94
Advective flow	k_0^* (m^2)	$7 \cdot 10^{-19}$
	α_2	3.5
	m	0.6
Non-advective flow	τ	1.0
	D_m (m^2/s)	$2 \cdot 10^{-10}$
		$2 \cdot 10^{-9}$
	$d_l = d_t$ (m)	0.12
Retention curve	p_0 (MPa)	0.105
	λ	0.205
	S_{rl}	0.10
	S_{ls}	1.00

Table 5.5: Backfill parameters used in the two-dimensional simulations. Backfill parameters used in the 2D simulations were the same as those used in the simulation of the water uptake test with 16 g/L, excepting backfill mechanical dispersivity, due to its dependency on the geometry, and k_0^* because of the reduction of average dry specific weight at the backfill compacted in situ at the ZEDEX gallery.

Matric suction was calculated by the code and osmotic suction was calculated by means of Van't Hoff equation (21) by using total concentrations of salts in the nodes computed by the code.

$$\pi = RT\sum_i C_i \rightarrow \psi_t = RT\sum_i C_i \left(CODE\_BRIGHT\right) + \psi_m \left(CODE\_BRIGHT\right) \qquad (21)$$

Figures 5.24 and 5.25 show the comparison between total suction measured at the six psychrometers and total suction calculated for the higher backfill molecular diffusion ($2 \cdot 10^{-10}$ m^2/s). Figures 5.26 and 5.27 show the same comparison when backfill molecular diffusion was $2 \cdot 10^{-9}$ m^2/s. Agreement between calculated and measured values is good in both cases.

Nevertheless, when backfill diffusion was higher the comparison showed better results. Only backfill molecular diffusion was different in both cases.

Both sections are fully saturated after 1530 days from the beginning of the saturation process for the low molecular diffusion and after 1570 days when using the high backfill molecular diffusion. Initial equivalent fractions of NaX and CaX_2 are 0.55 and 0.45 as it was shown in table 5.4. Figures 5.28 and 5.29 show the evolution of the equivalent fraction of the exchangeable cation NaX defined as equation (11) for both diffusions and figures 5.30 and 5.31 the evolution of the equivalent fraction of the exchangeable cation CaX_2 for both diffusions after 1450 days of the beginning of the saturation process. It can be observed an increase in the adsorbed Ca^{2+} concentration in the solid phase and a reduction of Na^+ in the solid phase (bentonite losses sodium). The sodium bentonite is being transformed into a calcium bentonite due to the exchange of sodium/calcium. This transformation may change the backfill behaviour if a long-term perspective is studied. Figures 5.32 and 5.33 show the molar concentration of Na^+ in the liquid phase for both diffusions. Figures 5.34 and 5.35 show the molar concentration of Ca^{2+} in the liquid phase for both backfill diffusions used in the calculations as well.

Figure 5.36 shows the intrinsic permeability calculated after 1450 days of saturation for the low backfill molecular diffusion and figure 5.37 for the high backfill diffusion. Evolution of this intrinsic permeability presented important variations, pointing out the molecular diffusion influence on reactive transport problem. Figure 5.38 shows the backfill osmotic suction calculated by means of Van't Hoff equation for the low molecular diffusion and figure 5.39 for the high molecular diffusion. The final osmotic suction is a little bit far from the measured values (1.7 MPa, in MX-80/sand mixtures) and far from the value provided by sensor W18 (A4/1/0,0). However, the total suction measured before the psychrometer broke down, around 1.0 MPa, could be not realistic because values provided by this kind of psychrometer are not reliable when free water gets into the sensor and chemical equilibrium might have not been reached at that moment.

These calculations show clearly that non-advective flow is the main mechanism controlling the transport of the chemical species. Two different values of molecular diffusion were used in the calculations to check out its importance. It was proved that if backfill diffusion is low it could happen that backfill is fully saturated, but chemical equilibrium may be still far from being reached. This could introduce a non-homogeneous backfill intrinsic permeability distribution. The non-homogeneous distribution may affect the saturated flow tests that will be performed in 2003 and 2004.

In order to take into account the effects of the host rock, some simulations were performed with granite. Figure 5.40 shows the geometry when host rock was considered. Granite was always saturated and there were two areas: a part where granite was non-altered and another area where granite was fractured and damaged after the blasting (Excavation Disturbed Zone - EDZ). The same backfill parameters were used in these calculations and parameters of granite are shown in table 5.6. Granite was assumed inert in these calculations.

Figures 5.41 and 5.42 show the evolution of total suction in sections A3 and A4 when backfill molecular diffusion was $2 \cdot 10^{-9}$ m^2/s and the host rock was considered. The results are very similar, what means that far away from the contact between the backfill and the rock, there is no influence on the flow; however, results close to the border are different if host rock is considered. Finally, granite was removed from the calculations because backfill long-term behaviour was the main purpose of the numerical analysis. By doing so, numerical

effectiveness of the calculations was improved, and lower convergence problems appeared. Moreover, a smaller mesh could be used and CPU time required for the calculations was optimised.

		GRANITE	ALTERED GRANITE	BACKFILL
Ion exchange reaction $k_{Na/Ca} = 0.4$	CEC (meq/100g)	0.0	0.0	20.94
Advective flow	k_0^* (m^2)	$1 \cdot 10^{-17}$	$1 \cdot 10^{-16}$	$7 \cdot 10^{-19}$
	α_2	0.0	0.0	3.5
	m	0.6	0.6	0.6
Non-advective flow	τ	1.0	1.0	1.0
	D_m (m^2/s)	$2.5 \cdot 10^{-10}$	$2.5 \cdot 10^{-9}$	$2 \cdot 10^{-9}$
	$d_l = d_t$ (m)	0.120	0.120	0.120
Retention curve	p_0 (MPa)	100.0	100.0	0.105
	λ	0.195	0.195	0.205
	S_{rl}	0.100	0.100	0.101
	S_{ls}	1.000	1.000	1.000

Table 5.6: Material properties used in the two-dimensional simulations when host rock was considered. Granite intrinsic permeability was obtained after Stenberg & Gunnarsson (1998).

5.8 SATURATED FLOW TESTS AT THE ZEDEX GALLERY

In order to check the effects of a non-homogeneous distribution of the intrinsic permeability, owing to its variation with total salt concentration in pore fluid a saturated flow test was simulated in agreement with the expected protocol of flow tests that will be carried out in the ZEDEX gallery throughout 2003 and 2004.

Clay Technology AB is planning to decrease the salinity of the injected water up to 12 g/L after full saturation of the backfill at the ZEDEX gallery. This value is supposed to be the salinity of the surrounding aquifer at Äspö, however, water salinity depends on the fracture water is collected from and the time water has been stored in that fracture.

In the simulations, salinity of injected water pressure was reduced from 16 g/L to 12 g/L and injected water pressure at mat D4 was reduced from 0.4 MPa to 0.1 MPa and water pressure at mats D3 and D5 was kept constant (figure 5.19). It is important to note that the final protocol of global flow tests has not been defined yet. As it was expected, computed backfill hydraulic conductivity decreased because of the reduction of salt concentration in pore fluid. Evolution of total collected flow of rate at mat D4 is depicted in figure 5.43. It was considered that the beginning of the saturated global flow tests was after 1485 days of the beginning of the backfill saturation process (water pressure at mat D4 is reduced). It is clear that evolution of the collected flow rate of water at mat D4 is not strongly dependent on the molecular diffusion. This is because of the similarity of calculated equivalent intrinsic permeabilities with both molecular diffusions as it is shown in figure 5.44.

Evolution of osmotic suction, calculated by means of Van't Hoff equation, is shown in figure 5.45. Equivalent fraction of the exchangeable cation NaX is depicted in figure 5.46 and equivalent fraction of exchangeable cation CaX_2 evolution is shown in figure 5.47. From these figures, it can be seen that the model predicts the transformation of the sodium bentonite into a calcium bentonite. The transformation process is very slow and strongly dependent on molecular diffusion. It was also checked out that salinity in injected water controls the pore fluid chemistry at long term. Figures 5.48, 5.49 and 5.50 show the evolution of ions Na^+, Ca^{2+} and Cl^- in pore fluid.

It is possible to calculate an equivalent global intrinsic permeability from the total flow rate of water collected at mat D4 (figure 5.43) at, for instance, 333 years after the beginning of the saturation process for both molecular diffusions. If gravity is disregarded in those calculations and two-dimensional effects are not considered, the flow of rate divided by two will be the approximate flow rate of water coming from one of the sections.

$$\left.\frac{Q}{2}\right|_{A4}^{low\ diff} \simeq S\cdot k_0^{eq}\,\frac{\gamma_\ell}{\mu_\ell}\cdot\nabla h\big|_{A4} \rightarrow k_0^{eq}\big|_{A4}^{low\ diff} = \frac{2.96\cdot10^{-9}\ m^3/s}{7.8\,m^2\cdot8.23\cdot10^6\,m^{-1}s^{-1}\cdot33.2} = 1.39\cdot10^{-18}\ m^2$$
$$\left.\frac{Q}{2}\right|_{A4}^{high\ diff} \simeq S\cdot k_0^{eq}\,\frac{\gamma_\ell}{\mu_\ell}\cdot\nabla h\big|_{A4} \rightarrow k_0^{eq}\big|_{A4}^{high\ diff} = \frac{2.93\cdot10^{-9}\ m^3/s}{7.8\,m^2\cdot8.23\cdot10^6\,m^{-1}s^{-1}\cdot33.2} = 1.37\cdot10^{-18}\ m^2 \quad (22)$$

Where S is the total surface of the mats (7.8 m^2), μ_ℓ is the liquid dynamic viscosity, γ_ℓ is the liquid specific weight and ∇h is the total head gradient (33.2). The ratio between the specific weight and the viscosity was assumed as $8.23\cdot10^6$ $m^{-1}s^{-1}$ corresponding to viscosity of pure water at 15ºC and liquid density of an aqueous solution 2% of mass of NaCl (Lide & Frederikse, 1997). Both equivalent permeabilities are similar as it was expected from the evolution of the collected flow of rate at mat D4 for both backfill molecular diffusions.

It is possible to estimate an equivalent intrinsic permeability if water perpendicularly flows in 1D conditions across N layers of soil (equation 23). Each layer of soil has its own intrinsic permeability, k_0^i, and its thickness, l_i.

$$k_0^{eq} = \frac{\sum_{i=1}^{N} l_i}{\sum_{i=1}^{N} \frac{l_i}{k_0^i}} \quad (23)$$

If equivalent intrinsic permeability is calculated using equation (23) from figure 5.43, the value obtained is a little bit higher (around $1.5\cdot10^{-18}$ m^2 for both backfill molecular diffusions) than the value estimated from the total flow rate of water collected at mat D4. The estimated equivalent intrinsic permeabilities are a little bit lower than those could be calculated by using the evolution of intrinsic permeability in line AB-BC depicted in figure 5.43. Section AB-BC is more pervious than other parts, close to the top and bottom of the considered geometry, where two-dimensional effects are much more important.

Finally, estimated backfill intrinsic permeability is low enough to assure the functionality of the barrier. It is not expected an important influence of the non-homogeneous distribution of intrinsic permeability on the saturated flow tests because of the low bentonite content and the

salinity of water used to saturate the backfill in the ZEDEX gallery. However, influence of different backfill permeability in the ground or in the roof on the global flow tests will be much more significant as it was checked out after performing some pulse tests in section A4 (chapter 4).

5.9 "DISTURBING" FLOW EFFECTS AT THE ZEDEX GALLERY

Because of the variation of dry specific weight of backfill after compaction it is expected an important variation of hydraulic conductivity depending on this parameter. Some hydraulic conceptual models accounting for the variation of dry specific weight were simulated, however, this information has not been added in this thesis. In addition to the heterogeneity of backfill permeability after compaction, some "disturbing" effects may affect the flow in situ. These factors are briefly summarised below.

Backfill and host rock were assumed isotropic and homogeneous materials in the numerical simulations. However, this approach could not be so realistic. It is well known that main flow in crystalline rocks, as granite in the Fennoscandian shield, is through fractures. Moreover, after the excavation of the ZEDEX drift by means of blasting (even careful blasting), new cracks connecting those fractures were opened close to the gallery (Stenberg & Gunnarsson, 1998).

Figures 5.51 and 5.52 show the water pressure measured in different boreholes drilled in the host rock after the excavation of the ZEDEX gallery. It is clear that, depending on the position and length of the borehole, important variations of measured water pressure are observed, ranging from few kPa up to 3500 kPa. Even, there are some boreholes where water pressure increased as water pressure at mats increased, which means that some fractures and cracks are connected to each other (Goudarzi et al. 2002). For instance, water pressure at borehole named UR103 (A3/R/1.5-2.0) is more or less 125 kPa (figure 5.51). This borehole is placed in section A3, it was drilled in the roof, it is 2.0 meters long, and water pressure is being measured in the section from 1.5 to 2 meters. In parallel with those results, measured water pressure in borehole named UR104 (A3/R/4.0-5.0) is around 3500 kPa. This value is close to the hydrostatic value (≈ 4000 kPa) and it is constant throughout the project. This borehole is also placed at the roof of section A3, it is 5 meters long, and water pressure is being measured in the inner part of the borehole (1 meter of section). Nevertheless, the evolution of the 30/70 or 0/100 backfill pore water pressure in the ZEDEX gallery shows that pore water pressure has not been higher than 500 kPa and it is totally related to the water pressure injected into the mats (Goudarzi et al. 2002). This probably means that some fractures are not directly connected to the backfill and some of them are connected. Therefore, there is an important uncertainty related to the boundary conditions in the host rock and the behaviour of such a medium.

Moreover, fractures may introduce a strong three-dimensional behaviour when simulating flow problems in nature. Figure 5.53 shows the evolution of total suction of two psychrometers placed in section A3 in the third layer. They are placed at the mid horizontal plane of the drift close to the right wall and left wall. Both psychrometers monitored similar evolution of the saturation process. When free water got in the devices they broke down and no sense measurements were recorded. From this figure, it could be assumed that the saturation process is more or less symmetric at the ZEDEX gallery. Nevertheless, figure 5.54 shows the evolution of two different psychrometers also placed in the third layer of section A3 but in the perpendicular direction to those shown in figure 5.53. The psychrometers are

placed at the symmetry vertical plane of the tunnel. It is clear that there is no symmetric behaviour as sensor named W10 (A3/3/0,R-0.5), placed close to the roof, measured a slower saturation process than psychrometer named W12 (A3/3/0,R+0.5), close to the floor of the tunnel. These measurements are compared with the calculations carried out. Figure 5.55 shows the predicted evolution of total suction at these two psychrometers. It is clear that evolution of psychrometer W10 is reproduced but evolution in psychrometer W12 is not correctly simulated. The response of psychrometer W12 means that water is arriving before than expected through a preferential flow path or, most likely, from the host rock in contact with the backfill in the ground (where EDZ is) due to the higher number of fractures after the excavation of the gallery and the contact of the lower mats with the EDZ. Evidences of flow in fracture media are very clear when visiting the ÄHRL. Some pictures of different galleries at the third level (-450 m below the ground surface) are shown in figures 5.56, 5.57 and 5.58. From these figures is clear that water only flows through some fractures and where no fractures are observed or fractures are not connected to those water bearing fractures, granite is dry. In these conditions, it is also difficult to establish correct flow boundary conditions in the granite surrounding the backfill.

From the results of the hydraulic tests performed in chapter 4, it was concluded that backfill does not present anisotropic behaviour at the range of dry specific weight considered (Mata & Ledesma, 2003). It is believed that backfill swelling capacity is big enough to assure an isotropic behaviour at this range of dry specific weights. Backfill swelling capacity may erase the effects of compaction method for the compaction effort considered in this work (Pusch, 1982 and Villar, 2002). However, the effects of compaction on other natural soils may have a significant influence on the permeability measurements (Mitchell, 1993). It could be possible that anisotropy were important at higher degrees of compaction or in non-swelling clays.

The existence of a *significant* osmotic flow could explain the increase and curvature of the evolution of total suction measured by some psychrometers installed in situ (figure 3.11, chapter 3). This flow might introduce a "drying" effect that actually the formulation cannot take into account. Although it has been shown in the literature that this flow can be easily disregarded, the author does not have enough information to conclude that the osmotic flow cannot be of some importance, within the range of salt concentration considered, type of soil, degree of saturation, and porosity in situ. Osmotic flow would produce an extra flow of water from backfill placed at inner parts of a section to backfill close to the mats, where salt concentrations are bigger.

Finally, the existence of preferential flow paths could alter the saturation process. After the compaction process of a layer in the ZEDEX gallery, a flat surface was produced. The contact between each layer could introduce a preferential flow surface as checked by (Mata et al. 2002b) after in situ Lefranc constant and variable head tests in compacted silt by means of a vibratory soil compactor. Figure 5.59 shows the contact between two silt compacted layers. However, this effect was studied numerically by introducing preferential flow paths along the contact of the layers in the simulations by means of joint hydraulic linear elements of constant thickness. It was checked that necessary permeability of these "simulated fractures" in order to reproduce the results measured by the psychrometers was almost three orders of magnitude higher than backfill permeability. Therefore, it is believed that this cannot be a realistic situation due, probably, to the backfill swelling capacity.

The existence of some of these effects cannot be proved before backfill is fully saturated. Moreover, some of them only can be checked if a dismantlement process of the whole project

is carefully planned. However, it is important to note that, though the approach presented in this chapter was successful, those "disturbing" flow effects should not be disregarded.

5.10 CONCLUSIONS

A fully coupled hydro-chemical approach was used to study the current saturation process of a MX-80 sodium bentonite and crushed granite rock mixture (30/70 by mass) compacted in situ at the ZEDEX gallery in the Äspö Hard Rock Laboratory in the Swedish Island of Äspö. The interest of this study was focused on the influence of salt concentration in the water used to saturate the backfill on the hydraulic behaviour of this mixture.

Some oedometer tests were carried out with different salt concentration in the hydration water (0 g/L, 6 g/L and 16 g/L). From these tests an experimental law between the intrinsic permeability and the total concentration of salts in the liquid phase was determined and therefore, an empirical model of intrinsic permeability. This empirical model was implemented in a finite element code to take into account the hydro-chemical coupling observed in different laboratory test results. Moreover, backfill water retention properties and a MX-80 sodium bentonite and sand mixture (30/70 by mass) were experimentally investigated. The influence of the hydration with different concentrations of salt in the water used to saturate the specimens was also considered. Osmotic suction was determined from the drying retention curve in a bentonite-sand mixture mixed and hydrated with salt water. Some water uptake tests performed by Clay Technology were simulated and calibrated by means of this new formulation. Backfill intrinsic permeability and liquid phase relative permeability were then obtained from this calibration process. All this information was then used to reproduce the evolution of the saturation process in the ZEDEX gallery. The evolution of total suction at six psychrometers installed in-situ was successfully reproduced using the formulation. Osmotic suction was calculated by means of Van't Hoff equation. This equation usually provides lower osmotic suction than those measured by means of psychrometric techniques as shown by Mata et al. (2002a). In these calculations, osmotic flow was not computed but it could be introduced as a driving force in the code easily.

The results showed that the hydro-chemical approach was able to explain the variation of the hydraulic behaviour when changes in pore fluid chemistry were considered. The sodium bentonite transformed into a bentonite with higher calcium content in its solid phase. In these conditions of dry specific weight (16.6 kN/m^3), low content of bentonite of the mixture (30% by mass) and the range of salt concentrations considered, the hydraulic conductivity increased more than 6 times as salt concentration in injected water increased up to 16 g/L. It is important to study this kind of problems with this type of formulation when chemical effects are expected to be significant. A complete characterisation of the geochemical initial conditions and the evolution of chemical variables are required in order to improve these computations. Moreover, a more complex geochemical model should be posed and solved to consider the main reactions occurring in this kind of bentonites. The calculations also showed that diffusion is an important parameter to be determined when the hydro-chemical problem is solved. The consistent results obtained in this case confirm the utility of these frameworks when studying coupled hydro-chemical hydration problems. Full backfill saturation at the ZEDEX gallery can be reached at the beginning of 2003, therefore, saturated flow tests will be performed in order to analyse, for instance, backfill permeability, anisotropy, interaction with the host rock or flow in jointed medium.

The performance of a saturated flow test was simulated and no important differences were observed when backfill molecular diffusion was changed. Moreover, a non-homogeneous distribution of the intrinsic permeability was of little importance on the study of the global saturated flow test. This means that saturated flow tests can be carried out and analysed without taking into account the variation of intrinsic permeability due to salt water and error committed should not be important. This is because the coupling between the hydraulic and chemical problems is not very strong in this case since the backfill bentonite content is low and the range of salinity is low.

Some effects can alter the evolution of the saturation process in the ZEDEX gallery. These factors have been pointed out. Some are more important than others, but all of them are difficult to study at this stage of the project and it would be really interesting to consider a plan to dismantle the project in order to investigate the possible existence of these factors.

5.11 REFERENCES

Acar, Y.B. & Olivieri, I. (1989). Pore fluid effects on the fabric and hydraulic conductivity of laboratory-compacted clay. *Transportation Research Record*, **1219**, p. 144-159.

Appelo, C.A.J. & Postma, D. (1993). Geochemistry, groundwater and pollution. Balkema, Rotterdam, The Netherlands.

Arya L.M., Leij F.J., Shouse P.J. & van Genuchten, M.Th. (1999). Relationship between the hydraulic conductivity function and the particle-size distribution. *Soil Sci. Soc. Am. J.*, **63** (5), p.1063-1070.

Barbour, S.L. & Yang, N. (1993). A review of the influence of clay-brine interactions on the geotechnical properties of Ca-montmorillonite clayey soils from Western Canada. *Can. Geotech. J.*, **30**, p. 920-934.

Bear, J (1972). Dynamics of fluids in porous media. Dover Publications, Inc.

Clay Technology (19979 and 2002). Personal communication.

Di Maio, C. (1996). Exposure of bentonite to salt solution: osmotic and mechanical effects. *Géotechnicque*, **46** (4), p. 695-707.

Dixon, D.A., Gray, M.N. & Thomas, A.W. (1984). A study of the compaction properties of potential clay-sand buffer mixtures for use in nuclear fuel waste disposal. *Eng. Geology*, **21**, p. 247-255.

Elzeftawy, A. & Cartwright, K. (1981). Evaluating the saturated and unsaturated hydraulic conductivity of soils. Permeability and Groundwater Contaminant Transport, ASTM STP 746, Zimmie, T.F. & Riggs, C.O. (Eds.), American Society for Testing and Materials, Philadelphia, p. 168-181.

Fernandez, F. & Quigley, R.M. (1988). Viscosity and dielectric constant controls on the hydraulic conductivity of clayey soils permeated with water-soluble organics. *Can. Geotech. J.*, **25**, p. 582-589.

Fernandez, F. & Quigley, R.M. (1991). Controlling the destructive effect of clay-organic liquid interactions by application of effective stresses. *Can. Geotech. J.*, **28**, p. 388-398.

Fredlund, D.G. & Rahardjo, H. (1993). Soil Mechanics for Unsaturated Soils. John Wiley & Sons, Inc. New York.

Fredlund, M.D., Fredlund, D.G. & Wilson, G.W. (1997). Prediction of the soil-water characteristic curve from grain-size distribution and volume-mass properties. In NONSAT'97, *Proc. of the 3rd Brazilian Symposium on Unsaturated Soils, Rio de Janeiro*, Vol **1**, p. 13-23.

Garcia-Bengochea, I. & Lovell, C.W. (1981). Correlative measurements of pore size distribution and permeability in soils. In: Permeability and Groundwater contaminant

transport, ASTM STP 746, Zimmie, T.F. & Riggs, C.O. (Eds.), American Society for Testing and Materials, Philadelphia, p. 137-150.

Gens, A., García-Molina, A. J., Olivella, S., Alonso, E. E., & Huertas, F. (1998). Analysis of a full scale in situ test simulating repository conditions. *Int. J. for Num. and Analyt. Methods in Geomechanics*, **22**, p. 515-548.

Gens, A. & Olivella, S. (2000). Non-isothermal multiphase flow in deformable porous media. Coupled formulation and application to nuclear waste disposal. *In Developments in Theoretical Geomechanics*, Smith & Carter (Eds.), Balkema, Rotterdam, p. 619-640.

Goudarzi, R., Gunnarsson, D., Johannesson, L-E. & Börgesson, L. (2002).Äspö Hard Rock Laboratory. Backfill and Plug Test. Sensors data report (period 990601-020101). Report Nº 4. International Progress Report **IPR-02-10**. SKB, Sweden.

Guimarães, L. (2002). *Análisis multi-componente no isotermo en medio poroso deformable no saturado*. PhD thesis, Universidad Politécnica de Cataluña, Barcelona, Spain. (In Spanish).

Guimarães, L., Gens, A. & Olivella, S. (1999). THM and reactive transport coupling in unsaturated porous media. *Proc. 7th Int. Symp. Oon Numerical Models in Geomech.*, NUMOG VII, p. 303-308.

Guimarães, L., Gens, A., Sánchez, M. & Olivella, S. (2001). A chemo-mechanical model for unsaturated expansive clays. *International Workshop Clay behaviour: Chemo-mechanical coupling*. Di Maio, C., Hueckel, T. and Loret, B. (Eds.), Maratea, Italy.

Guimarães L., Gens, A. & Olivella, S. (2002). Modelling the geochemical behaviour of an unsaturated clay subjected to heating and hydration. *Proc. 3rd Int. Conf. on Unsaturated Soils,*.UNSAT 2002, Jucá, J.F.T., de Campos, T.M.P. & Marinho, F.A.M. (Eds.), Recife, Brazil, Vol. **1**, p. 71-76.

Harvie, C. & Weare, J. (1980). The prediction of mineral solubilities in natural water: the Na-K-Ca-Cl-SO_4-H_20 system to high concentration at 25ºC. *Geochimica et Cosmochimica Acta*, **44**, p. 981-997.

Harvie, C., Greenberg, J. & Weare, J. (1987). A chemical equilibrium algorithm for highly non-ideal multiphase systems: Free Energy minimization. *Geochimica et Cosmochimica Acta*, **51**, p. 1045-1057.

Hueckel, T., Kaczmareck, M. & Caramuscio, P. (1997). Theoretical assessment of fabric and permeability changes in clays affected by organic contaminants. *Can. Geotech. J.*, **34**, p. 588-603.

Hueckel, T., Tao, F., Cassiani, G. & Pellegrino, A. (2001). Chemical softening and hardening of geomaterials in situ. *Computer Methods and Advances on Geomechanics*, (Desai et al., Eds.). Balkema, Rotterdam, **1**, p. 743-748.

Huyakorn, P.S. & Pinder, G.F. (1983). Computational methods in subsurface flow. Academic Press, Inc. New York.

Iyer, B. (1990). Pore fluid extraction-Comparison of saturation extract and high-pressure squeezing. *Physico-Chemical Aspects of Soil and Related Materials. ASTM STP 1095*, K.B. Hoddinott and R.O. Lamb, Eds., American Society for Testing and Materials, Philadelphia, p. 159-170.

Johannesson, L.E., Börgesson, L. & Sandén, T. (1998). Backfill materials based on crushed rock (part 2). Geotechnical properties determined in laboratory. ÄHRL International Progress Report **IPR-99-23**, SKB, Sweden.

Kaczmarek, M., Hueckel, T., Chawla, V. & Imperiali, P. (1997). Transport through a clay barrier with the contaminant concentration dependent permeability. *Transport in Porous Media*, **29** (2), p. 159-178

Kim, H-T, Suk, T-W, Park, S-H & Lee, C-S. (1993). Diffusivities for ions through compacted Na-bentonite with varying dry bulk density. *Waste Management*, **13**, p. 303-308.

Kosugi, K. (1996). Lognormal distribution model for unsaturated soil hydraulic properties. *Water Resources Research*, **32** (12), p. 2697-2703.

Kovács, G. (1981). Seepage Hydraulics. Developments in water science (10). Elsevier Scientific Publishing Company, Amsterdam.

Lapierre, C., Lerouil, S. & Locat, J. (1990). Mercury intrusion and permeability of Louiseville clay. *Can. Geotech. J.*, **27**, p. 761-773.

Lehikoinen, J., Muurinen, A., Melamed, A. & Pitkänen, P. (1997). Determination of porewater chemistry in compacted bentonite. In *Scientiphic Basis for Nuclear Waste Management*, **XX**. Gray, W.J. & Triay, I.R. (Eds.), *Material Research Society*, **465**, p. 1011-1018. Pennsylvania.

Lichtner, P. (1996). Continuum formulation of multicomponent-multiphase reactive transport. *Reviews in Mineralogy*, **34**, p. 1-81.

Lide, D.R. & Frederikse, H.P.R. (1997). CRC Handbook of Chemistry and Physics. A ready-reference book of chemical and physical data. CRC Press, New York.

Marshall, T.J. (1958). A relation between permeability and size distribution of pores. *J. Soil Sci.*, **9**, p. 1-8.

Mata, C., Guimarães, L., Ledesma, A., Gens, A. & Olivella, S. (2001). A hydro-geochemical analysis of the saturation process with salt water of a bentonite crushed granite rock mixture in an engineered nuclear barrier. In *6th Int. Workshop Key Issues on Waste Isolation Research*, p. 643-663, Paris, November, 2001

Mata, C., Romero, E. & Ledesma, A. (2002a). Hydro-chemical effects on water retention in bentonite-sand mixtures. *Proc. 3rd Int. Conf. on Unsaturated Soils,*.UNSAT 2002, Jucá, J.F.T., de Campos, T.M.P. & Marinho, F.A.M. (Eds.), Recife, Brazil, Vol. **1**, p. 283-288.

Mata, C., Alonso, M. & Alonso, E.E. (2002b). Construcción de dos terraplenes de ensayos en la zona de la futura presa de tierras del Albagés (Les Garrigues, Lérida). Project report for REGSA. (In Spanish). Barcelona, Spain.

Mata, C. & Ledesma, A. (2003). Permeability of a bentonite-crushed granite rock using different experimental techniques. (Accepted for publication in *Géotechnique*).

Mehnert, E. & Jennings, A.A. (1985). The effect of salinity-dependent hydraulic conductivity on saltwater intrusion episodes. *J. Hydrol.*, **80**, p. 283-297.

Miehe, R., Jockwer, N., Wieczorek, K. & Rothfuchs, T. (2000). Qualification of clay barriers in underground repository systems. EUROSAFE 2000, Forum for Nuclear Safety, Köln, Germany, 6-7 November 2000.

Mingarro, E., Rivas, P., del Villar, L.P., de la Cruz, B., Gómez, P., Hernández, A., Turrero, M.J., Villar, M.V., Campos, R. & Cozar, J. (1991). Characterization of Clay (Bentonite)/Crushed Granite Mixtures to Build Barriers Against the Migration of Radionuclides: Diffusion Studies and Physical Properties. Technical Report EUR 13666 EN. Luxembourg: Commission of the European Communities.

Mitchell, J.K. (1993). Fundamentals of soil behaviour. 2nd Edition. John Willey & Sons, Inc. NY.

Molenaar, M.M. & Huyghe, J.M. (2001). An electro-chemo-mechanical mixture formulation of shale. *International Workshop Clay behaviour: Chemo-mechanical coupling*. Di Maio, C., Hueckel, T. and Loret, B. (Eds.), Maratea, Italy.

Murad, M. & Cushman, J. (1998). A generalised Biot's model for non-isothermal consolidation of clays incorporating physico-chemical effects. *Poromechanics*, Thimus et al. (Eds.), Balkema, Rotterdam, p. 111-116.

Muurinen, A. (2002). Personal communication.

Muurinen, A. & Lehikoinen, J. (1998a). Pore fluid chemistry in compacted bentonite. In Preprints of Contributions to the Workshop on Microstructural Modelling of Natural and Artificially Prepared Clay Soils with Special Emphasis on the Use of Clays for Waste Isolation, Pusch, R. (Ed.), Lund, Sweden, 12-14 October.

Muurinen, A. & Lehikoinen, J. (1998b). Evolution of the pore fluid chemistry in compacted bentonite. In Scientific Basis for Nuclear Waste Management XXI. Mckinley, I.G. & McCombie, C. (Eds.). *Mat. Res. Soc. Proc.*, p. 415-422. Pennsylvania.

Nielsen, D.R., van Genuchten, M. Th. & Biggar, J.W. (1986). Water flow and solute transport in the unsaturated zone. *Water Res. Res.*, **22** (9), p. 89S-108S.

Olivella, S., Carrera, J., Gens, A., & Alonso, E. E. (1994). Nonisothermal Multiphase Flow of Brine and Gas Through Saline Media. *Transport in Porous Media*, **15**, p. 271-293.

Olivella, S., Gens, A., Carrera, J. & Alonso, E. E. (1996). Numerical formulation for a simulator (CODE_BRIGHT) for the coupled analysis of saline media. *Engineering Computations*, **13**, p. 87-112.

Olsen, H.W. (1962). Hydraulic flow through saturated clay. *Proc. 9th National Conference on Clays and Clay minerals*, p. 131-161.

Pusch, R. (1982). Mineral-water interactions and their influence on the physical behaviour of highly compacted Na bentonite. *Canadian Geotechnical Journal*, **19**, 381-387.

Push, R., Karland, O. & Muurinen, A. (1989). Transport and microstructural phenomena in bentonite clay with respect to the behaviour and influence of Na, Cu and U. Technical Rerport, **TR-89-34**, SKB, Sweden.

Romero, E., Gens, A. & Lloret, A. (1999). Water permeability, water retention and microstructure of unsaturated compacted Boom clay. *Engineering Geology*, **54**, p. 117-127.

Romero, E., Alonso, E.E., García, I. & Knobelsdorf, J. (2002). Microstructural changes affecting air permeability through an unsaturated 80/20 sand-bentonite mixture. In Preprints of Contributions to the Workshop on Microstructural Modelling of Natural and Artificially Prepared Clay Soils with Special Emphasis on the Use of Clays for Waste Isolation, Pusch, R. (Ed.), Lund, Sweden.

Russo, D. & Bresler, E. (1977). Analysis of the saturated-unsaturated hydraulic conductivity in a mixed sodium-calcium soil. *Soil Sci. Soc. Am. J.*, **41**, p. 706-710.

Stenberg, L. & Gunnarsson, D. (1998). Characterisation of the ZEDEX drift in advance of the Backfill and Plug Test. Progress Report **HRL-98-10**. SKB, Sweden.

Suarez, D.L. & Šimůnek, J. (1997). UNSATCHEM: Unsaturated water and solute transport model with equilibrium and kinetic chemistry. *Soil Sci. Soc. Am. J.*, **61**, p. –1633-1646.

Thomas, H.R., Cleall, P.J. & Hashm, A.A. (2001). Thermal-hydraulic-chemical-mechanical (THCM) behaviour of partly saturated soil. *Computer Methods and Advances on Geomechanics*, Desai et al. (Eds.), Balkema, Rotterdam, **1**, p. 743-748.

Tuli, A., Kosugi, K. & Hopmans, J.W. (2001). Simultaneous scaling of soil water retention and unsaturated hydraulic conductivity functions assuming lognormal pore-size distribution. *Adv. Water Resources*, **24**, p. 677-688.

van Olphen, H. (1963). An introduction to clay colloid chemistry. Interscience publishers, John Wiley & Sons. New York.

Villar, M.V. (2002). Thermo-hydro-mechanical characterisation of a bentonite from Cabo de Gata. A study applied to the use of bentonite as sealing material in high radioactive waste repositories. Technical Publication **04/2002**, ENRESA, Madrid.

Watabe, Y., Leroueil, S. & Le Bihan, J.-P. (2000). Influence of compaction conditions on pore-size distribution and saturated hydraulic conductivity of a glacial till. *Can. Geotech. J.*, **37**, p. 1184-1194.

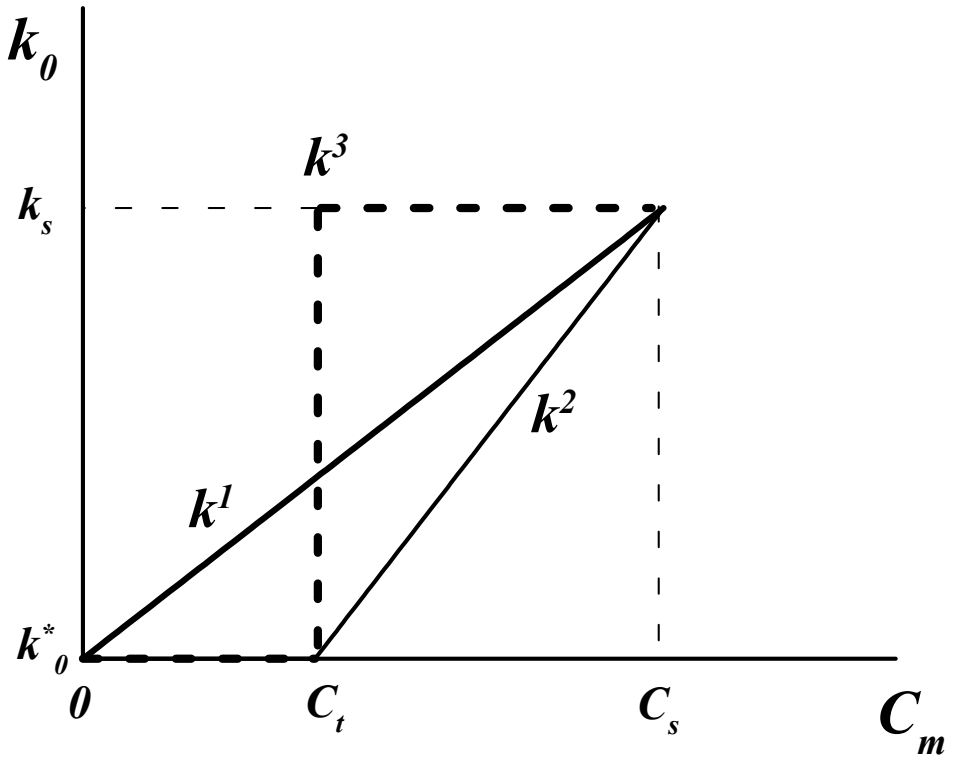

Figure 5.1: Hypothetical models for salinity-dependent intrinsic permeability after Mehnert & Jennings (1985).

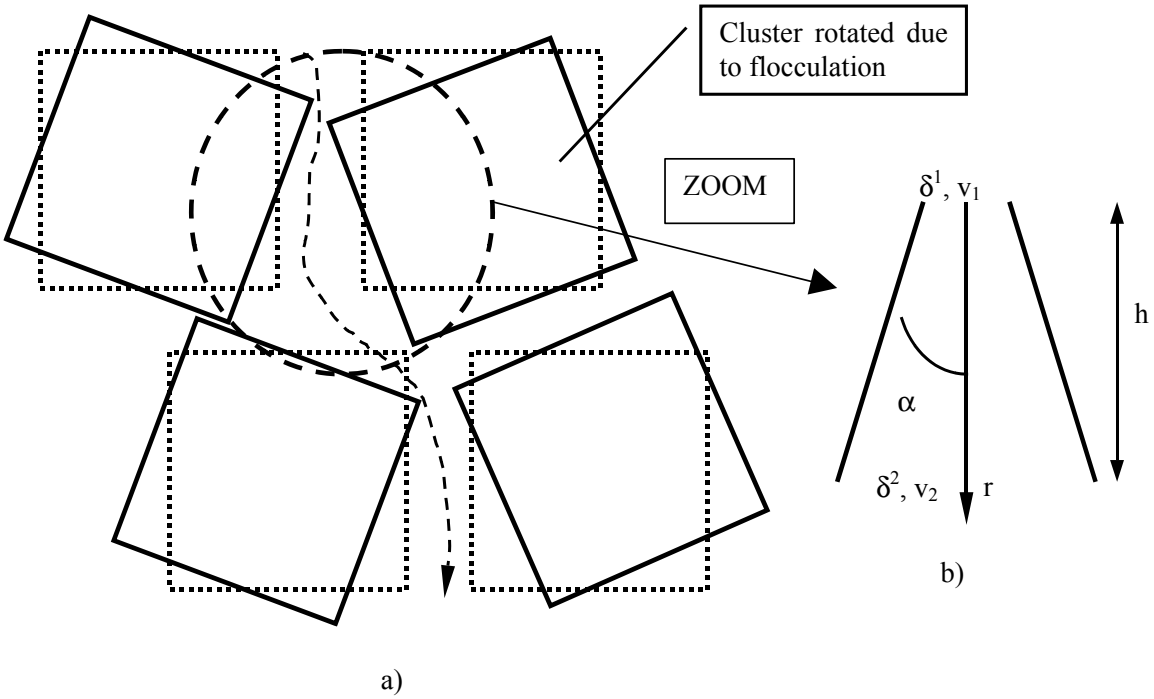

Figure 5.2: a) Flocculation flow model: rotation and deformation of the clusters forming divergent channels. b) Flow through a single divergent channel. (Hueckel et al. 1997).

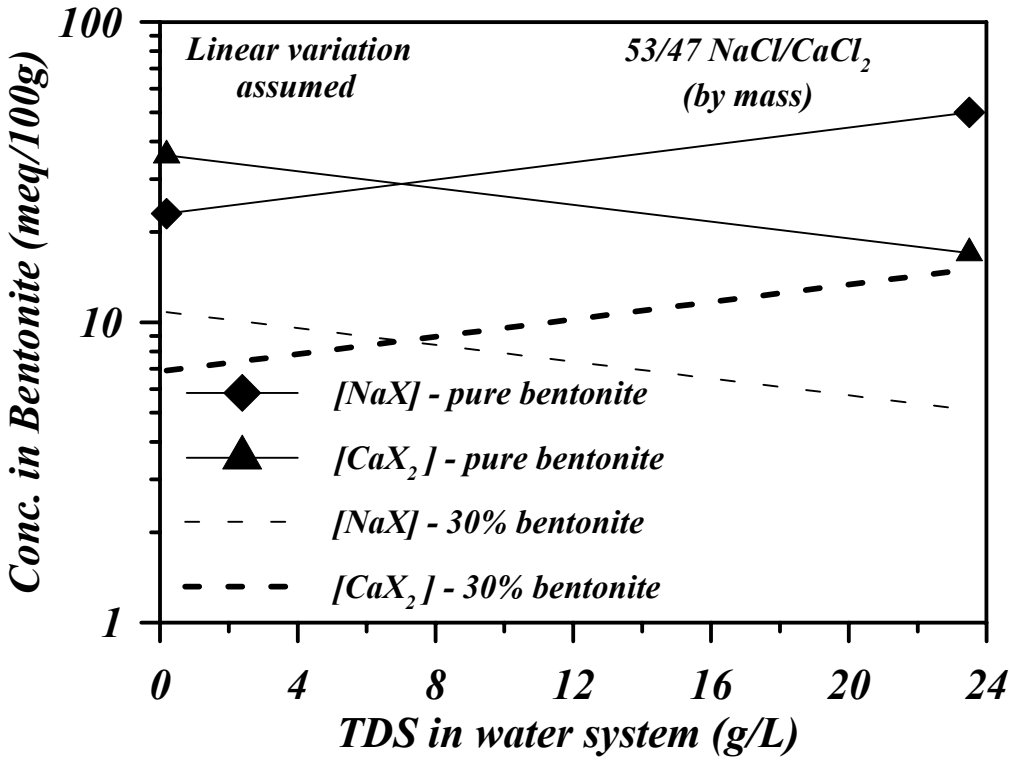

Figure 5.3: Equilibrium concentrations of NaX and CaX_2 in MX-80 bentonite for two total dissolved salt (TDS) concentrations in injected water at a bentonite/water ratio of 15 kg/m^3 (after Muurinen & Lehikoinen, 1998b).

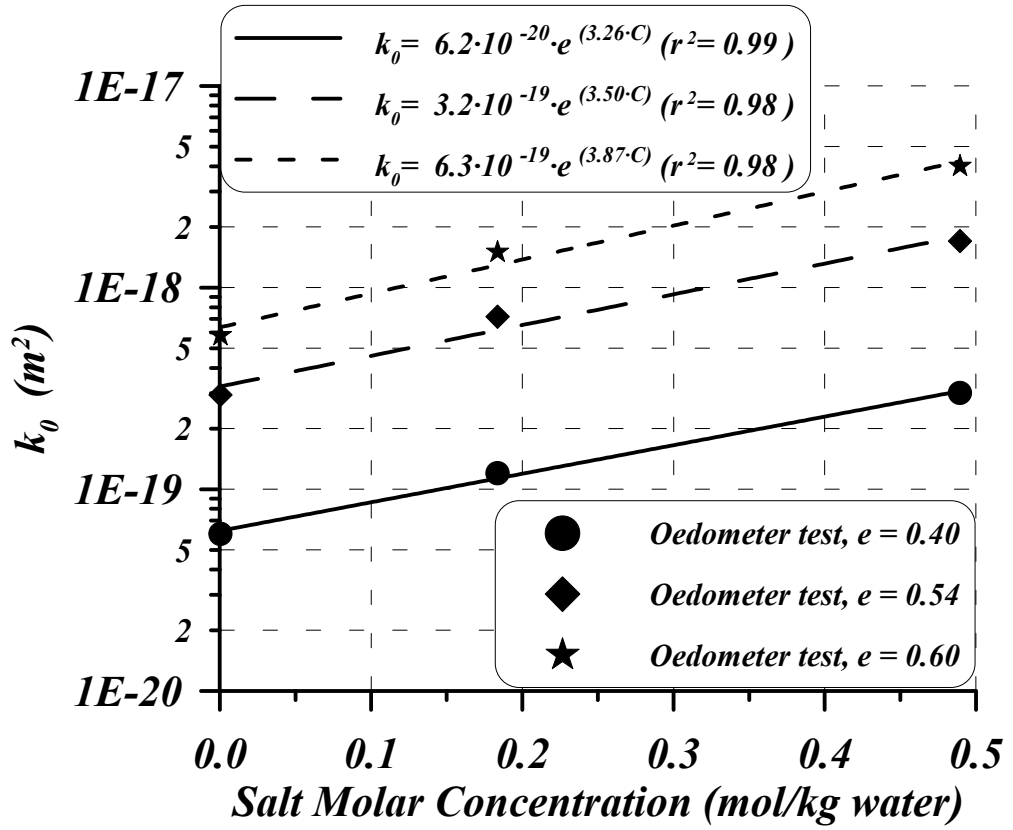

Figure 5.4: Variation of intrinsic permeability with salt concentration in injected water in the three oedometer tests performed on compacted backfill specimens. It was assumed that total salt concentration in injected water was very close or it was representative of the pore fluid concentrations.

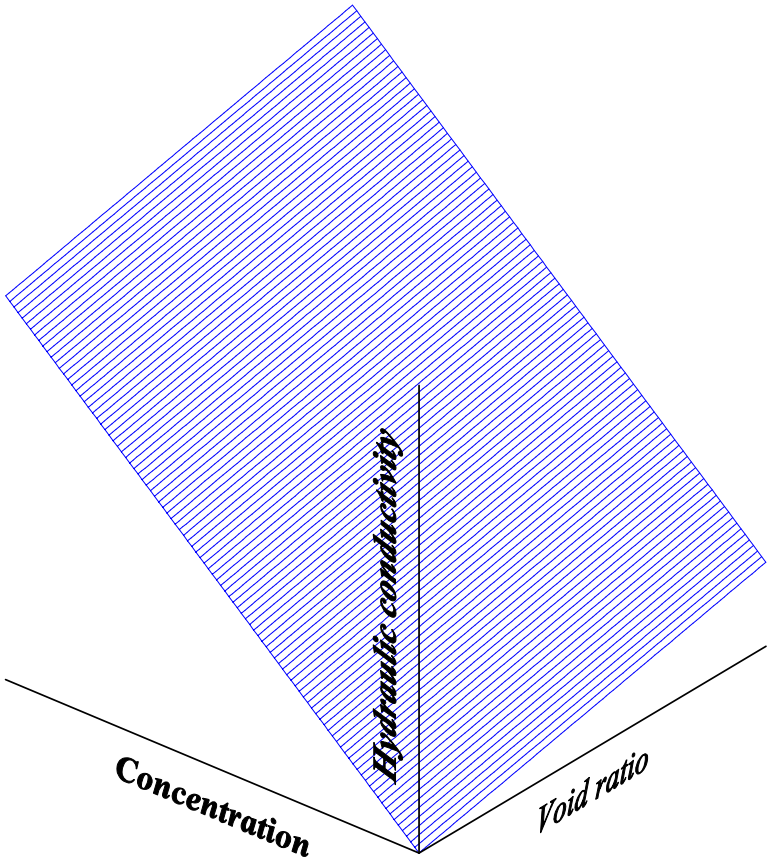

Figure 5.5: Shape of the empirical model for the saturated hydraulic conductivity taking into account the concentration of chemical species in pore fluid and the variation of void ratio. Hydraulic conductivity axis in log scale.

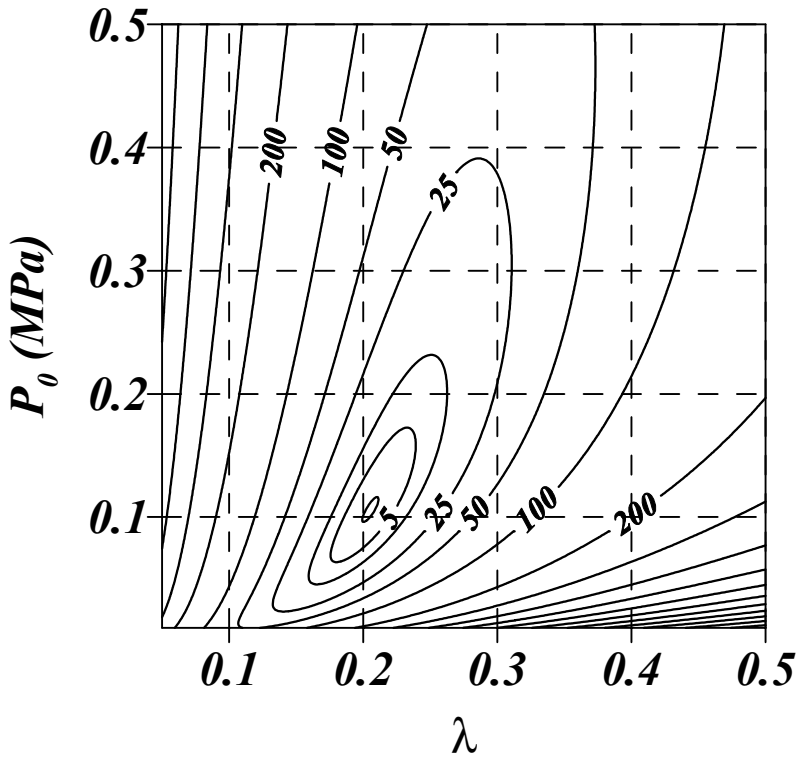

Figure 5.6: Contours map of the objective function of the retention curve assuming the Van Genuchten model. Only two parameters were back-analysed. Values in the contours are in MPa^2.

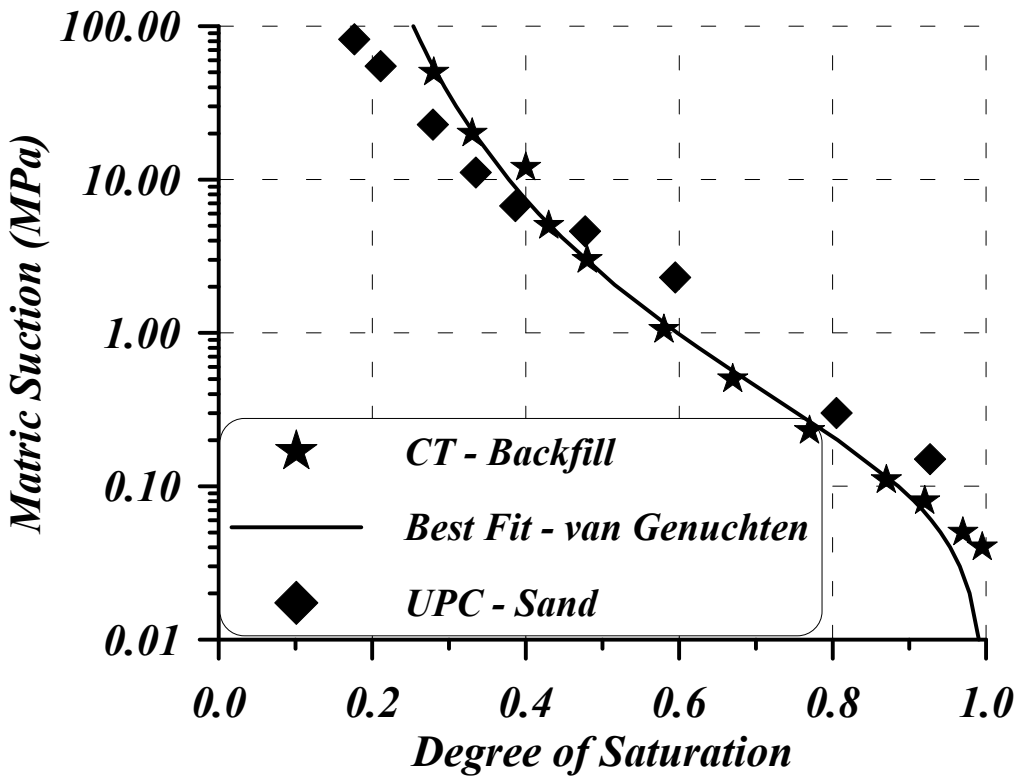

Figure 5.7: Matric suction (wetting path) for the bentonite-sand mixture and its comparison with the matric suction relationship measured by Clay Technology (1997). The fit of this last retention curve was used in the calculations.

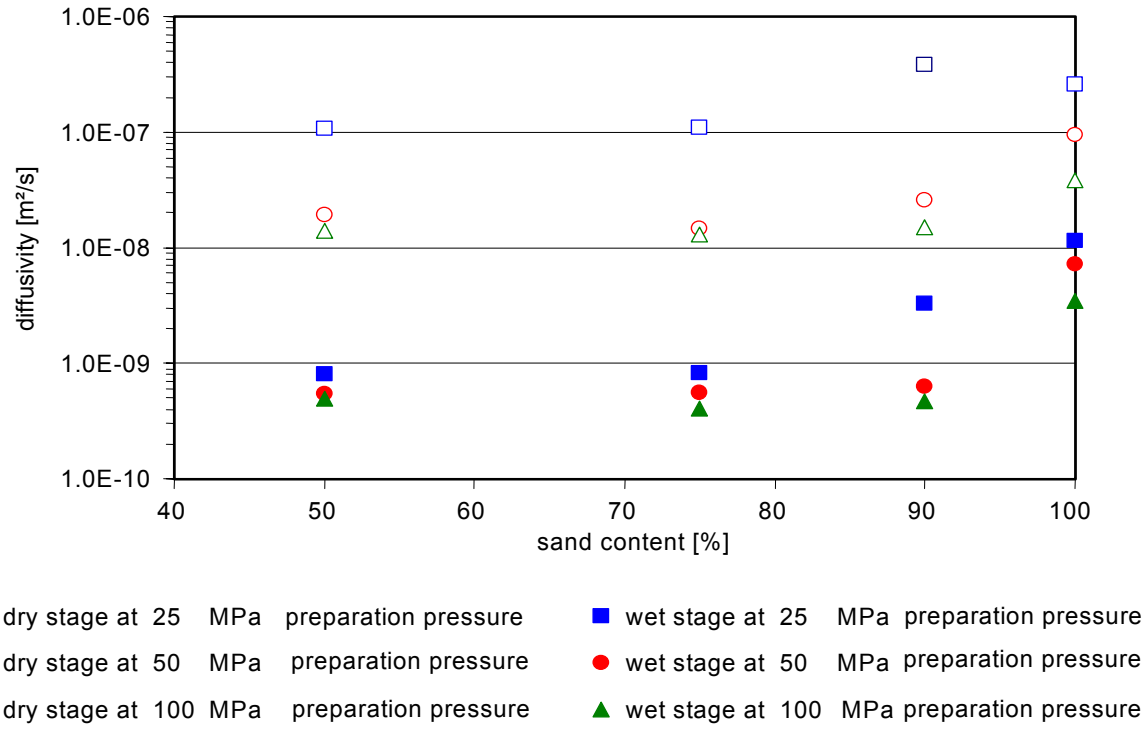

Figure 5.8: Results of different gas diffusion tests on bentonite – sand mixtures at different densities after compaction, dry and wet specimens and varying the sand content of the mixtures (Miehe et al. 2000). The bentonite used in these test is a calcium bentonite (calcigel). Dry specific weights were not provided, only the compaction pressure.

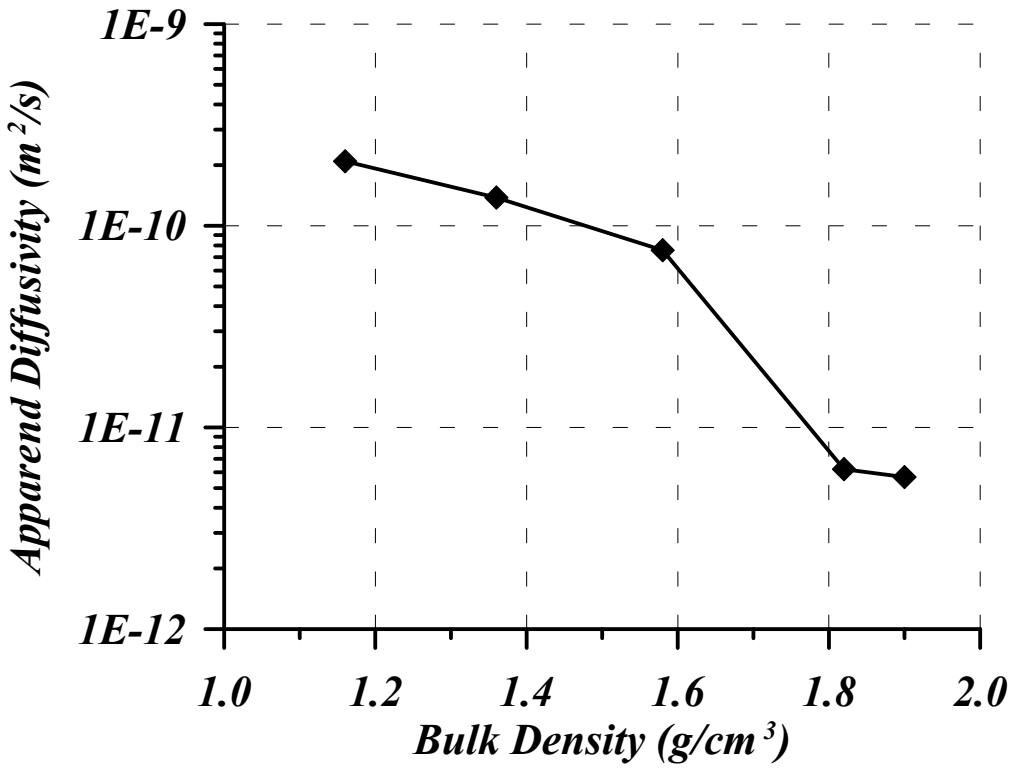

Figure 5.9: Evolution of chloride diffusion estimated after tests performed in compacted specimens of MX-80 sodium bentonite (Kim et al. 1993).

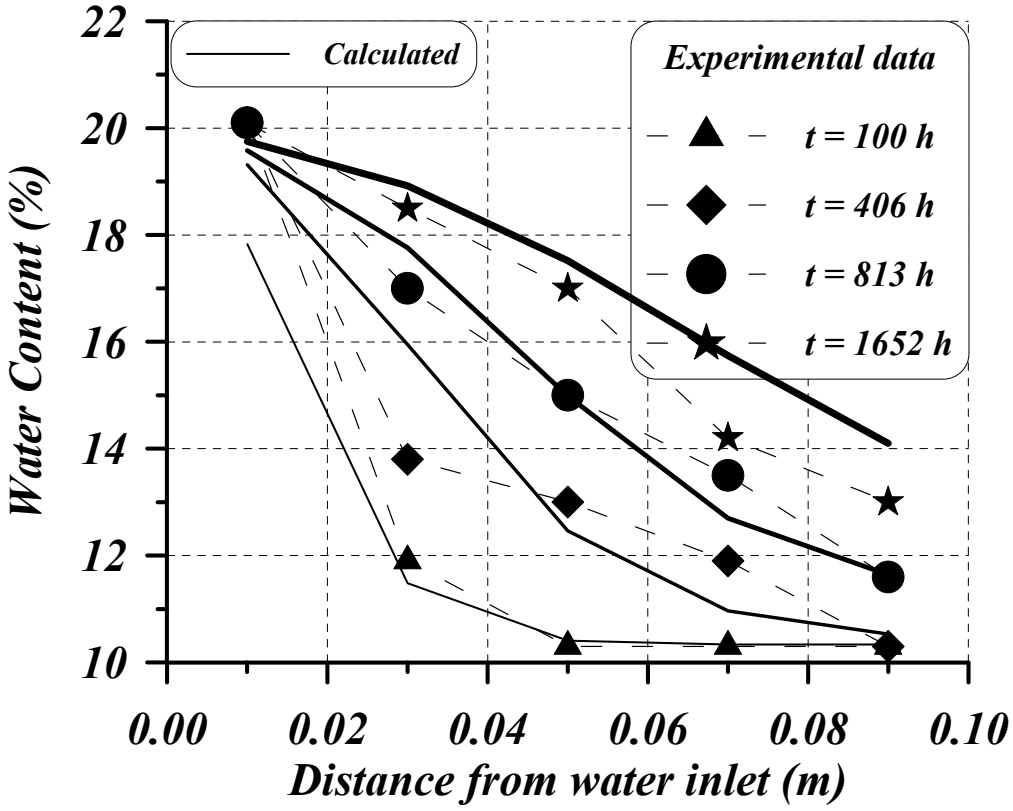

Figure 5.10: Numerical simulation of the water uptake tests performed on the backfill hydrated with saltwater (16 g/L). The diffusion used was $2 \cdot 10^{-10}$ m^2/s.

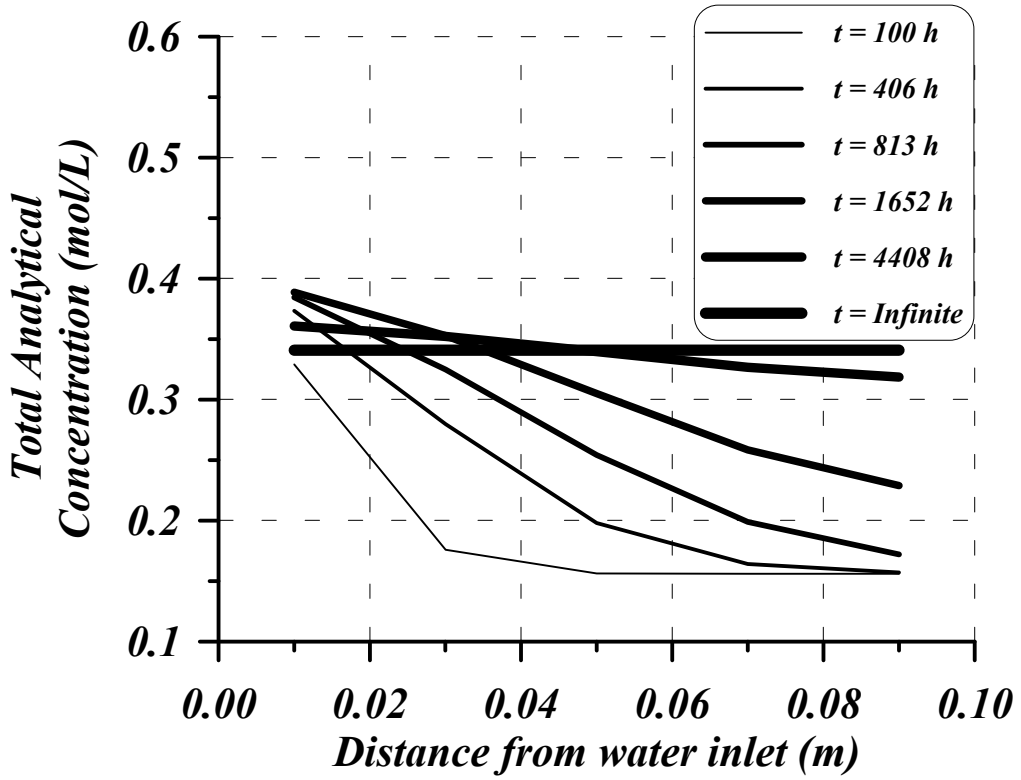

Figure 5.11: Calculated evolution of the total analytical concentration of salt in the pore water during the saturation process.

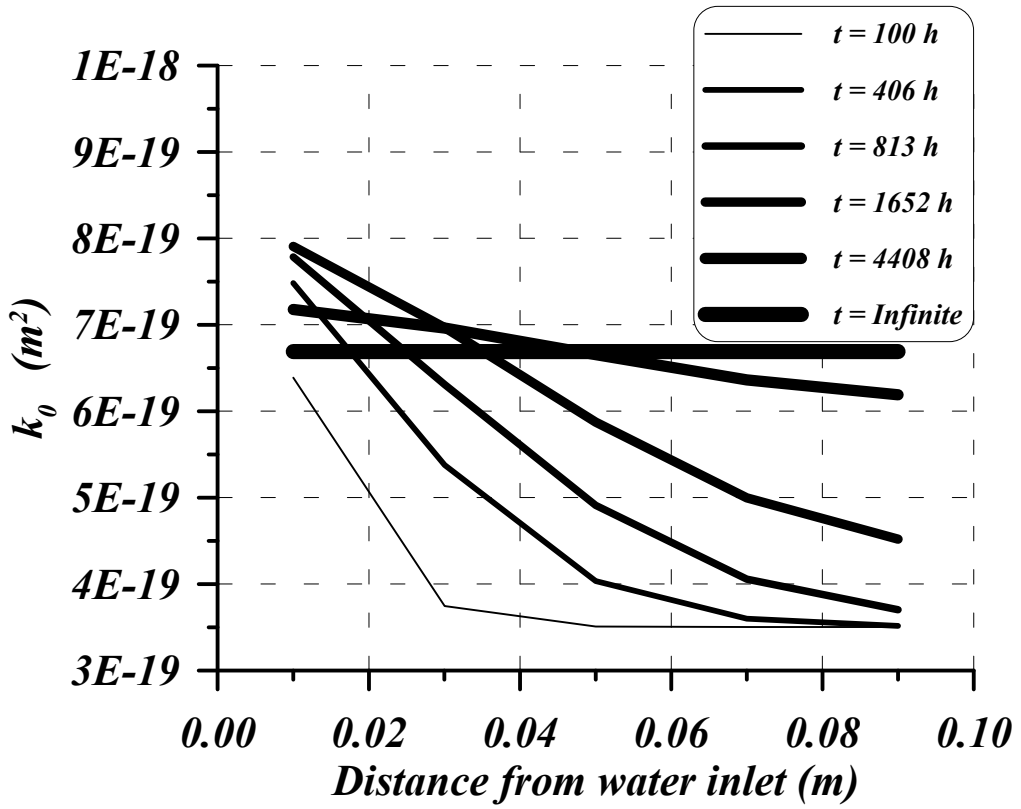

Figure 5.12: Evolution of the intrinsic permeability calculated when the 16 g/L water uptake test was simulated with this formulation. It can be observed that hydraulic conductivity reached a maximum value close to the water inlet and then, decreased.

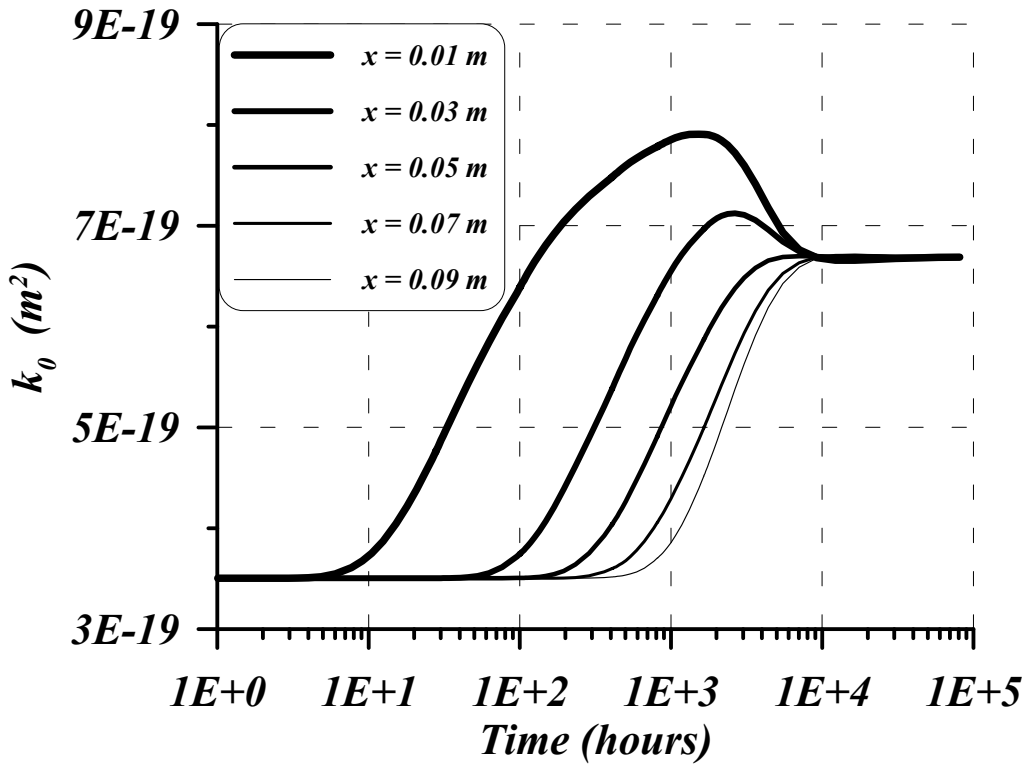

Figure 5.13: Time evolution of the calculated intrinsic permeability during the saturation process of a 10 cm length backfill specimen (WUT). X is the distance from the water inlet.

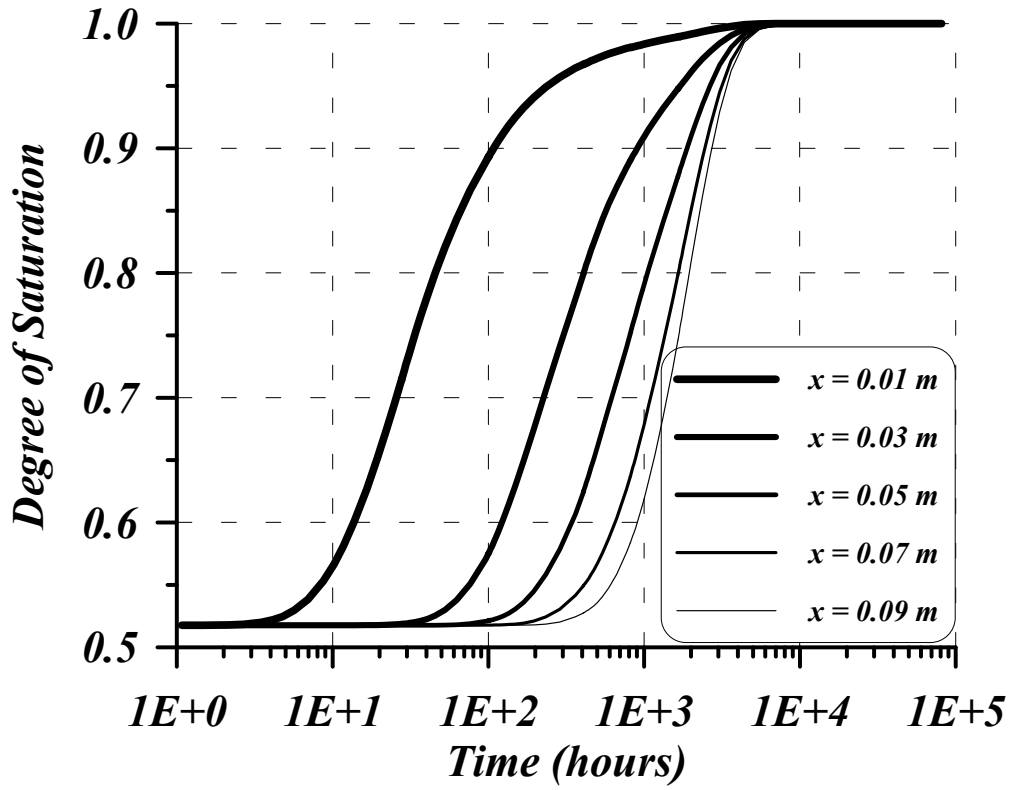

Figure 5.14: Time evolution of the calculated degree of saturation during the saturation process of a 10 cm length backfill specimen (WUT). X is the distance from the water inlet. Backfill saturation is reached after 5000 hours, however, chemical equilibrium has not been reached yet (after 9000 hours, see figure 5.13).

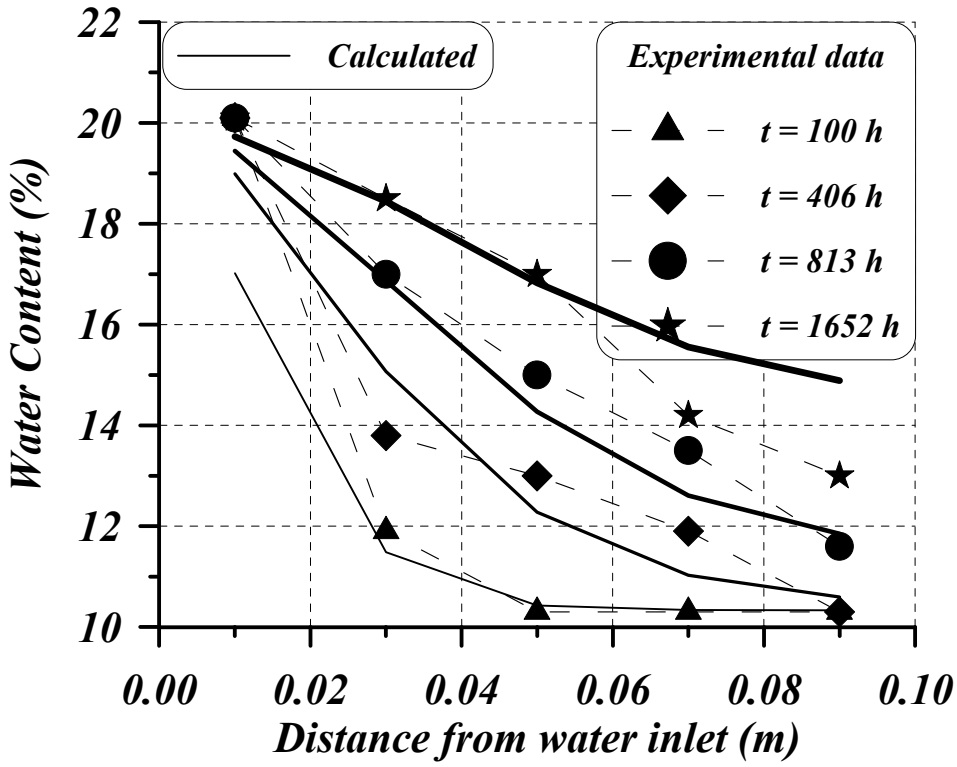

Figure 5.15: Numerical simulation of the water uptake tests performed on the backfill hydrated with saltwater (16 g/L). The diffusion used was $2 \cdot 10^{-9}$ m^2/s. The fit was even better than the obtained by using the lower backfill diffusion.

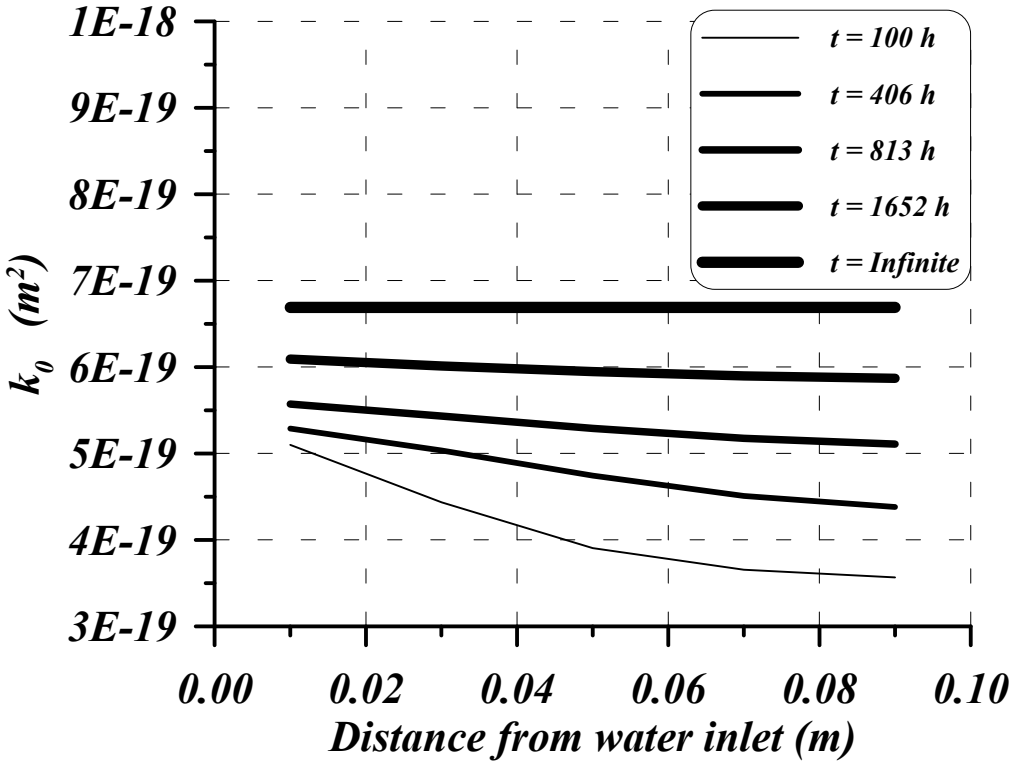

Figure 5.16: Evolution of the intrinsic permeability calculated when the 16 g/L water uptake test was simulated with this formulation using a diffusion value of $2 \cdot 10^{-9}$ m^2/s. It can be observed that hydraulic conductivity kept increasing uniformly during the wetting process showing a different evolution to the case with a smaller diffusion.

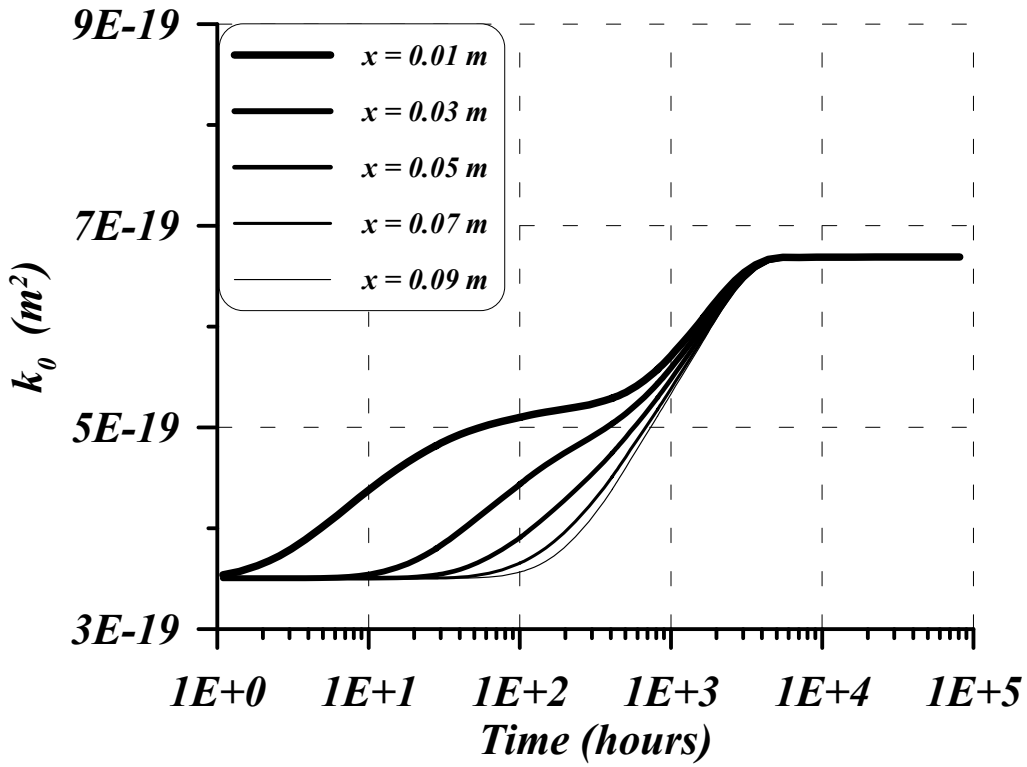

Figure 5.17: Time evolution of the calculated intrinsic permeability during the saturation process of a 10 cm length backfill specimen (WUT) using a backfill diffusion of $2 \cdot 10^{-9}$ m^2/s. X is the distance from the water inlet. Chemical equilibrium is reached after 5500 hours.

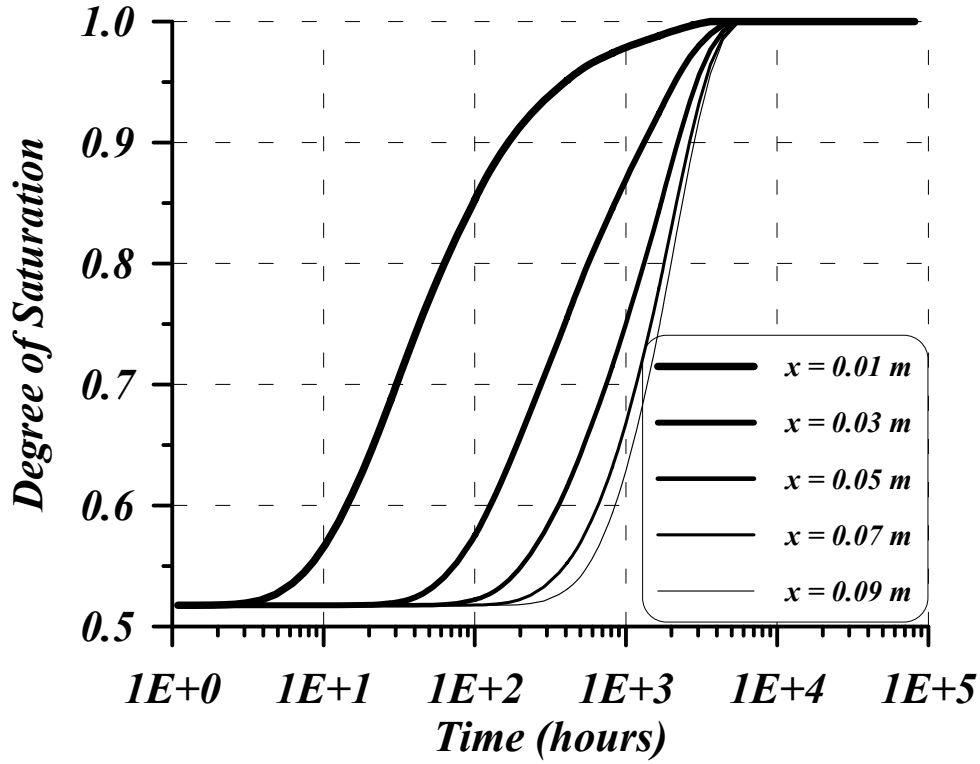

Figure 5.18: Time evolution of the calculated degree of saturation during the saturation process of a 10 cm length backfill specimen (WUT). X is the distance from the water inlet. Backfill saturation is reached after 6000 hours. In this case, chemical equilibrium and water potential equilibrium are reached at similar times.

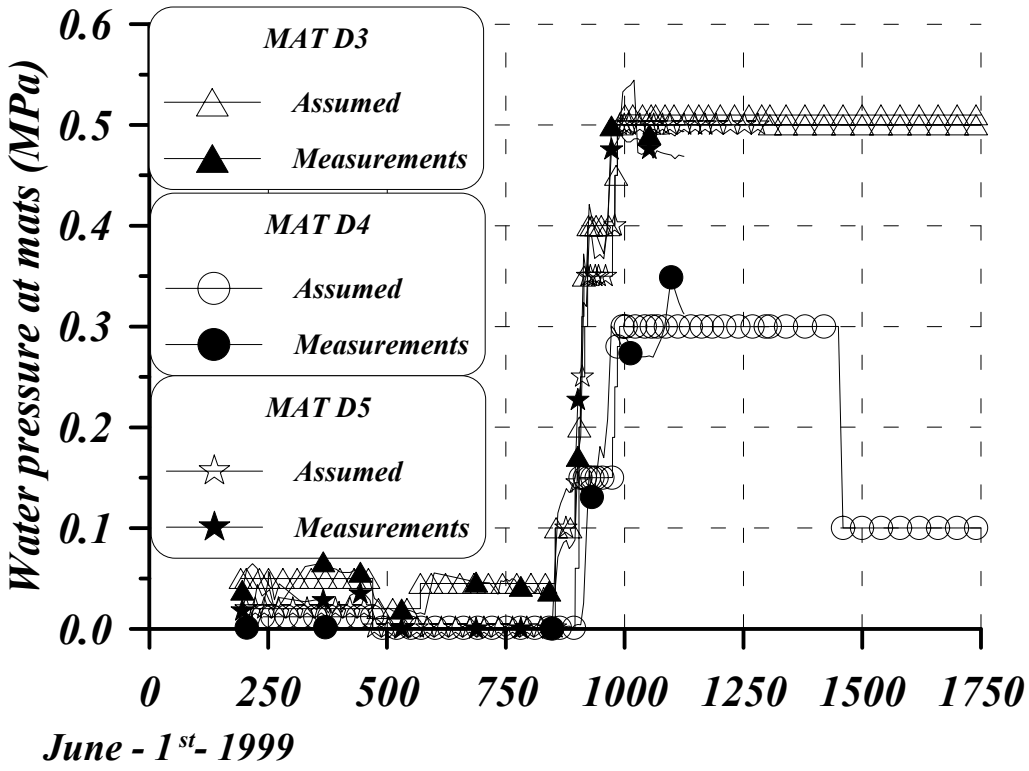

Figure 5.19: Injected water pressure at mats placed between the sections of backfill at the ZEDEX gallery (after Goudarzi et al. 2002).

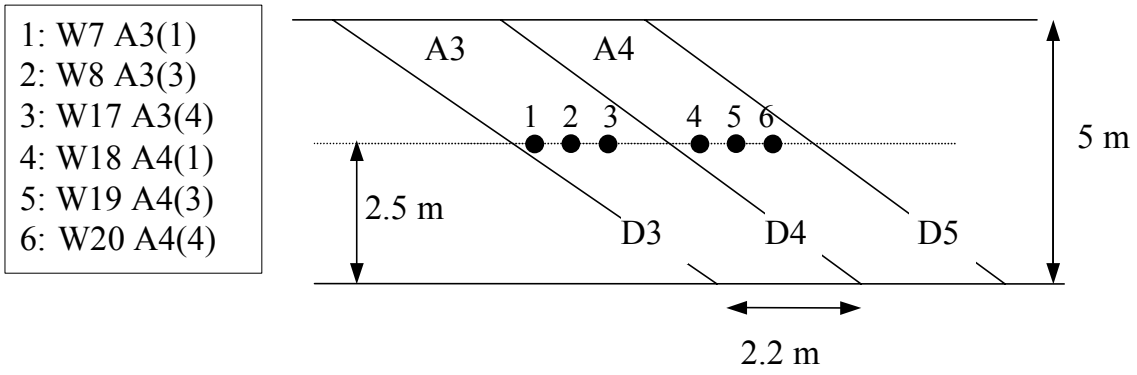

Figure 5.20: Geometry solved in the two dimension simulations and location of the six psychrometers studied. However, in these two-dimensional calculations, granite was not considered because of its little influence on the results. A3(1) means section A3 first layer.

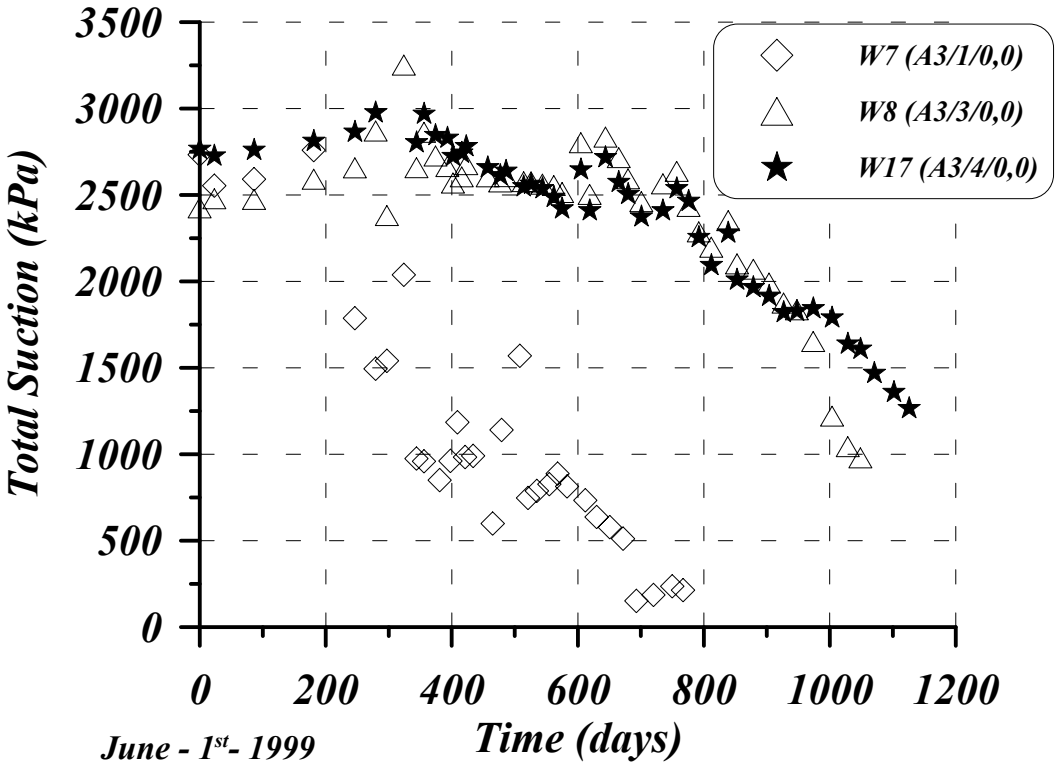

Figure 5.21: Evolution of the total suction measured in 3 psychrometers placed in section A3 at the ZEDEX gallery (after Goudarzi et al. 2002).

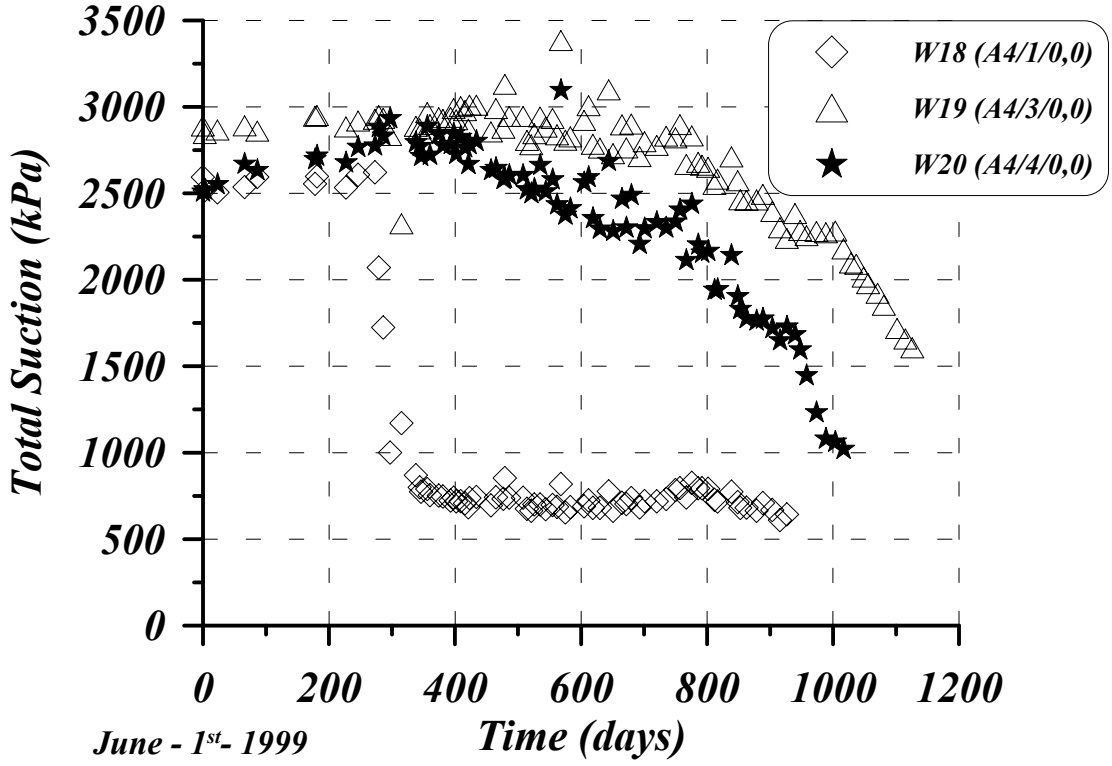

Figure 5.22: Evolution of the total suction measured in 3 psychrometers placed in section A4 at the ZEDEX gallery (after Goudarzi et al. 2002).

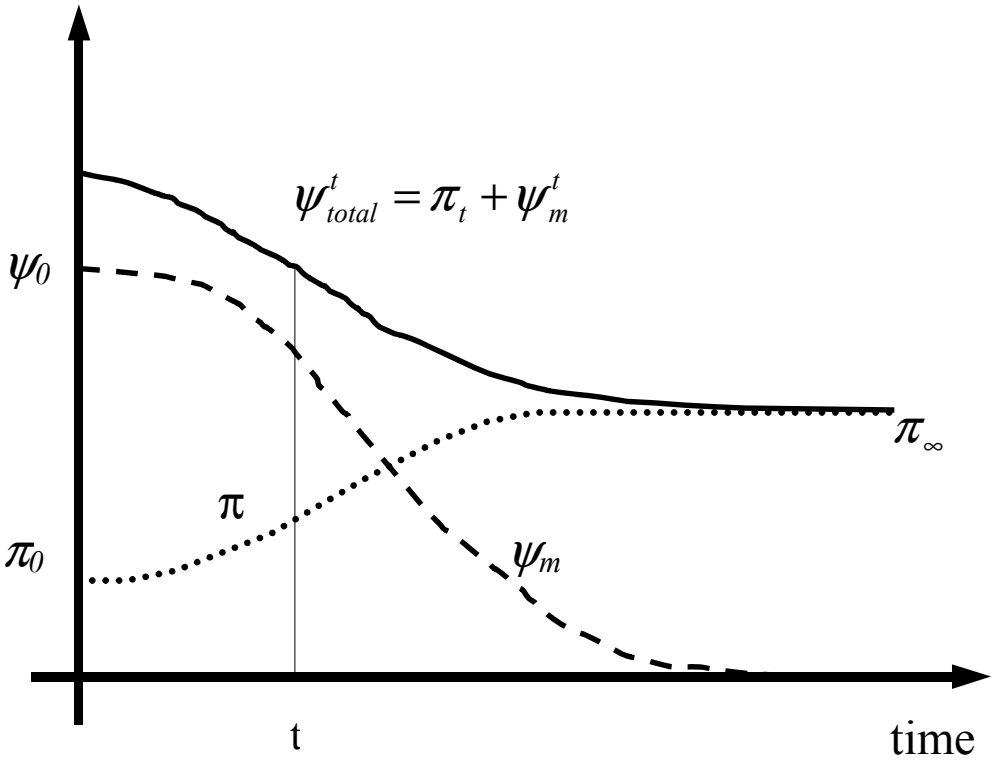

Figure 5.23: Evolution of osmotic, π, matric, ψ_m, and total suction, ψ_t, in a representative elementary volume of soil being saturated by salt water. Soil diffusion is high enough to assure that advective flow of water and salts and non-advective flow of ions have similar times.

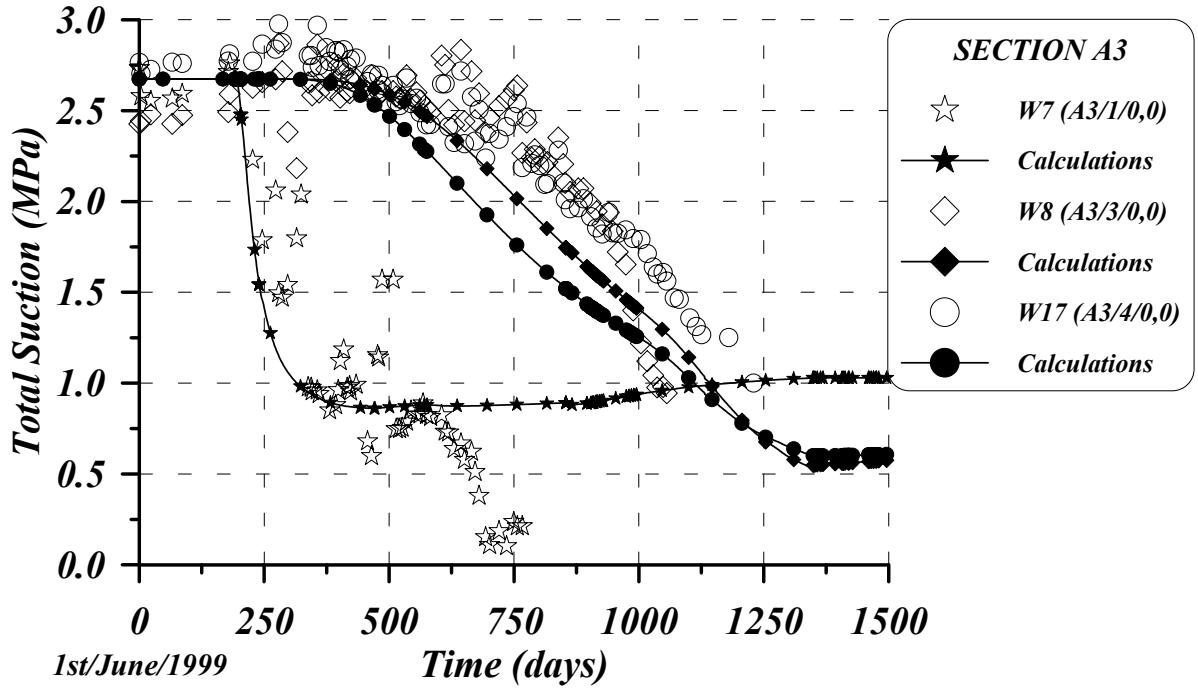

Figure 5.24: Comparison between the computed values of the total suction by means of the hydro-chemical simulation and the measured total suction in 3 psychrometers in section A3. Backfill molecular diffusion used was $2 \cdot 10^{-10}$ m^2/s.

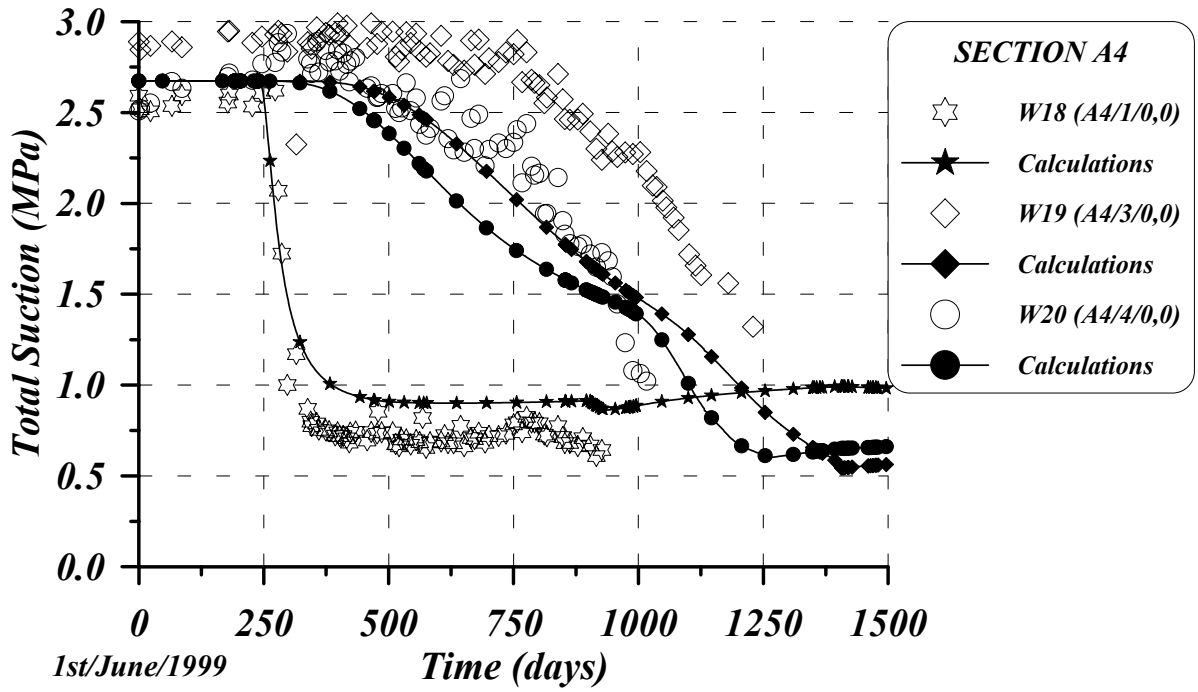

Figure 5.25: Comparison between the computed values of the total suction by means of the hydro-chemical simulation and the measured total suction in 3 psychrometers in section A4. Backfill molecular diffusion used was $2 \cdot 10^{-10}$ m^2/s.

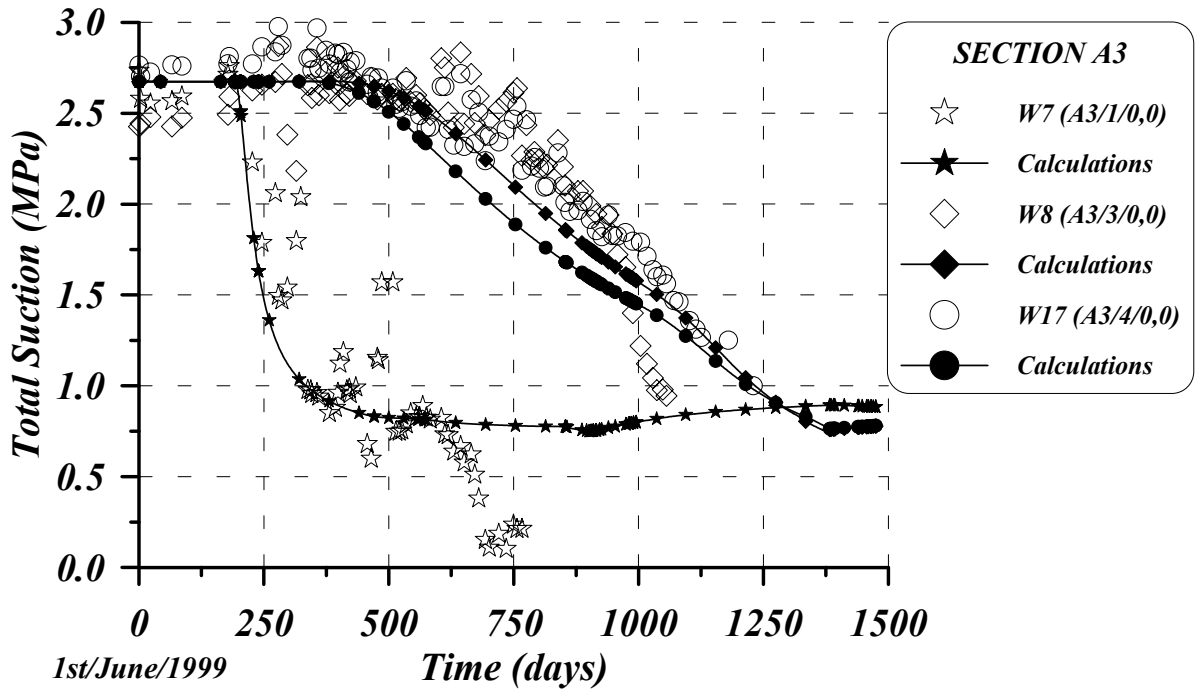

Figure 5.26: Comparison between the computed values of the total suction by means of the hydro-chemical simulation and the measured total suction in 3 psychrometers in section A3. Backfill molecular diffusion used was $2 \cdot 10^{-9}$ m^2/s.

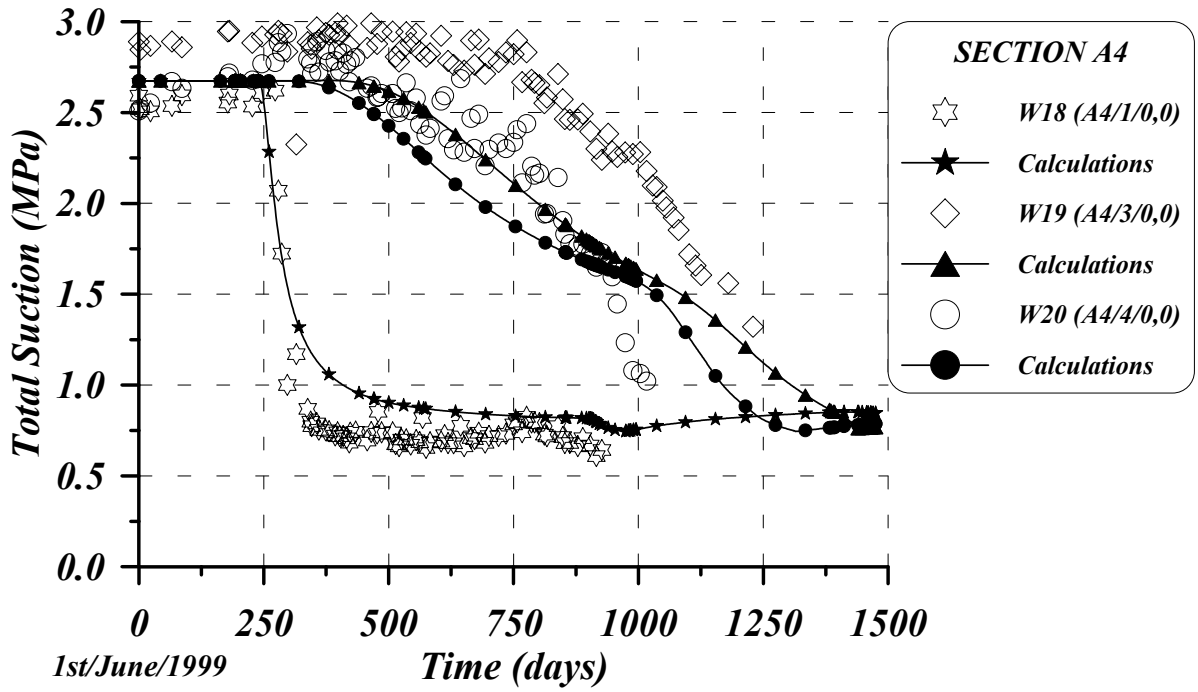

Figure 5.27: Comparison between the computed values of the total suction by means of the hydro-chemical simulation and the measured total suction in 3 psychrometers in section A4. Backfill molecular diffusion used was $2 \cdot 10^{-9}$ m^2/s.

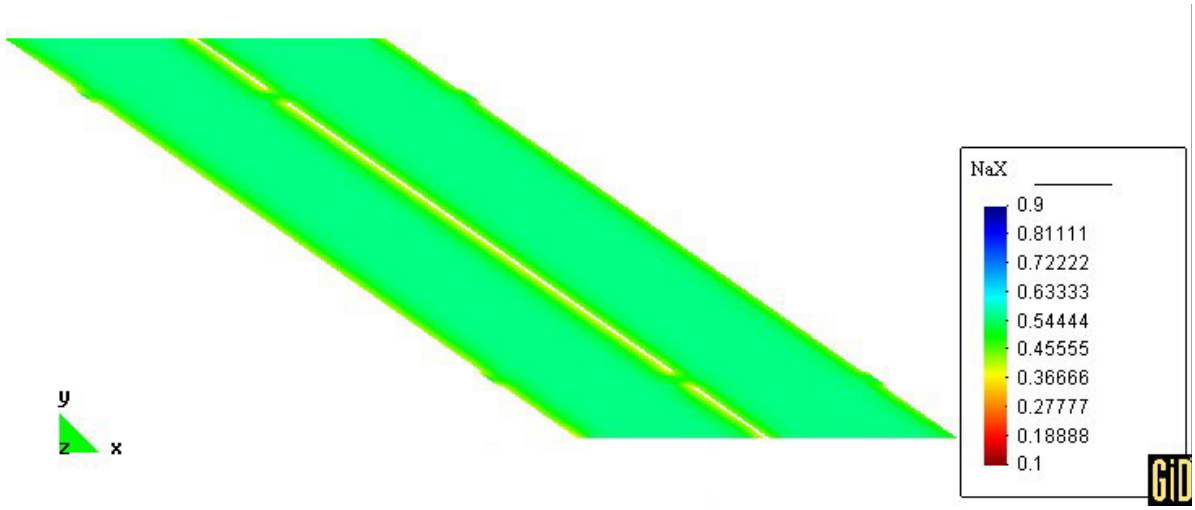

Figure 5.28: Equivalent fraction of the exchangeable cation NaX in the backfill at 1450 days when backfill molecular diffusion was $2 \cdot 10^{-10}$ m^2/s.

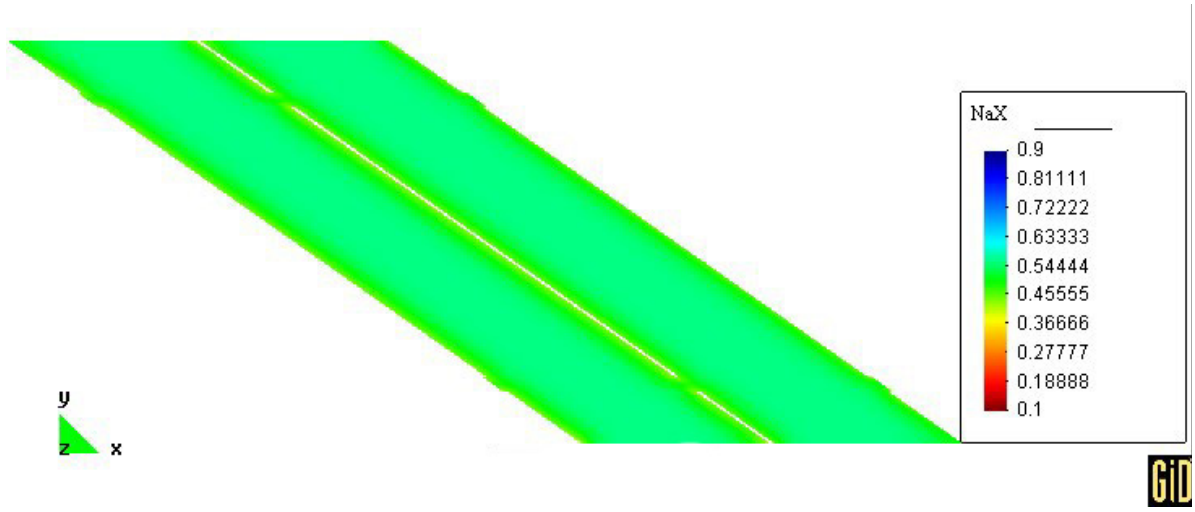

Figure 5.29: Equivalent fraction of the exchangeable cation NaX in the backfill at 1450 when backfill molecular diffusion was $2 \cdot 10^{-9}$ m^2/s.

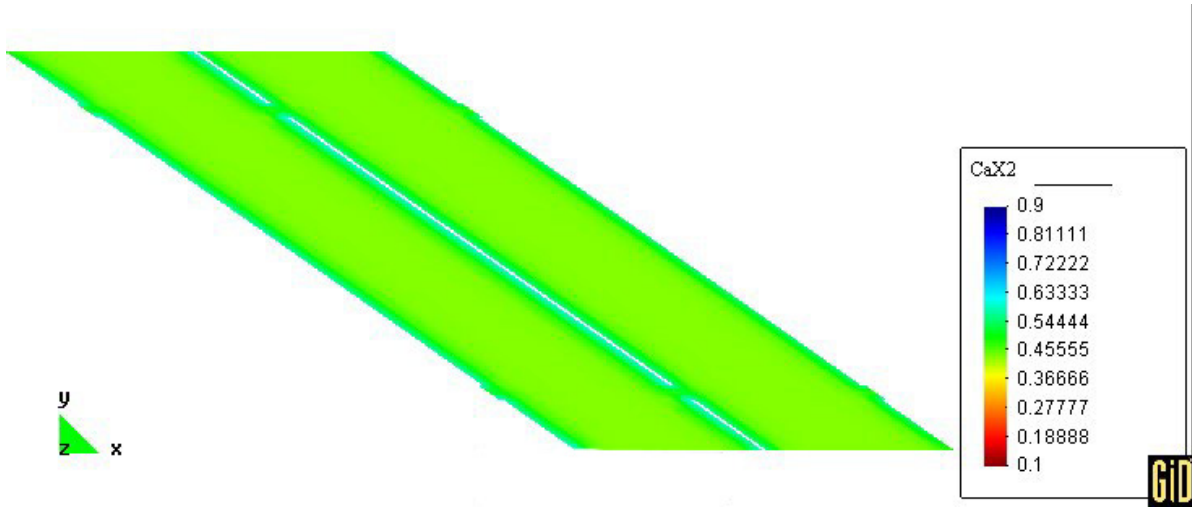

Figure 5.30: Equivalent fraction of the exchangeable cation CaX_2 in the backfill at 1450 days when backfill molecular diffusion was $2 \cdot 10^{-10}$ m^2/s.

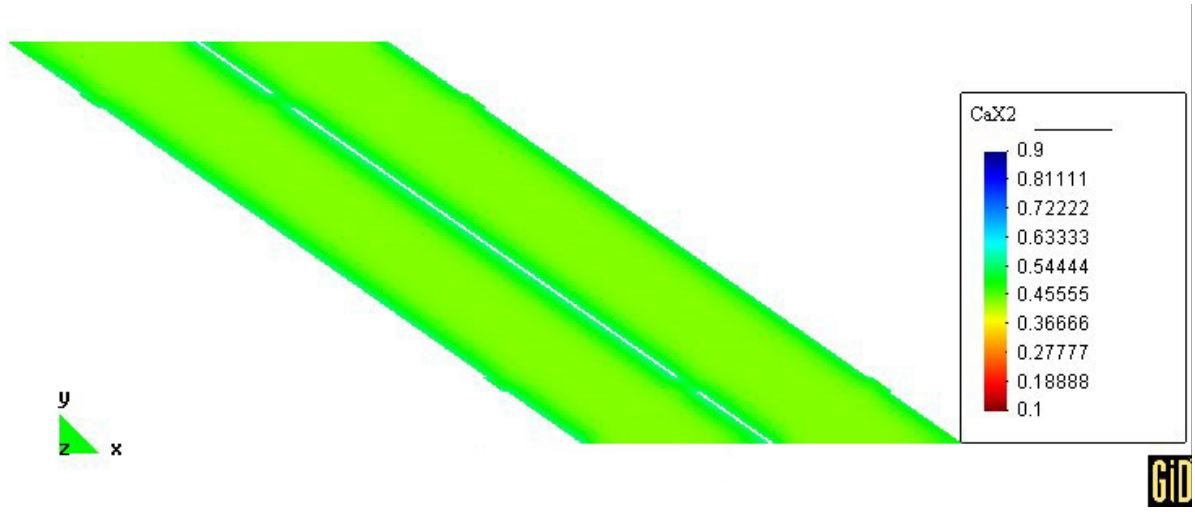

Figure 5.31: Equivalent fraction of the exchangeable cation CaX_2 in the backfill at 1450 days when backfill molecular diffusion was $2 \cdot 10^{-9}$ m^2/s.

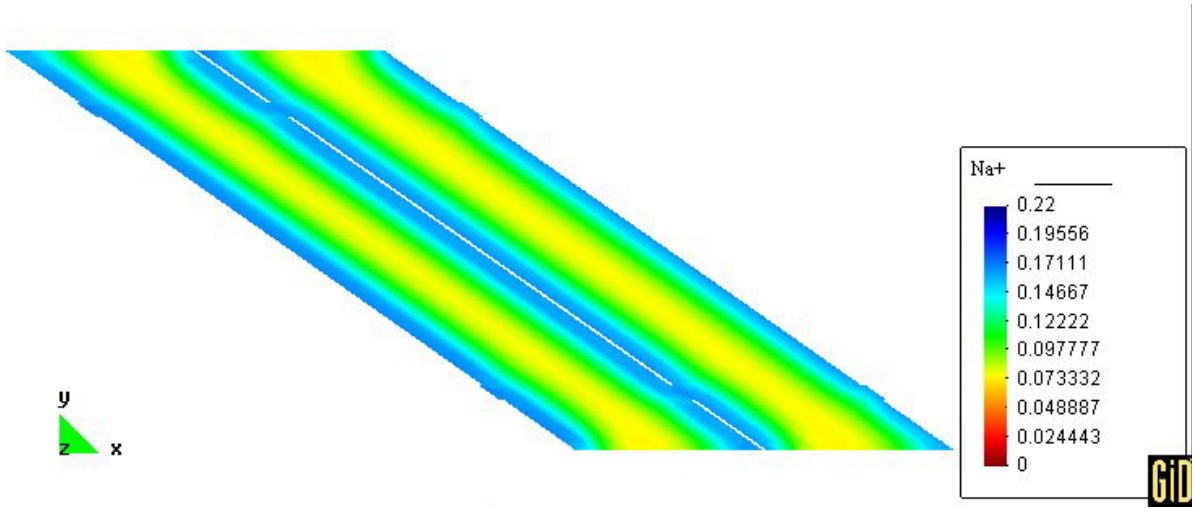

Figure 5.32: Molar concentration (mol/L) of Na^+ in backfill liquid phase at 1450 days when backfill molecular diffusion was $2 \cdot 10^{-10}$ m^2/s.

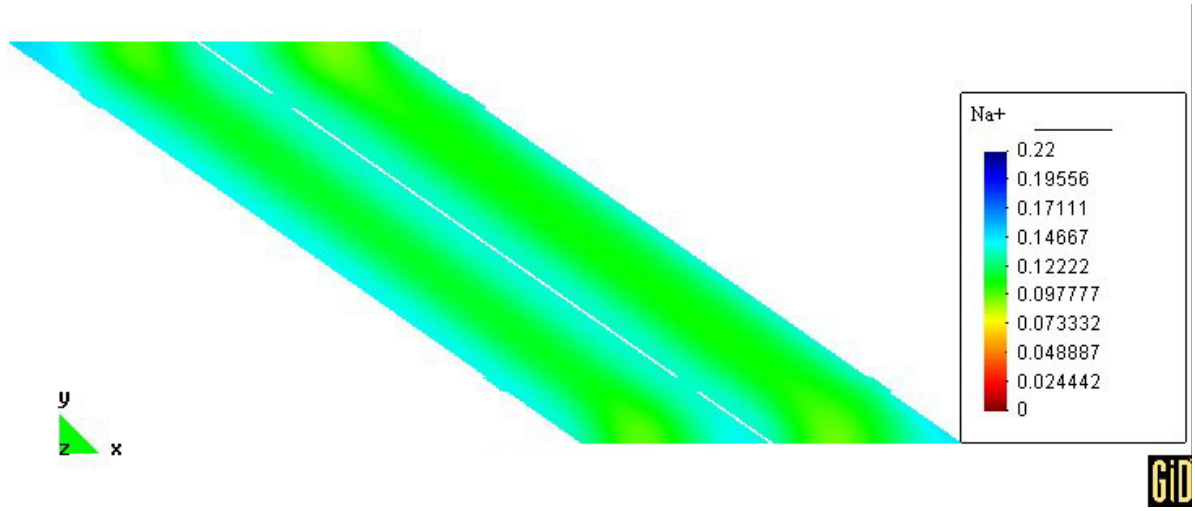

Figure 5.33: Molar concentration (mol/L) of Na^+ in backfill liquid phase at 1450 days when backfill molecular diffusion was $2 \cdot 10^{-9}$ m^2/s.

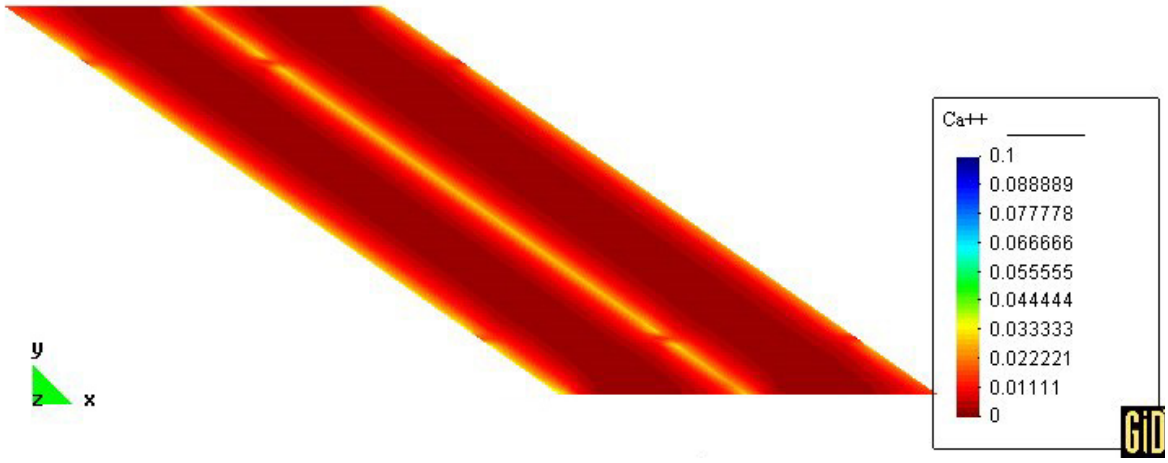

Figure 5.34: Molar concentration (mol/L) of Ca^{2+} in backfill liquid phase at 1450 days when backfill molecular diffusion was $2 \cdot 10^{-10}$ m^2/s.

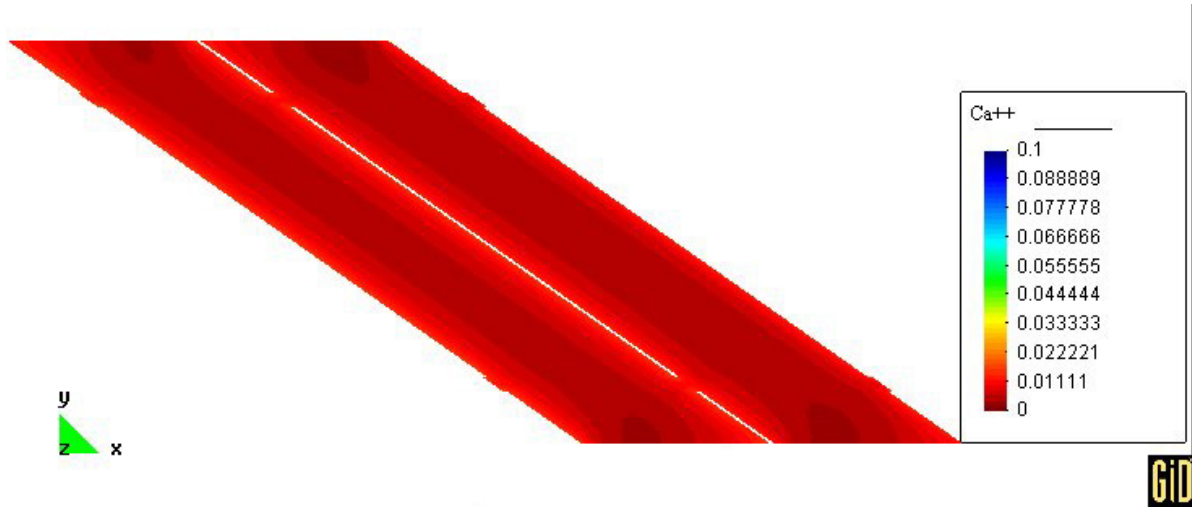

Figure 5.35: Molar concentration (mol/L) of Ca^{2+} in backfill liquid phase at 1450 days when backfill molecular diffusion was $2 \cdot 10^{-9}$ m^2/s.

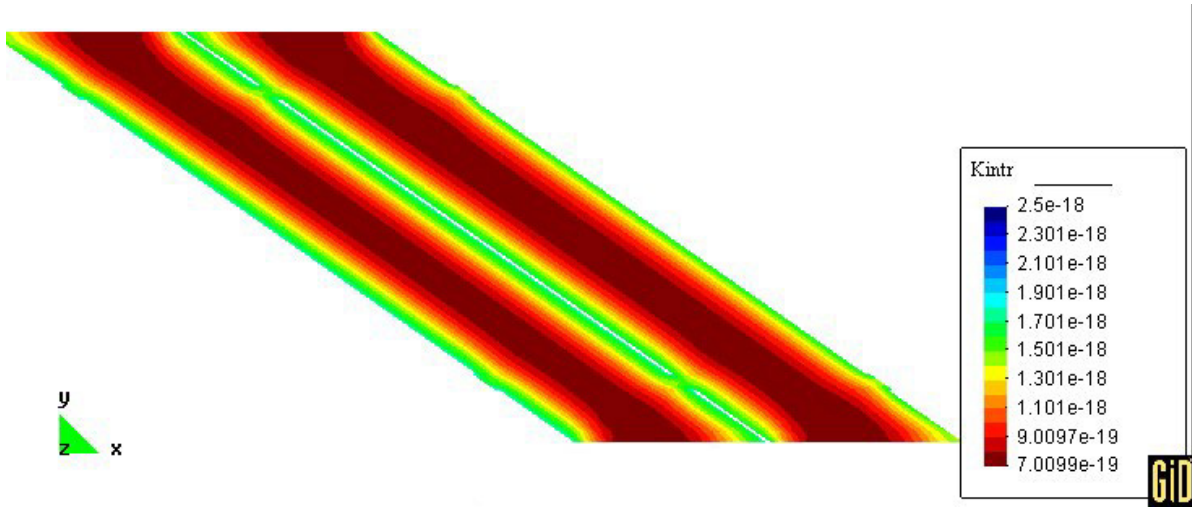

Figure 5.36: Backfill intrinsic permeability (m^2) after 1450 days when backfill molecular diffusion was $2 \cdot 10^{-10}$ m^2/s.

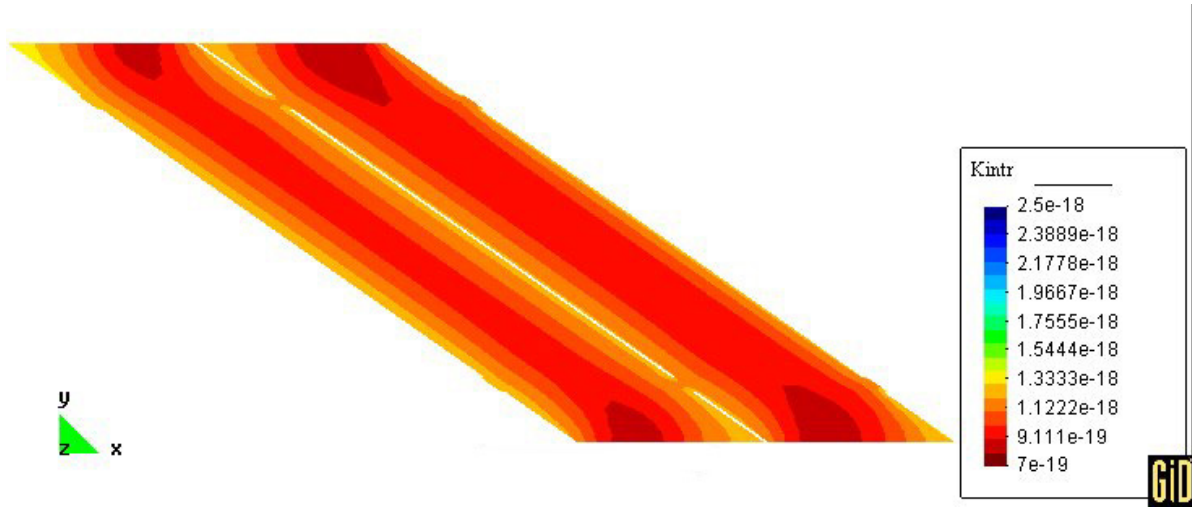

Figure 5.37: Backfill intrinsic permeability (m^2) after 1450 days when backfill molecular diffusion was $2 \cdot 10^{-9}$ m^2/s.

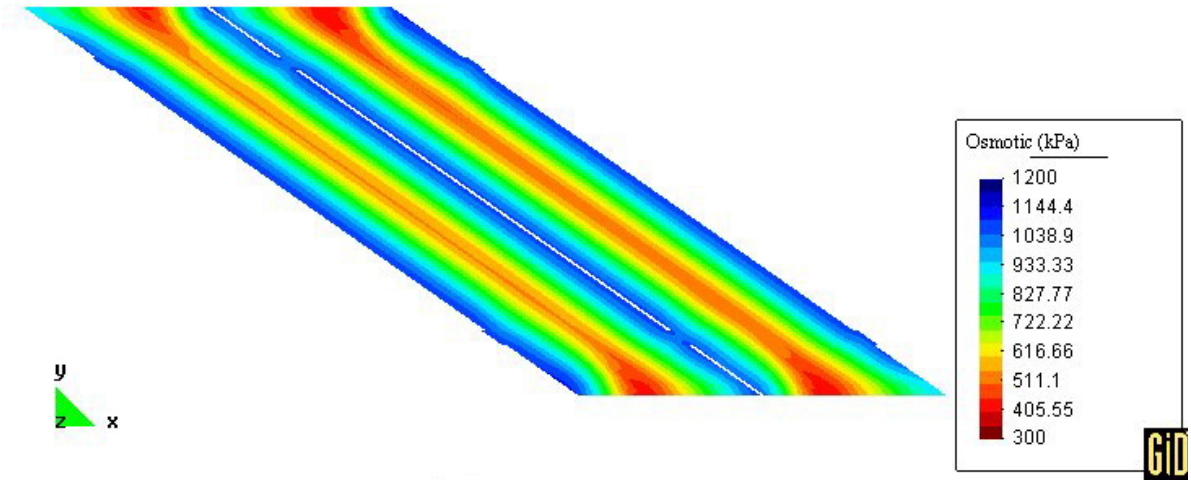

Figure 5.38: Computed backfill osmotic suction at 1450 days when backfill molecular diffusion was $2 \cdot 10^{-10}$ m^2/s.

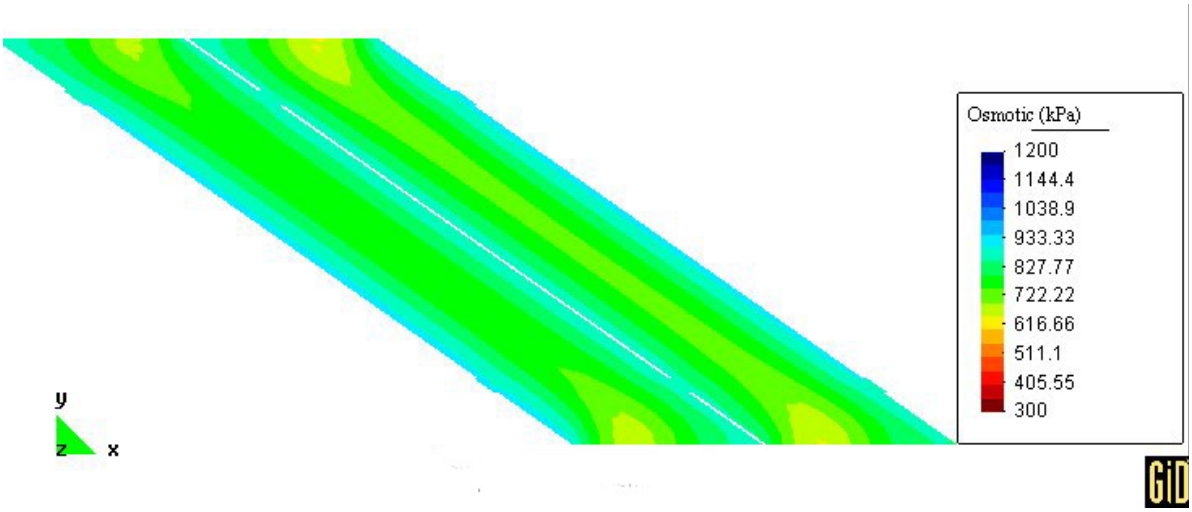

Figure 5.39: Computed backfill osmotic suction at 1450 days when backfill molecular diffusion was $2 \cdot 10^{-9}$ m^2/s.

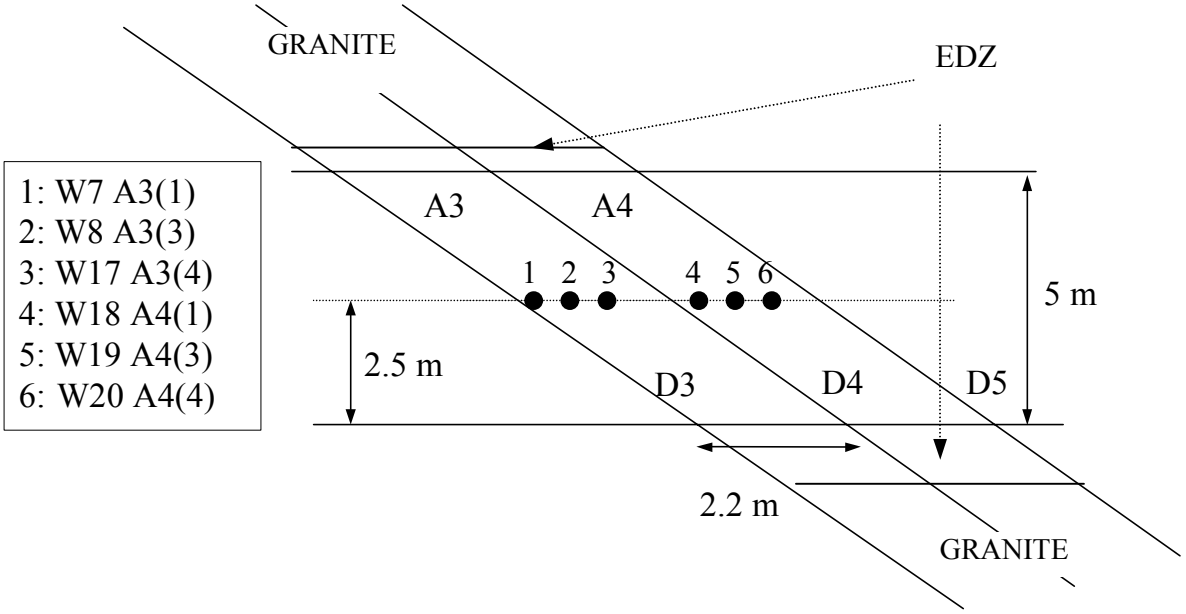

Figure 5.40: Geometry solved in the two dimension problems and location of the six psychrometers studied when host rock was considered in the calculations. Water pressure in the rock was prescribed to 0.4 MPa and water coming from the mat contained 6 g/L of salts. EDZ is the altered granite rock after the excavation of the gallery.

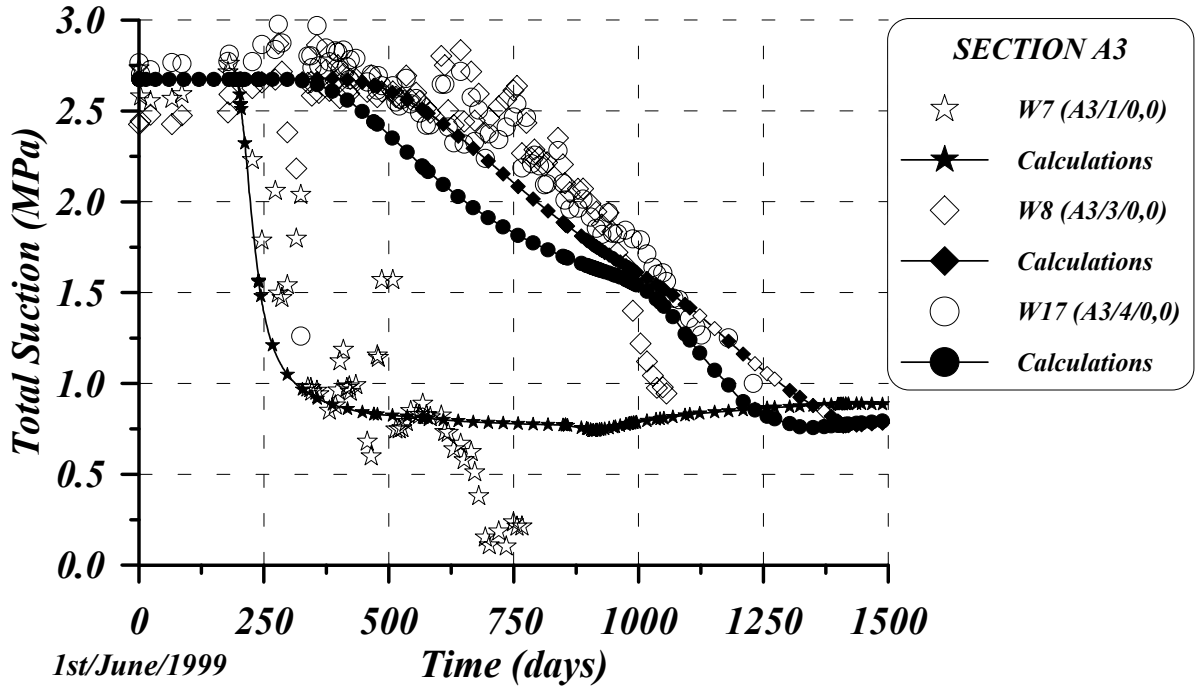

Figure 5.41: Comparison between the computed values of the total suction by means of the hydro-chemical simulation and the measured total suction in 3 psychrometers in section A3. Backfill molecular diffusion used was $2 \cdot 10^{-9}$ m^2/s. In this case, host rock was considered as shown in figure 5.40. It is clear that no important differences appear if rock is considered or not far from the boundaries.

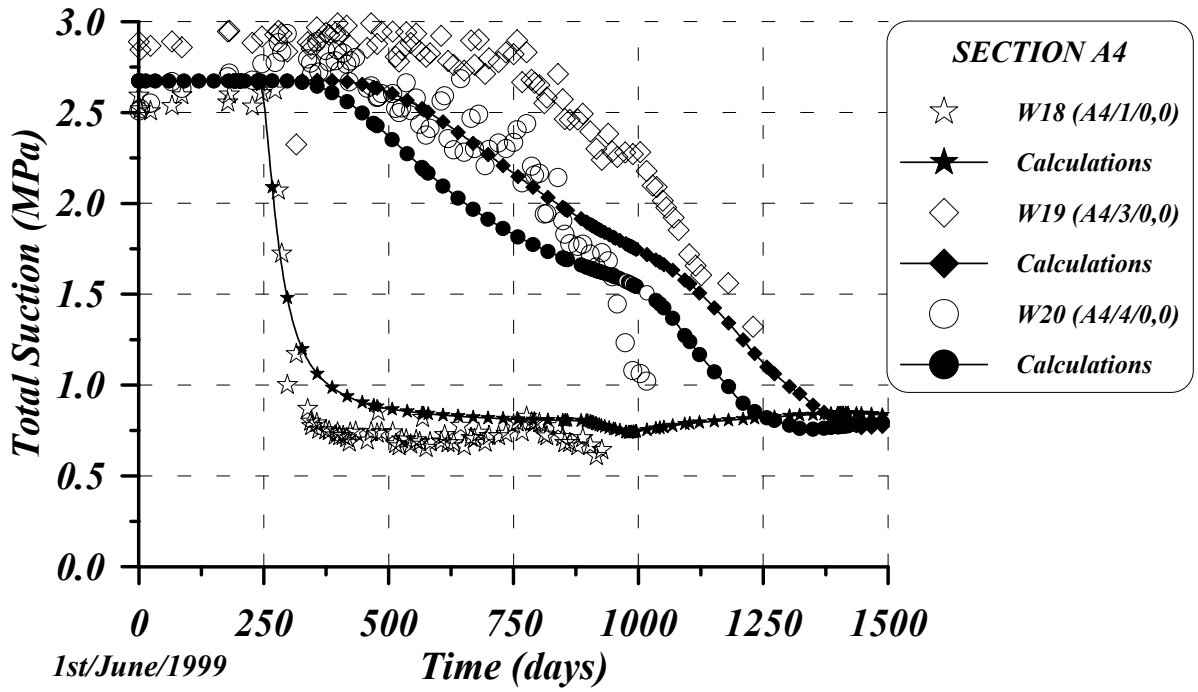

Figure 5.42: Comparison between the computed values of the total suction by means of the hydro-chemical simulation and the measured total suction in 3 psychrometers in section A4. Backfill molecular diffusion used was $2 \cdot 10^{-9}$ m^2/s. In this case, host rock was considered as shown in figure 5.28. It is clear that no important differences appear if rock is considered or not far from the boundaries.

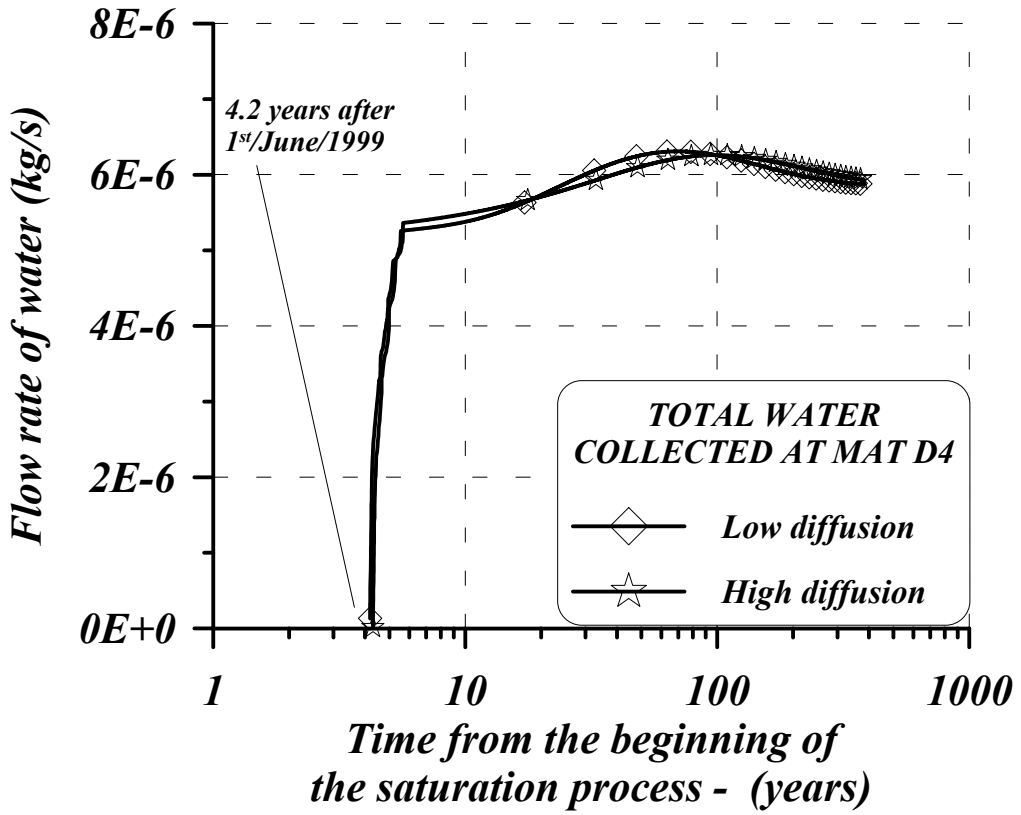

Figure 5.43: Evolution of total flow rate of water collected at mat D4 when injected water pressure was reduced in this mat up to 0.1 MPa. A comparison of the results when both molecular diffusions were used is shown. The reduction of water pressure takes place after 4.07 years (1485 days) of the beginning of the saturation process. Water is collected at mat D4 after 4.2 years of the beginning of the saturation process.

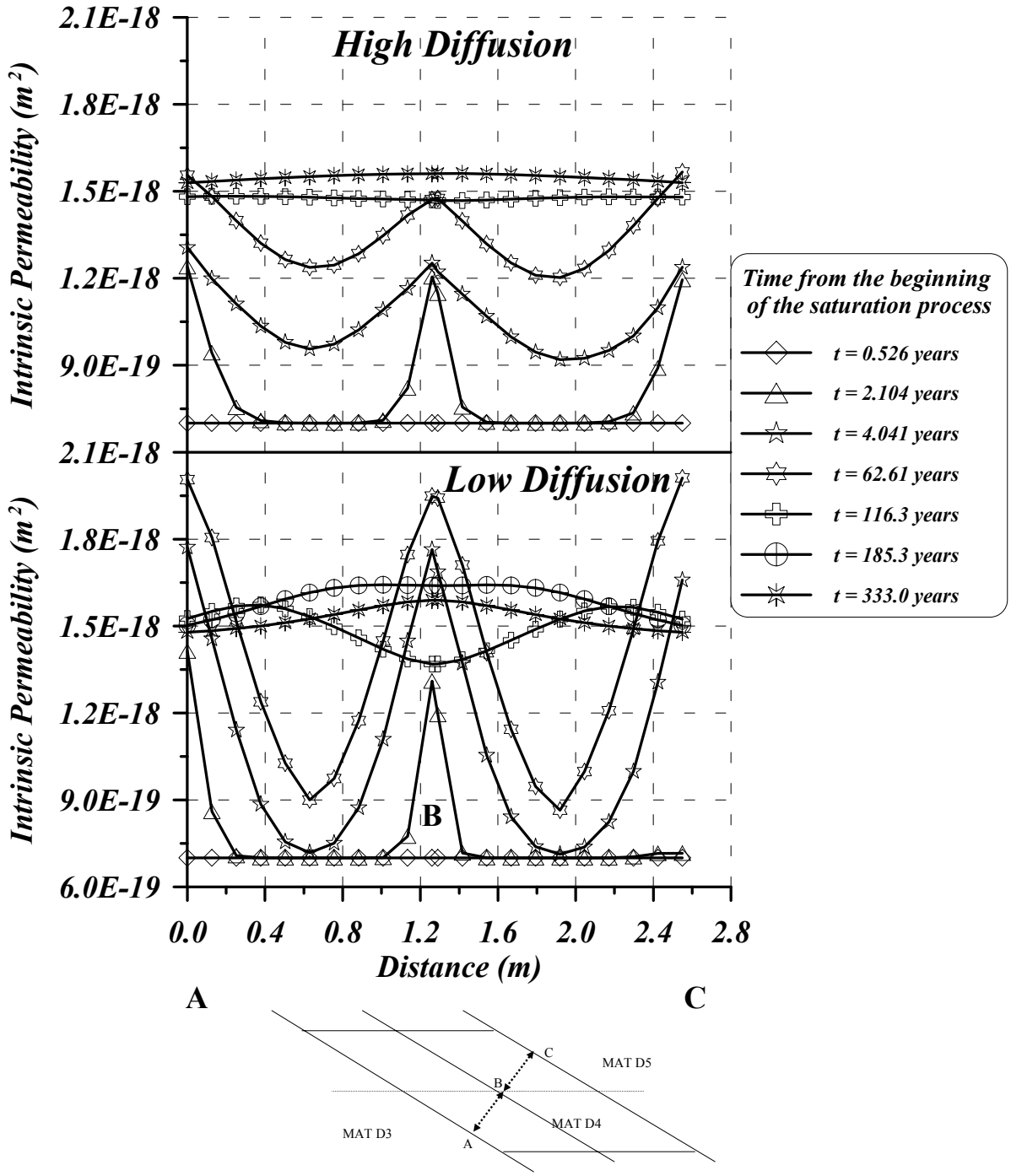

Figure 5.44: Evolution of intrinsic permeability in a perpendicular line from mat D3 to D5 in sections A3 and A4 for both molecular diffusions. It is necessary to point out that the origin of time in this figure is the beginning of the saturation process. The evolution of injected water pressure at mats is shown in figure 5.19. After 1480 days (4.07 years) water pressure at mat D4 is reduced up to 100 kPa and salinity of incoming water at the three mats is reduced from 16 g/L to 12 g/L.

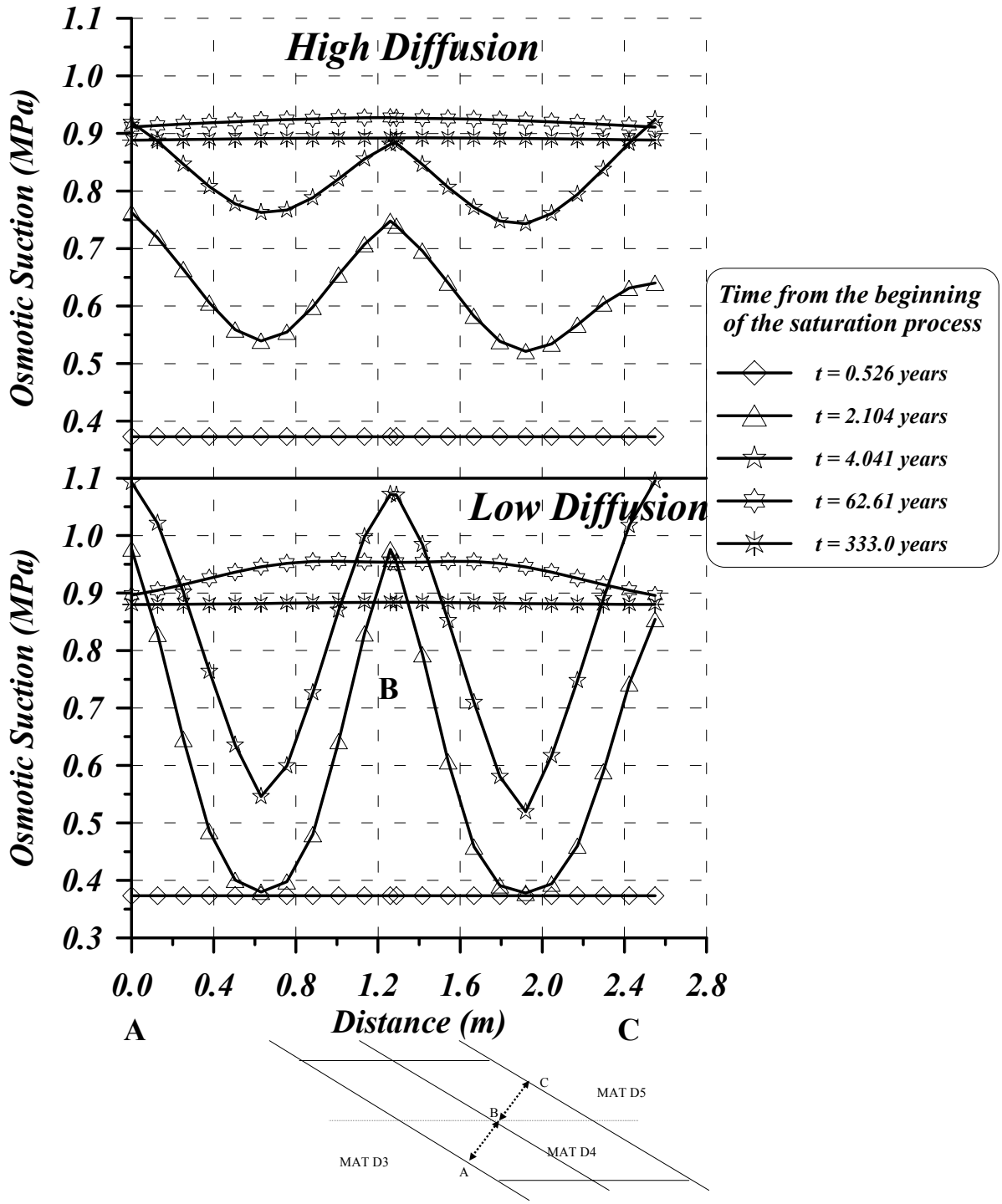

Figure 5.45: Evolution of osmotic suction along section AB-BC when injected water pressure was reduced in mat D4 up to 0.1 MPa and water contained 12 g/L of salts.

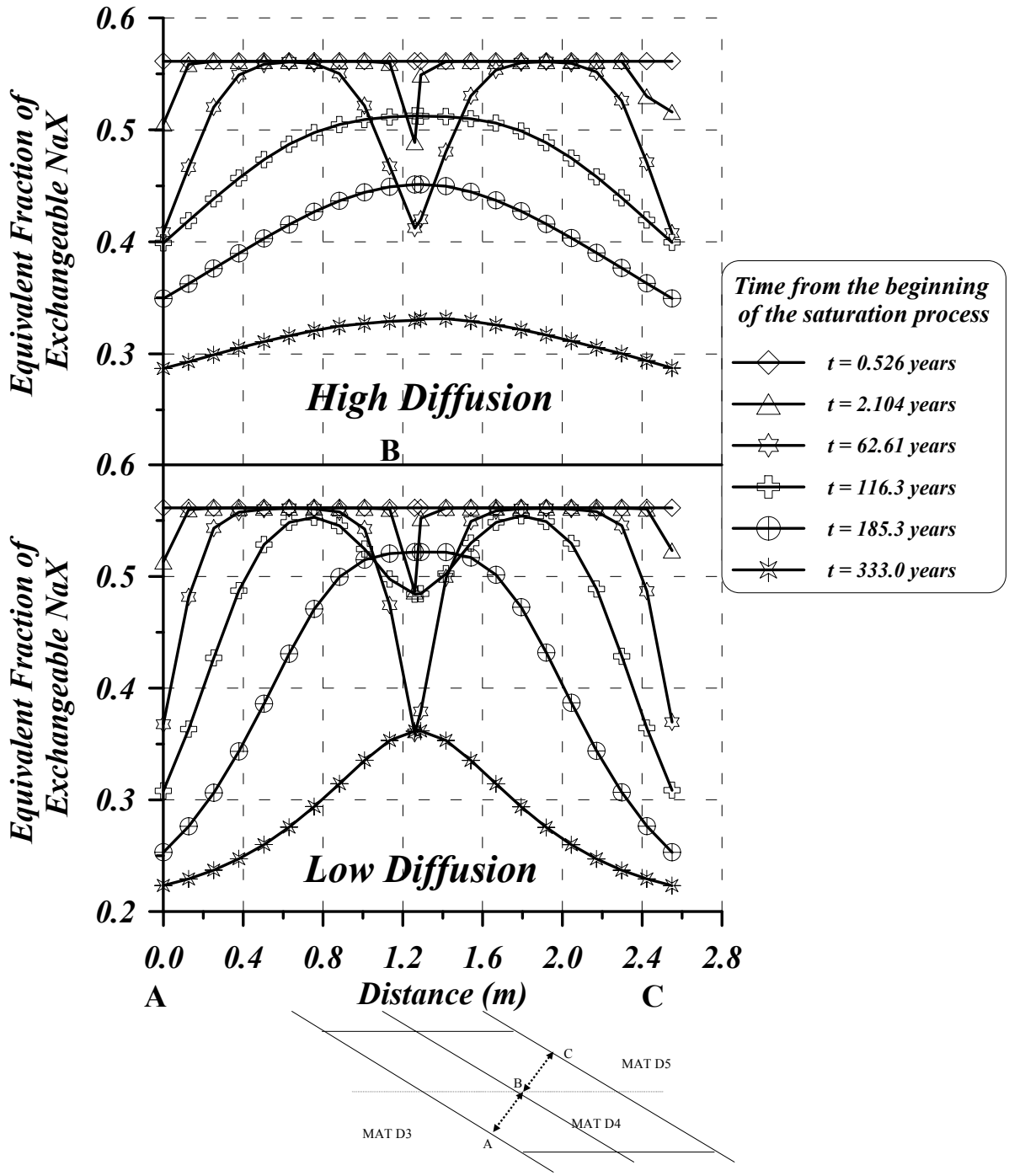

Figure 5.46: Evolution of equivalent fraction of exchangeable NaX along section AB-BC when injected water pressure was reduced in mat D4 up to 0.1 MPa and water contained 12 g/L of salts.

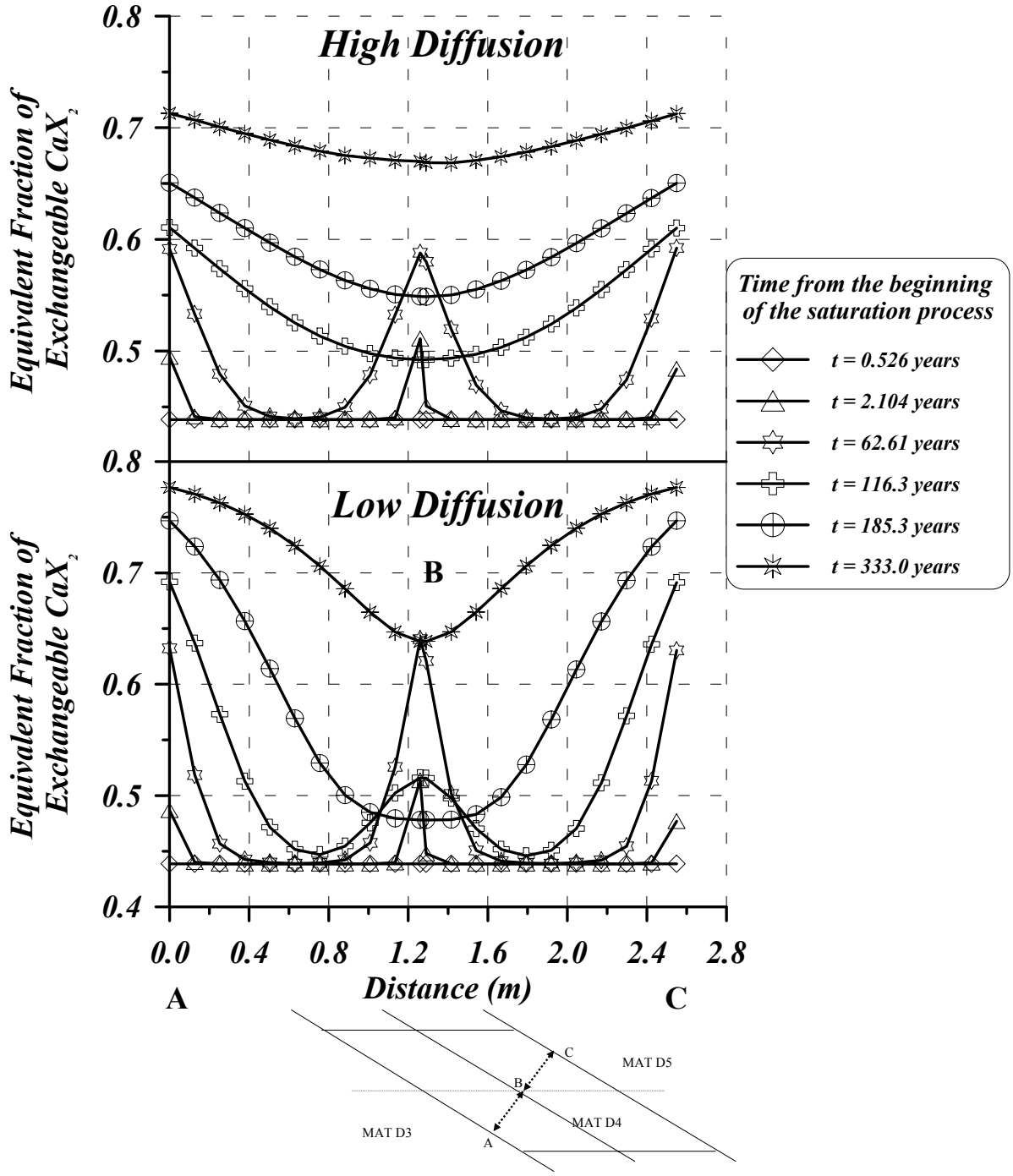

Figure 5.47: Evolution of equivalent fraction of exchangeable CaX_2 along section AB-BC when injected water pressure was reduced in mat D4 up to 0.1 MPa and water contained 12 g/L of salts.

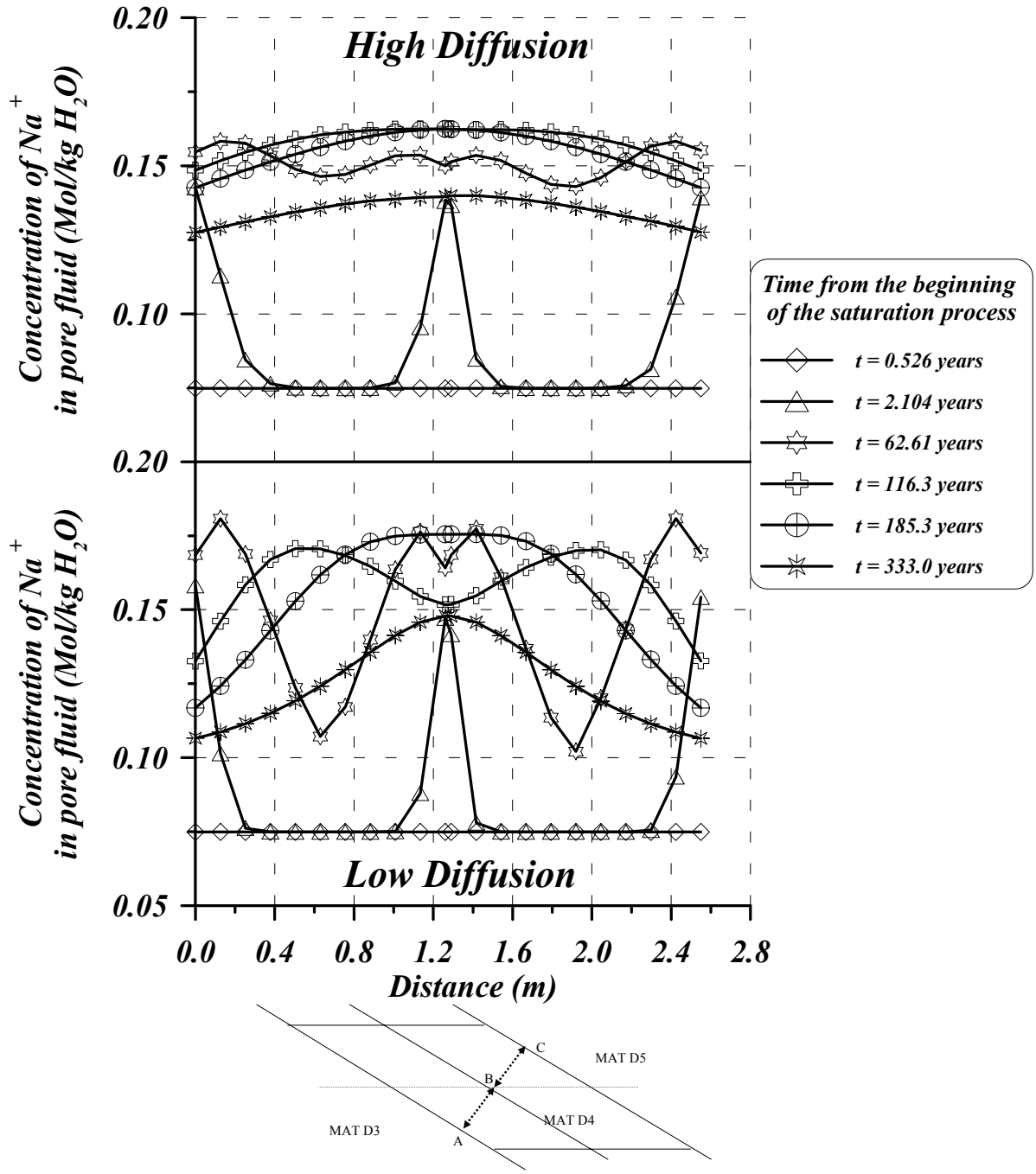

Figure 5.48: Evolution of concentration of ion sodium in pore fluid along section AB-BC when injected water pressure was reduced in mat D4 up to 0.1 MPa and water contained 12 g/L of salts.

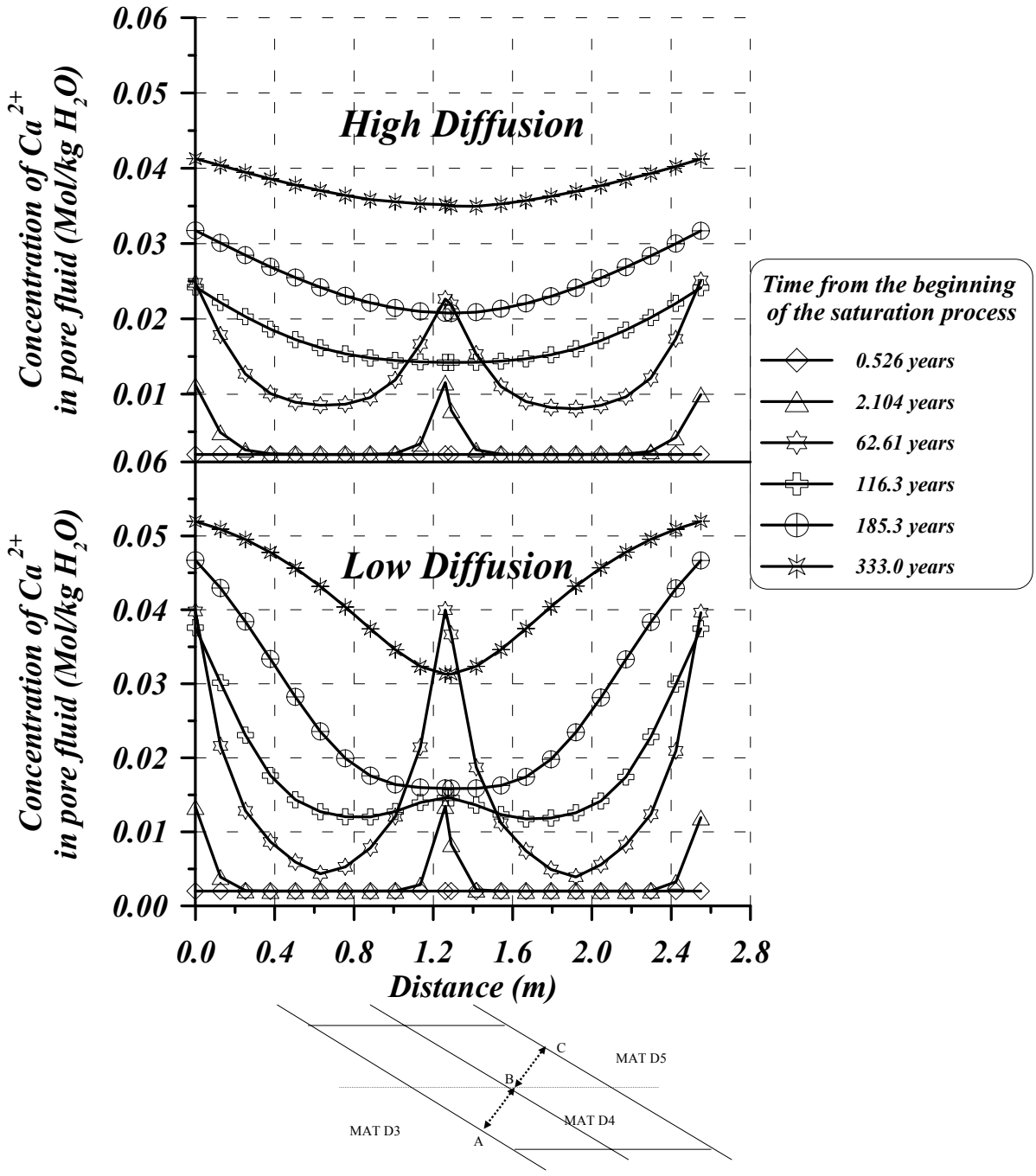

Figure 5.49: Evolution of concentration of ion calcium in pore fluid along section AB-BC when injected water pressure was reduced in mat D4 up to 0.1 MPa and water contained 12 g/L of salts.

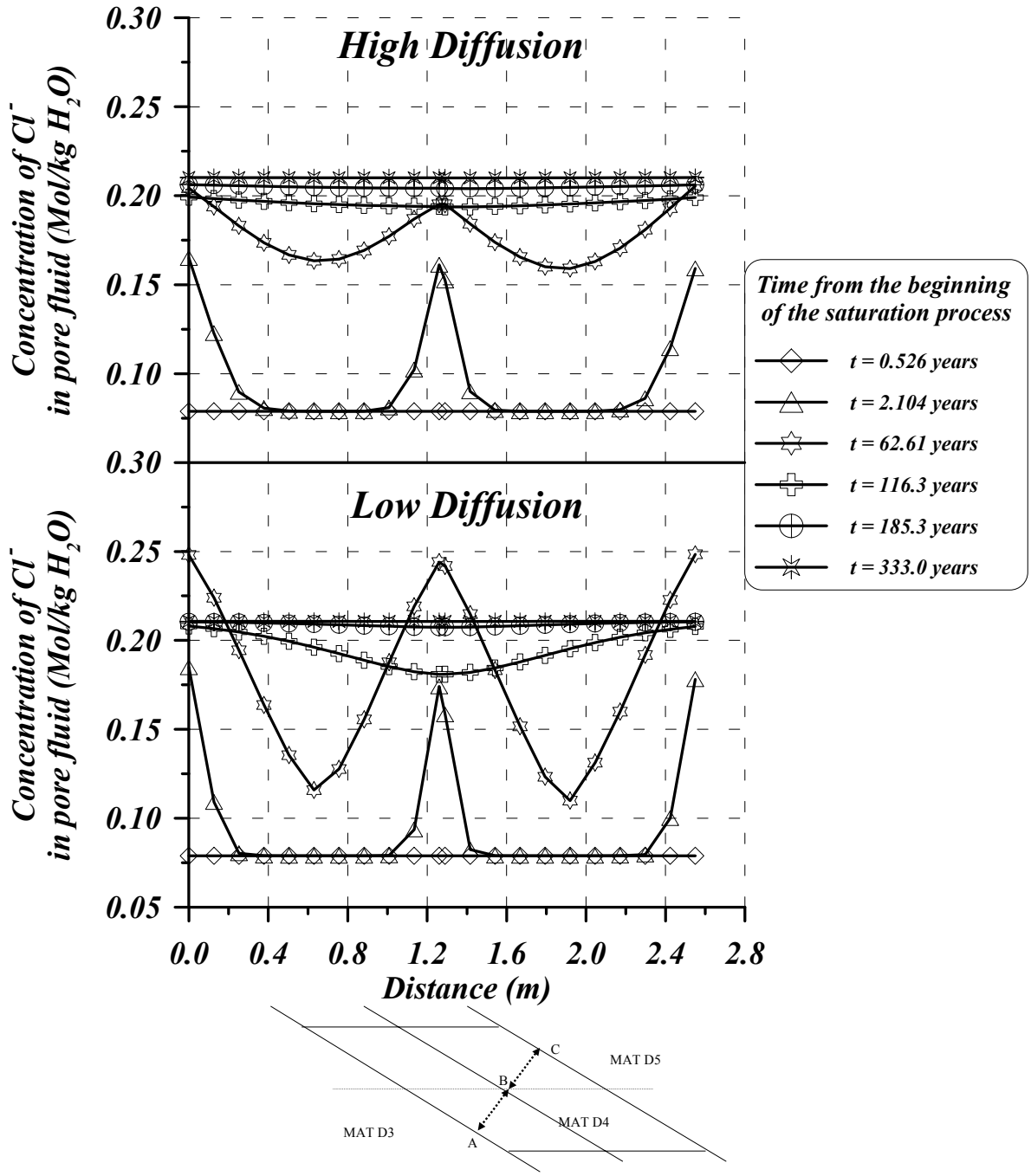

Figure 5.50: Evolution of concentration of ion chloride in pore fluid along section AB-BC when injected water pressure was reduced in mat D4 up to 0.1 MPa and water contained 12 g/L of salts.

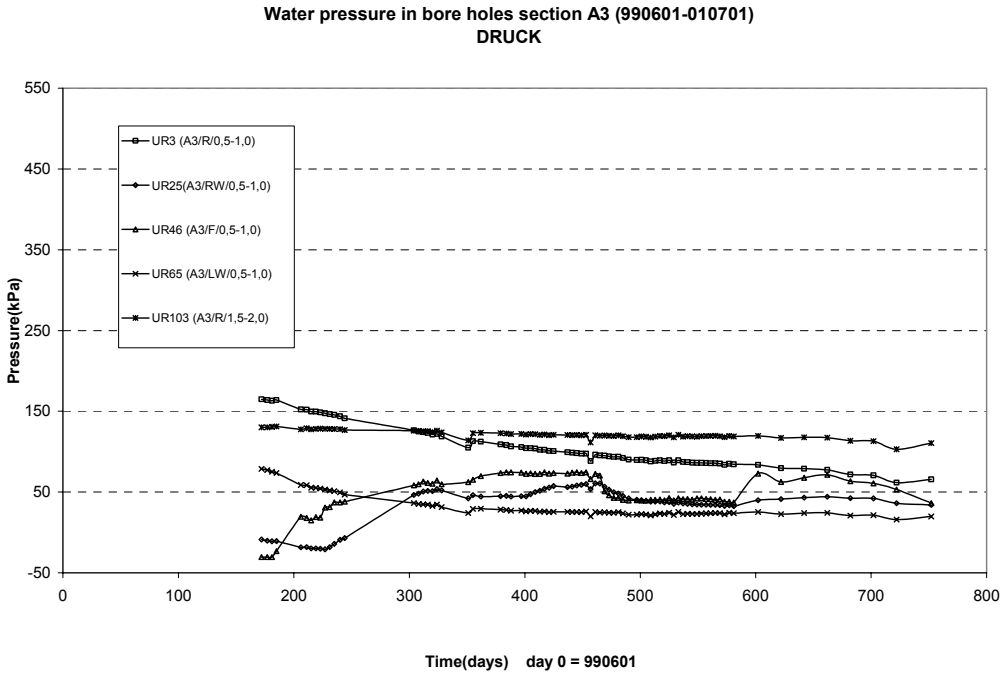

Figure 5.51: Evolution of water pressure measured in different boreholes excavated in the rock, in section A3 at the ZEDEX gallery (Goudarzi et al. 2002).

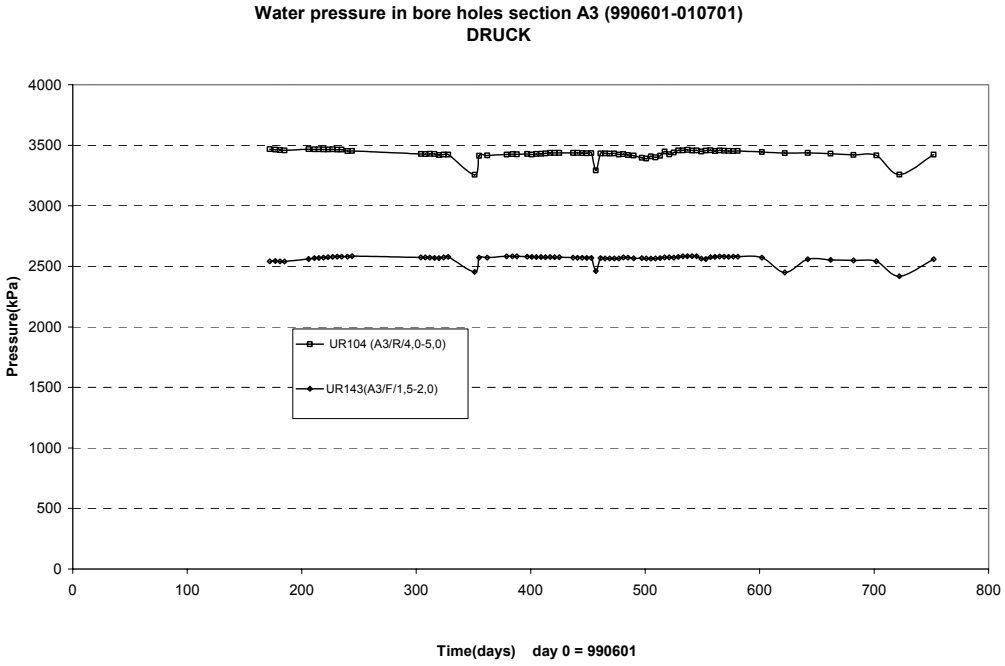

Figure 5.52: Evolution of the measured water pressure at two different boreholes that were excavated from the ZEDEX gallery in section A3 (Goudarzi et al. 2002).

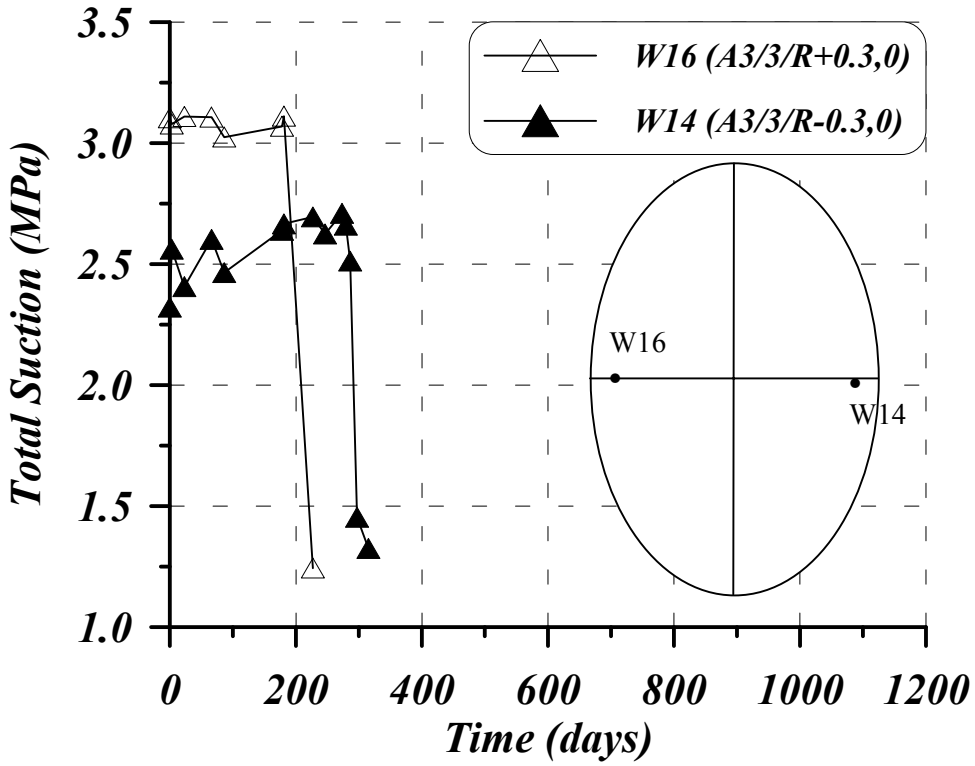

Figure 5.53: Evolution of total suction of two Wescor PST-55 psychrometers placed in the section A3 at the ZEDEX gallery (Goudarzi et al. 2002). Both psychrometers measured similar saturation evolution. When free water got in the devices, they might break down.

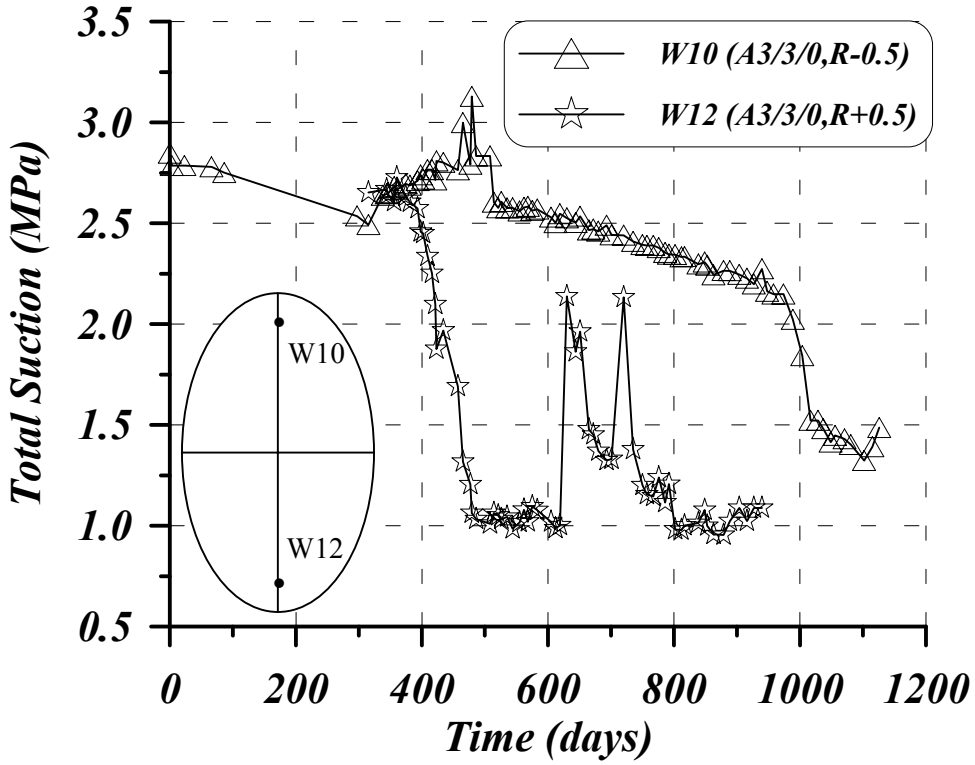

Figure 5.54: Evolution of total suction of two Wescor PST-55 psychrometers placed in the section A3 at the ZEDEX gallery (Goudarzi et al. 2002). It can be observed that different evolution of the saturation process is being monitored.

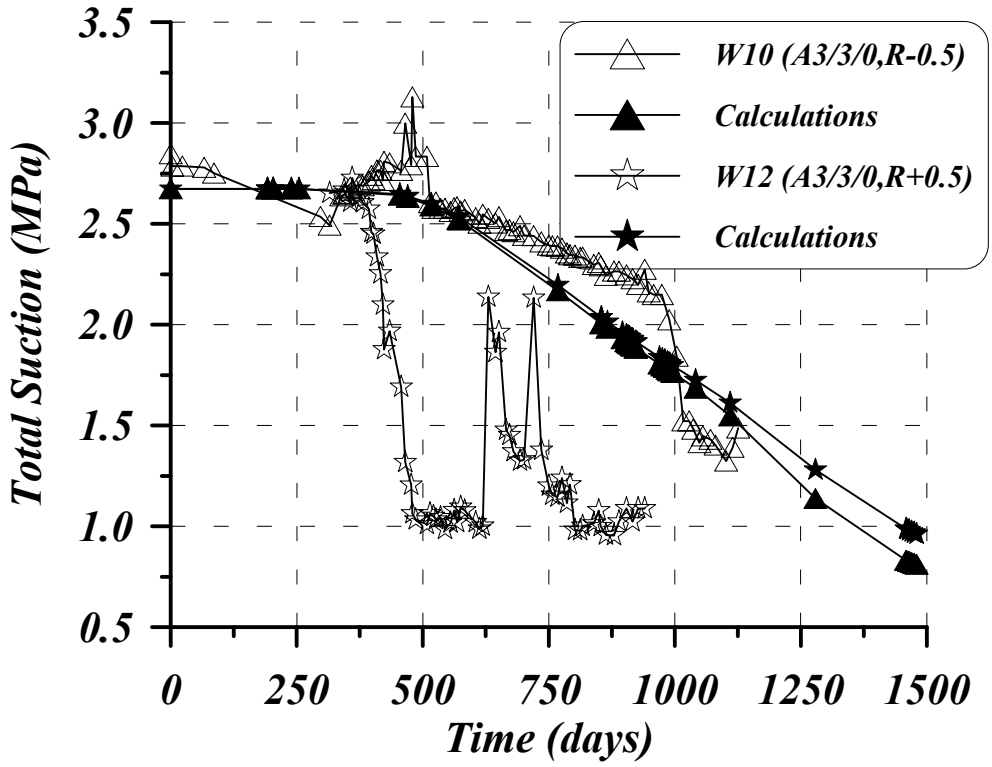

Figure 5.55: Evolution of total suction of two Wescor PST-55 psychrometers placed in the section A3 at the ZEDEX gallery (Goudarzi et al. 2002) compared with the predicted results by the code. It can be observed that the model assumed is able to explain the evolution of psychrometer W10 where water comes from the mats, but it is not able to predict the evolution observed in psychrometer W12.

Figure 5.56: Detail of the gallery excavated by blasting closed to the ZEDEX gallery entrance. As water bearing fractures are not present in the area of the picture, the formation seems to be “dry”.

Figure 5.57: Detail of the main gallery excavated by TBM at the third level (-450 m below the ground surface). Water flows through a fracture. Therefore, there is a part where oxidation processes occur and other part where granite seems to be “intact”.

Figure 5.58: Wider view of the main tunnel excavated by TBM. It is also clear that there are water bearing fractures and non-connected fractures.

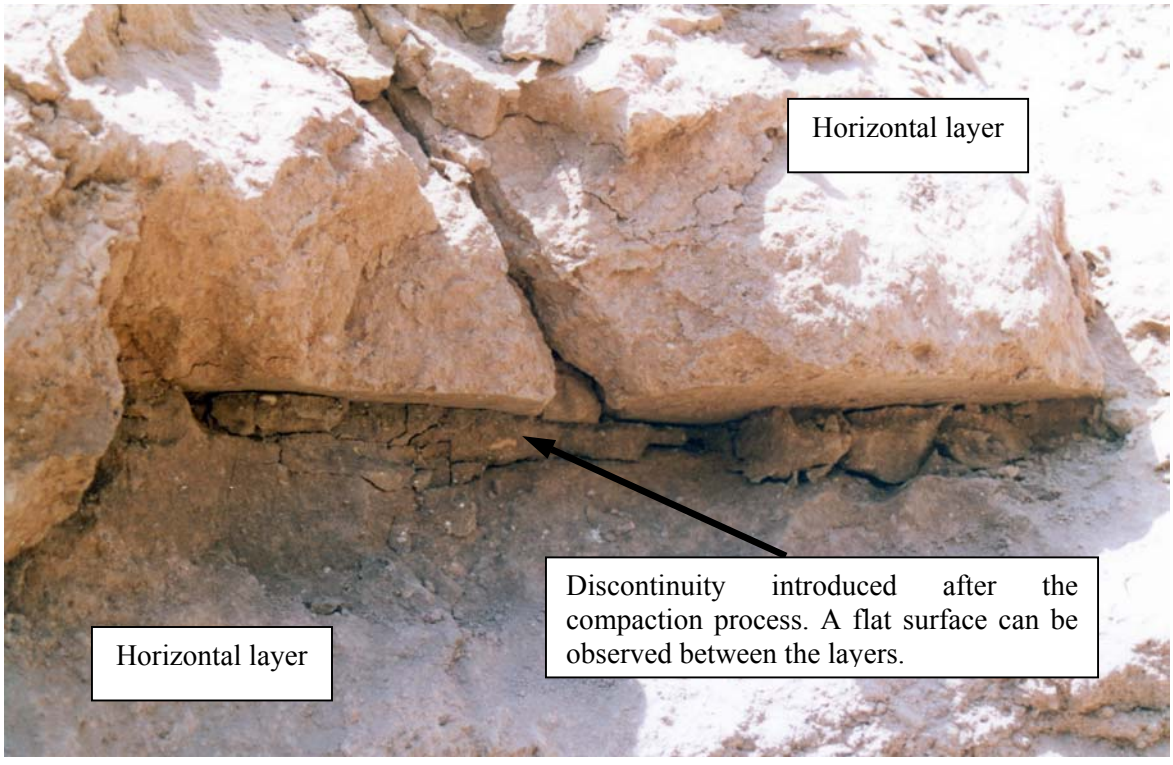

Figure 5.59: Discontinuity between two horizontal layers in an embankment. The soil is a sedimentary silt and the compactor used was a vibratory soil compactor (Mata et al. 2002b).